The University of Texas at Arlington

Department of Chemistry and Biochemistry

The evaluation of environmental contaminants using static headspace gas chromatography mass spectrometry, vacuum ultraviolet detection and ionic liquids

Dissertation Defense

Emmanuel Varona – Torres

Advisor: Kevin A. Schug

May 2021

Dedication

This work is dedicated to:

My parents and grandmother:

Juan & Grace Varona and Abuela Angie

My brother, sister and brother in law:

Cheito Varona and Angeles & Daniel Reyes

My Wife:

Karmarie Varona

My nieces and nephews:

Alana & Daniel Reyes, Christopher, Maximus, Charles & Mia Varona and Amaris Rodriguez

Thank you for your unconditional support, encouragement, inspiration and patience.

Acknowledgements

From the bottom of my heart, thank you to my mentor Prof. Kevin A. Schug, for your guidance and support.

I would like to thank the Collaborative Laboratories for Environmental Analysis and Remediation (CLEAR), UT-Arlington, for their financial support for my research.

Special thanks to the Shimadzu Center for Advance Analytical Chemistry, UT-Arlington, for allowing me to use their state-of-the-art facilities for research. Restek Corp. for their continuous interest and support for my research.

Table of Contents

Dedication 2

Acknowledgments 3

List of Figures: 8

List of Tables: 12

Summary 14

1. Gas Chromatography 17

1.1 Introduction 17

1.2 Principles of Gas Chromatography 18

1.3 Theory 18

1.3.1 Thermodynamic Relationship in Chromatography 18

1.3.2 Plate Theory 21

1.3.3 Rate Theory 22

1.4 Gas Chromatography Detectors 24

1.4.1 Mass Spectrometry 24

1.4.2 Vacuum Ultraviolet Spectroscopy 26

1. References 32

2. Headspace Gas Chromatography (HS-GC) 34

2.1 Introduction 34

2.2 Static Headspace Extraction (SHE) 35

2.2.1 Automated Gas-Tight Syringe Injection 35

2.2.2 Pressure loop System 37

2.3 Static Headspace Extration (SHE) Theory 40

2.3.1 Physicochemical Relationships 43

2.3.2 Effect of Temperature 44

2. References 45

3. The Characterization of BTEX in Variable Soil Compositions Near Unconventional Oil and Gas Development 47

3.1 Introduction 47

3.2 Materials and Methods 54

3.2.1 Air Quality Analysis 54

3.2.2 Soil Analysis 54

3.2.3 Remediation Plots 56

3.2.4 Chemicals 56

3.2.5 BTEX Analysis 57

3.2.6 Instrumentation and Parameters 57

3.2.7 Statistical Analysis 59

3.2.8 Limitation in Data for Interpretation 60

3.3 Results and Discussion 60

3.3.1 Characterizing Atmospheric Contamination 60

3.3.2 Time Series Soil Analyses 67

3.3.3 Geospatial Analyses 73

3.3.4 Variable Soil Composition 77

3.3.5 BTEX Volatilization, Sequestration, and Remediation 79

3.4 Conclusion 82

3. References 83

4. Room Temperature Ionic Liquids (RTILs) 87

4.1 Introduction 87

4.2 Room Temperature Ionic Liquids as co-Solvent in Headspace Analysis 88

4 References 91

5. Matrix-effect-free Determination of BTEX in Variable Soil Compositions Using Room Temperature Ionic Liquids co-Solvents in Static Headspace Gas Chromatography mass spectrometry 93

5.1 Introduction 93

5.2 Materials and Methods 96

5.2.1 Standards and Chemicals 96

5.2.2 Instrumentation and Parameters 96

5.2.3 Preparation of Spiked Samples 98

5.2.4 Statistical Analysis 99

5.2.5 Soil Samples 99

5.3 Results and Discussion 99

5.3.1 Exploratory Experiments 99

5.3.2 Optimization of HS Equilibration Time 100

5.3.3 EPA Method with CRM Soils 103

5.3.4 Optimized Method with CRM Soils 106

5.3.5 Method Validation 110

5.3.6 Soil Sample Analysis 111

5.4 Conclusions 112

5. References 114

6. Thermodynamic Characterization of Interactions Between Environmental Contaminants and RTILs by Static Headspace Gas Chromatography Vacuum Ultraviolet Detection 117

6.1 Introduction 117

6.2 Materials and Methods 119

6.2.1 Standards and Chemicals 119

6.2.2 Instrumentation and Parameters 120

6.2.3 Headspace Vial Volume Determination 121

6.2.4 Sample Preparation 122

6.2.5 Background Measurements of RTILs 123

6.2.6 Pseudo-Absolute Quantification 124

6.3 Results and Discussion 128

6.3.1 RTILs Background Vapors 128

6.3.2 Exploratory Experiments 128

6.3.3 Kp Determination of VOCs in RTILs at Varying Temperatures 132

6.3.4 van't Hoff Plots for Determination of Enthalpy and Entropy 140

6.4 Conclusion 146

6.References 147

Conclusion 148

List of Figures

Figure 1.1: Representation of van Deemter curve 23

Figure 1.2: Schematic of the GC-VUV instrument 28

Figure 1.3: Deconvolution of overlapping signals in chromatogram for m- and p-Xylenes 29

Figure 2.1: Schematic diagram of 6-Port 2-position pressure loop system 38

Figure 2.2: Headspace vial containing a sample: V_G, volume of the gas phase, V_s, volume of the sample phase 40

Figure 3.1. Soil texture is classified by the percent sand, silt, and clay in relation to the soil triangle 51

Figure 3.2. Sampling locations (gray dots) in relation to UD production sites (tan rectangles), and BTEX emission sources (red flame icons) in the study 55

Figure 3.3. Ambient (A) benzene, (B) toluene, and (C) total xylene isomer concentrations and around pad site #1 in the study area. 62

Figure 3.4. Ambient (A) benzene, (B) toluene, and (C) total xylene isomer concentrations and around pad site #2 in the study area. 63

Figure 3.5. Ambient (A) benzene, (B) toluene, and (C) total xylene isomer concentrations and around pad site #3 and #4 in the study area 64

Figure 3.6. Ambient (A) benzene, (B) toluene, and (C) total xylene isomer concentrations and around pad site #5 in the study area. 65

Figure 3.7. Total soil BTEX concentrations detected in rounds 1–4 as visualized cumulatively 68

Figure 3.8. Geospatial analysis for the soil samples collected during rounds 1–4 (A–D). 72
Figure 3.9. Total soil BTEX concentrations with respect to the prevailing wind position from the nearest BTEX emissions source for rounds 1–4 (A–D). 76
Figure 3.10. Total BTEX detected in the various soil types collected throughout the study (A) and in rounds 1–4 (B–E). 78
Figure 3.11. Two plots with 4, 10’ x 10’ quadrants were constructed 5ft. apart from each other to evaluate remediation strategies in contaminated soils. 81
Figure 4.1. Commonly used cations and anions for the synthesis of RTILs. 88
Figure 4.2. Structure of RTILs being investigated. 90
Figure 5.1. Soil texture is classified by the percent sand, silt and clay in relation to the soil texture triangle 94
Figure 5.2. Chromatogram of sample 5, with complete separation of xylene isomers. 98
Figure 5.3. Calibration curves for benzene, toluene, ethylbenzene and xylene isomers 101
Figure 5.4 HS heating time optimization for benzene, toluene, ethylbenzene, and xylene isomers 102
Figure 5.5. Low concentration calibration curves for benzene, toluene, ethylbenzene, and xylene isomers utilizing EPA 5021A 105
Figure 5.6. Low concentration calibration curves for benzene, toluene, ethylbenzene, and xylene isomers utilizing [MTEOA][$MeOSO_3$] 107

Figure 5.7 Broad concentration calibration curves for benzene, toluene, ethylbenzene, and xylene isomers utilizing [MTEOA][$MeOSO_3$]. 108

Figure 5.8. Calibration curves for benzene, toluene, ethylbenzene and xylenes isomers utilizing [EMIM][NTF2] as a HS solvent 109

Figure 6.1. Chemical structures of RTILs being investigated. 119

Figure 6.2. Chromatogram of analytes of interest with water as the HS solvent. 121

Figure 6.3. Chromatograms and peak identification of background vapor in RTILs.123

Figure 6.4. Chromatograms and peak identification of clean RTILs. 124

Figure 6.5. Recorded cross-sections 127

Figure 6.6. Chemical structure of the analytes being investigated. 127

Figure 6.7. Optimization of heating equilibration times in [EMIM] [ESO_4] using cyclohexane as internal standard. 133

Figure 6.8. Chromatogram of analytes of interest in [MTEOA][$MeOSO_3$] at 110 ℃. 138

Figure 6.9A. Partition coefficients obtained at varying temperatures using PAQ for analytes investigated in [EMIM] [ESO_4] 138

Figure 6.9B. Partition coefficients obtained at varying temperatures using PAQ for analytes investigated in [EMIM] [DEP]. 139

Figure 6.9C. Partition coefficients obtained at varying temperatures using PAQ for analytes investigated in [EMIM] [NTF2]. 139

Figure 6.9D. Partition coefficients obtained at varying temperatures using PAQ for analytes investigated in [MTEOA] [$MeOSO_3$]. 140

Figure 6.10. van't Hoff plots and calculated ΔH and ΔS values A) cyclohexane, B) benzene, C) octane, D) toluene, E) chlorobenzene, F) ethylbenzene, G) m-xylene, H) p-xylene and I) o-xylene in all 4 RTILs. 141

List of Tables

Table 3.1. Variable soils textures collected across sampling rounds 1-4. 56

Table 3.2. MS-MRM parameters 59

Table 3.3. R^2 values obtained from the calibration curves of each of the compound in the different soil matrices. 68

Table 3.4. Meteorological conditions prior to and during the time of sampling. 72

Table 5.1. Multiple reaction monitoring mode transition and settings for BTEX detection. 98

Table 5.2 LOQ and % recovery determination using BTEX CRM soil Wt Wt^{-1} dilution with CRM sand. Concentrations are in pg g^{-1} 111

Table 5.3 Quantitative data of samples (3 and 5) utilizing all 3 CRM calibration curves. ng g^{-1} 112

Table 6.1. Determination of headspace vial volume (V_V). 122

Table 6.2. Average cross-sections of analytes in the 125 – 240 nm range. 126

Table 6.3. Average Kp determination of VOCs in water at 70 ℃ by the VPC and PAQ method 131

Table 6.4. Calculated actual volume of sample per analyte that reached the GC at 70 ℃. 131

Table 6.5. Average Kp determination of VOCs in [EMIM] [ESO_4] at 70 ℃ by the VPC and PAQ method 134

Table 6.6. Average Kp determination of VOCs in [EMIM] [DEP] at 70 ℃ by the VPC and PAQ method 135

Table 6.7. Average Kp determination of VOCs in [MTEOA] [$MeOSO_3$] at 70 ℃ by the VPC and PAQ method 136

Table 6.8. Average Kp determination of VOCs in [EMIM] [NTF2]] at 70 ℃ by the VPC and PAQ method 136

Summary

In analytical chemistry the term “headspace” refers to the vapor that forms above a sample (liquid or solid) in a closed container. Headspace (HS) sampling is the method to promote partition between volatile components from the sample matrix and then analyzed by gas chromatography (GC). HS is an excellent technique to introduce a “clean” vapor sample into the GC and avoids introduction of non-volatile components from the sample matrix and often used for determination of volatile organic compounds (VOCs) with minimal or no additional sample preparation.

Concerns about the environmental impact of fossil fuel extraction techniques (i.e., hydraulic fracturing and other well stimulation techniques) have risen due to its expansion in the United States and other countries. Robust atmospheric studies have attributed to the emissions of rogue greenhouse gases and VOCs to mechanical inefficiencies commonly found in the midstream production process, such as gas flaring stations, condensate tanks, and pipelines. However, the interplay between fossil fuel extraction activities and soil quality has not received much attention. Utilizing headspace gas chromatography mass spectrometry (HS-GC-MS) and an establish standard method by the Environmental Protection Agency (EPA), we present a study of soil near oil and gas production in verified emissions of volatile contaminants. The findings provide an initial indication of the interactions between atmospheric VOCs contamination events and the accumulation of those contaminants in soil where, varying soil texture was found to contribute to total amount detected.

Room temperature ionic liquids (RTILs) have received significant attention in HS analysis due to their unique physiochemical properties (i.e., negligible vapor pressures,

tunable thermal stabilities, tunable viscosities and wide liquid range). RTILs are salts in which ions are poorly coordinated, resulting in a liquid state at room temperature. The evaluation of RTILs as co-solvent in soil analysis, in an effort to increase sensitivity, reduce and normalized the matrix-effects associated with varying soil compositions. It was found that hydrophilic RTILs investigated, 1-ethyl-3-methylimidazolium ethylsulfate ([EMIM][ESO_4]), 1-ethyl-3-methylimidazolium diethyl phosphate ([EMIM][DEP]), tris(2-hydroxyethyl)methylammonium methylsulfate ([MTEOA][$MeOSO_3$]), reduced matrix-effect from varying soil composition thus, reducing the need to characterized and matrix-match soil textures for calibration purposes. It also reduced the analysis time and increased precision and accuracy for the quantification of VOCs in variable soil matrices relative to standard methods.

Understanding the thermodynamic interactions between an analyte and the sample phase is of paramount importance when eliciting a co-solvent in HS analysis. The partition coefficient (KP) is an equilibrium constant that describes the distribution of the analyte between two phases (i.e., sample phase/ gas phase). Kp determinations by HS-GC is acquired by two methods: vapor phase calibration (VPC) and phase ratio variation (PRV). Kp determinations of analytes in HS co-solvents can help guide the analyst in which to use for the analysis at hand. Here we demonstrate the ability of using a pressurized – loop HS system in conjunction with gas chromatography vacuum ultraviolet detection (HS-GC-VUV) to directly calculate the concentration of the analyte in the gas phase, by pseudo-absolute quantification (PAQ), thus allowing for quick determination of Kp and other thermodynamic properties such as enthalpy (ΔH)and entropy (ΔS) of the

system. The Kp determinations by PAQ were comparable to those obtained using the VPC method, with differences in the average values ranging <1 to 30%.

Chapter 1: Gas Chromatography

1.1 Introduction

In December of 1952, Archer J. P. Martin and Richard L. M. Synge were awarded the Nobel Prize in Chemistry for their development of partition chromatography. During his award speech, Martin went on to emphasizes the possibility of using a gaseous mobile phase, known as gas-liquid chromatography.[1] In fact, the possibility of using a gas as the mobile phase to perform chromatographic separations was first described in Martin and Synge's 1941 publication where they state "…separations of volatile substances should be possible in a column in which permanent gas is made to flow over gel impregnated with a nonvolatile solvent…".[2-3] A decade later, Anthony T. James and Martin reported the separation of volatile fatty acids by gas-liquid chromatography with nitrogen gas as the mobile phase and a stationary phase of silicone / stearic acid supported on diatomaceous earth.[4] This process is considered the starting point of gas chromatography (GC).

In 1955, PerkinElmer a U.S. based company introduced their first commercial gas chromatograph, the Model 154 Vapor Fractometer.[5] The Model 154 was the first gas chromatograph to use an oven to adjust column temperature; it also featured a flash vaporizer and a syringe injector. In 1961, PerkinElmer developed the Model 222, the first gas chromatograph with a resistance-heated packed column, which removed the difference between set and actual column temperature. An affiliate of PerkinElmer in Germany developed the Model F-6 in 1962.[6] This was the first "building block" gas chromatograph. It allowed the user to choose from various detectors and programed oven operations. During the 1967 Pittsburgh Conference on Analytical Chemistry and Applied

Spectroscopy (Pittcon) PerkinElmer released what they consider "…one of the finest GCs ever built…", the Model 900.[5] The Model 900 had many improvements over the older models. Six years later in 1973, Hewlett-Packard (HP) introduced its first gas chromatograph the HP 5830, which was the first microprocessor controlled analytical instrument ever made.[6] Later in 1981, Shimadzu launched the GC-8A, which revolutionized gas chromatograph system design by offering a smaller, compact size and a solid, die cast frame.[6]

1.2 Principles of Gas Chromatography

The International Union of Pure and Applied Chemistry (IUPAC) defines gas chromatography (GC) as "A separation technique in which the mobile phase is a gas. Gas chromatography is always carried out in a column".[7] In GC, the analyte is first converted into its vapor state (if not already in a gaseous state) by injection into the heated injection port, where it is transported through the column (stationary phase) by a gaseous mobile phase (carrier gas). The stationary phase is normally a nonvolatile liquid supported or bonded to a capillary wall or inert solid particles. Common carrier gases used today are hydrogen, nitrogen, and helium. Separation occurs as the gaseous analytes partition between the carrier gas and the stationary phase. Depending on the retention time of the analytes in the column, the analytes are eluted from the column at different times, at which point a detector can generate a signal for each analyte.

1.3 Theory

1.3.1 Thermodynamic Relationship in Chromatography

The chromatographic process involves the repeated transfer of analytes between a flowing mobile phase and a fixed stationary phase.[8] The analytes physicochemical

properties and the varying stationary and mobile phases, dictate the degree to which partitioning happens. Thus, analytes that interact heavily with the stationary phase will be retained longer. The analytes that do not interact heavily, will quickly flow through the system with the mobile phase. Even though equilibrium is never achieved, thermodynamic concepts can be used to characterize or obtain a better understanding of the molecular-scale energetics (i.e. free energy, enthalpy and entropy) of a system.[8]

The distribution of an analyte, X, between the mobile phase and the stationary phase (sp) at equilibrium is represented by equation 1.1.

$$[X]_{mp} \leftrightarrow [X]_{sp} \quad \text{(Equation 1.1)}$$

The distribution of the analyte between two phases (stationary/mobile phase) can be described by the partition coefficient (Kp), an equilibrium constant. The relationship between the retention factor (k) and Kp is shown in equation 1.2, using the phase ratio (β) expression, which is the ratio of the mobile phase volume to the stationary phase volume in the chromatographic system.

$$Kp = k \cdot \beta \quad \text{(Equation 1.2)}$$

The equilibrium constant (Kp) for an analyte that is partitioning between the mobile phase and stationary phase consists of the ratio of the concentration at equilibrium of the analyte in the stationary phase to that of the analyte in the mobile phase, as shown in equation 1.3.

$$Kp = \frac{[X]_{sp}}{[X]_{mp}} \quad \text{(Equation 1.3)}$$

Where (t_r) is the retention time; the retention factor is taken as the ratio of the adjusted retention time (t_r') to the dead time (t_O) as given in equation 1.4. It can be

regarded as the amount of time the analyte spends in the stationary phase (t_r') divided by the amount of time it spends in the mobile phase (t_O). The retention factor represents the ratio of amount of analyte in each phase at any time point. Thus, one can multiply by the phase ratio to obtain the equilibrium constant, as seen in equation 1.2.

$$t_r' = t_r - t_O \quad \text{(Equation 1.4)}$$

The equilibrium constant, Kp, can be related to Gibbs free energy change (ΔG), using the well-known equation 1.5:

$$\Delta G = -RTlnK \quad \text{(Equation 1.5)}$$

where R is the gas constant and T is the temperature (in Kelvin). The Gibbs free energy change is related to the change in enthalpy (ΔH) and the change in entropy (ΔS) as described by the Gibbs-Helmholtz equation (equation 1.6).

$$\Delta G = \Delta H - T\Delta S \quad \text{(Equation 1.6)}$$

Combining equation 1.5 and 1.6, one derives what is known as the linear form of the van't Hoff equation, given in equation 1.7. It relates the change in the equilibrium constant of a system to the change in temperature. Plotting $lnKp$ vs. $\frac{1}{T}$ allows for the determination of thermodynamic properties. After performing a linear regression analysis and obtaining a linear equation, multiplying both the slope and the intercept of the line by the gas constant one obtains ΔH and ΔS respectively.

$$lnKp = -\frac{\Delta H}{RT} + \frac{\Delta S}{R} \quad \text{(Equation 1.7)}$$

A spontaneous reaction, where the analyte favors interaction with the stationary phase occurs when ΔG is negative. A spontaneous reaction can be prompted by a decrease in ΔH becomes more negative or by a large increase in ΔS, which means that

even if ΔH is positive, a positive ΔS, multiplied by the temperature, could result in an overall negative ΔG, and thus, a favorable process.

1.3.2 Plate Theory

The Plate Theory was developed by Martin and Synge in 1941, to describe the mechanism of retention.[2] It allows for the calculation of the retention volume and column efficiency. The Plate Theory assumes that the analyte is at equilibrium with the mobile phase and stationary phase; although equilibrium between the phases does not actually occur. The column is divided in to what is referred to as "theoretical plates". Each theoretical plate is of a specific length; thus, the analyte will spend finite amount of time in each plate. The smaller the theoretical plate, the faster equilibrium could be achieved, thus more theoretical plates will exist in the column. The number of theoretical plates is a measure of column efficiency, by either reporting the number of theoretical plates (N) (the higher N, the better) (equation1.8), or by indicating the plate height; as the height equivalent to a theoretical plate ($HETP$) see equation 1.9. The smaller the calculated height, the better for separation.

$$N = 16\left(\frac{t_r}{w_b}\right)^2 = 5.54\left(\frac{t_r}{w_{\frac{1}{2}}}\right)^2 \text{ (Equation 1.8)}$$

$$HETP = \frac{L}{N} \text{ (Equation 1.9)}$$

In equation 1.8, w_b is the peak width, and w_b is the peak width at half-peak height, and L is the length of the column. Based on equation 1.8, columns behave as if they have different number of theoretical plates for different analytes. The Plate Theory does not

consider mass transfer kinetics and thus, reveals very little about factors that influence $HETP$ values. This theory also disregards the concept of analyte diffusion and flow path.

1.3.3 Rate Theory

Developed by Jan van Deemter and his colleagues at the Royal Dutch Shell, the Rate Theory describes the process of peak dispersion, also referred to as band broadening.[9] The Rate Theory provides an equation that allows for the calculation of differences in height equivalent to a theoretical plate (H) in terms of mobile phase velocity and other physiochemical properties of the analyte and the distribution system, as given in equation 1.10:

$$H = A + \frac{B}{u} + C_u \text{ (Equation 1.10)}$$

where u is the average velocity of the mobile phase, and the terms $A, B,$ and C are all factors that contribute to band broadening. Various forms of the van Deemter equations have been developed. Marcel J. E. Golay introduced the equation for height equivalent to a theoretical plate when using an open tubular column in GC as seen in equation 1.11.[10] Figure 1.1 shows a schematic representation of the van Deemter curve.

$$H = \frac{B}{u} + C_u \text{ (Equation 1.11)}$$

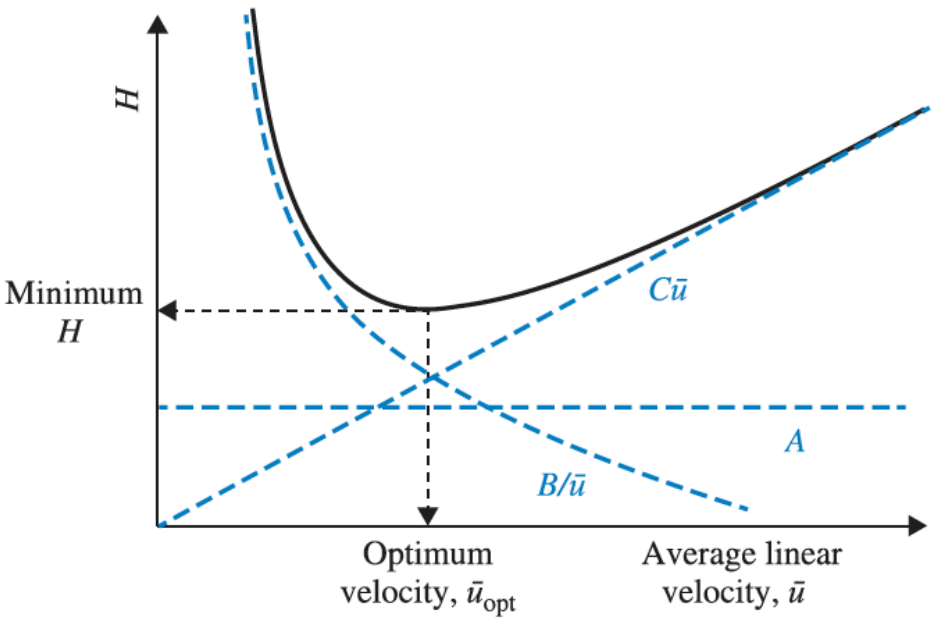

Figure 1.1: Representation of van Deemter curve-plot of plate height vs. average linear velocity. Reprinted with permission.[11]

The *A*- term represents *eddy diffusion,* which describes when an analyte zone migrates through a packed bed, the random individual flow paths around the particles of packing are of different lengths thus, causing band broadening. In GC when using open tubular columns this term can be neglected due to no packing.[10] The $\frac{B}{u}$- term represents molecular diffusion, which arises from the random molecular motion of analyte molecules in the mobile phase. The mobile phase moves through the column, the analyte molecules diffuse in all directions, diffusing to area of lower concentration. If the velocity of the mobile phase increases, molecular diffusion effects will be decreased. The Cu- term represents mass transfer interphase and describes the contribution from resistance to mass transfer in both the mobile phase and stationary phase. In GC, the resistance to mass transfer in the mobile phase is neglected due to the fast diffusivity in the gas phase. The analyte in the mobile phase will move ahead of the analyte in the stationary phase if the velocity of

the mobile phase is high and the analyte has a strong affinity to the stationary phase thus, leading to band broadening. High mobile phase velocity favors more band broadening. Stationary phase film thickness contributes to mass transfer. With a thicker film; the longer it takes the analyte to reach the interface, which leads to an increase in band broadening.

1.4 Gas Chromatography Detectors

When the analyte elutes from the column, they reach the detector. The detector then converts this interaction into an electrical signal that is received by the data system. The signal it receives is plotted vs. the time of injection, thus a chromatogram is produced. Various detectors exist. Some produce a signal for any analyte eluting from the column, while others only produce a signal for analytes with specific structures, functional groups, and or atoms. Here we will focus on only two detectors, the triple quadrupole mass spectrometer and the vacuum ultraviolet spectroscopic detector.

1.4.1 Mass Spectrometry

The mass spectrometer was developed during the hunt for the electron by Sir Joseph J. Thomson.[12] In the 1940's, mass spectrometry technology played a pivotal role in the Manhattan Project, a war time project that involved the separation of the fissionable ^{235}U isotope on a preparative scale and as leak detector in a UF_6 gaseous diffusion plant.[13] Mass spectrometry measurement deals with ions because of the ease of manipulating the motion and direction of them experimentally and detecting them. There are 3 basic steps in mass spectrometry analysis: ionization, separation and measurement.

The first step in mass spectrometry is ionization. This converts the analyte molecules or atoms into a gaseous ionic species. This step often requires the removal or

addition of electrons or protons. The energy transferred during an ionization may break the molecule into characteristic fragments. The second step is the separation and mass analysis of the molecular ions and their charged fragments on the basis of their mass-to-charge ratios (m/z). Mass-to-charge ratio by definition is the mass of the ion (m) divided by the number of charges (z) the ion carries.[13] And finally, the ion current due to the mass separated ions is measured, amplified and displayed in the form of a mass spectrum.

The ionization of the analyte is the first critical step in the analysis of any type of compound by MS. Depending on the sample phase, various ionization modes are available. Most common ionization sources for GC-MS are chemical ionization (CI), electron ionization (EI), and photoionization (PI). Herein, we will focus on electron ionization (EI). EI is considered one of the oldest modes of ionization, being first used in 1918 by Arthur J. Dempster.[14] It is the most popular ionization source for organic compounds with molecular masses less than 600 Da. It is restricted to thermally stable and relatively volatile compounds. In the process of EI, the gaseous analyte molecules are bombarded with a beam of typically 70 eV at low pressures usually around 10^{-5} – 10^{-6} torr. An electron from the target analyte molecule is expelled during this process to convert the analyte molecule to a positive ion with an odd number of electrons. The energy gained in excess by ionization of the analyte molecule causes it to dissociate into structurally specific smaller mass fragmented ions. Thus, allowing for the use as a finger print, diagnostic tool of the structure of the analyte.

Mass spectrometry can also operate in tandem form referred to as MS/MS. It essentially involves two mass spectrometry systems. The first system, performs mass selection of a desired target ion from a stream of ions produced from the ionization source.

The mass selected ion will then undergo unimolecular fragmentation in the intermediate region, the collision induced dissociation cell (CID) The second system, performs mass analysis of the product ions that were formed in the CID.

The triple quadrupole mass spectrometry (QqQ-MS) is considered an MS/MS technique. The quadrupole consists of four parallel metal rods. The mass separation is achieved by the stable vibratory motion of ions in a high-frequency oscillating electric field created by applying direct-current (DC) and radio-frequency (RF) potentials to each of these electrodes.[13] Under a set of defined DC and RF potentials, ions of specific m/z value pass through the geometry of the quadrupole rods. This mechanism is the same for both Q_1 and Q_3 thus, acting as mass filters. In QqQ-MS the collision cell (CID) or "q" only operates in the RF mode. By colliding with atoms of an inert gas such as, Ar, He, or N_2, ions are excited to a higher energy state. The fragmentation of the excited ion happens when the excitation energy exceeds the energy required to cleave a particular bond. Various scan operations exist when using MS/MS. The various scan modes in QqQ-MS are: precursor-ion scan, product-ion scan, neutral-loss scan, and selected-reaction monitoring also known as multiple-reaction monitoring (MRM). Focusing on MRM, here both Q_1 and Q_3 are set at a fixed m/z's, allowing only distinct fragment ion from the precursor ion to be detected. This mode is widely used for quantitative analysis due to the increased level of detection specificity. The increase in level due to the characteristic structural link that is maintained during the process between the mass selected precursor ion and its product ions.[13] Chemical noise is essentially eliminated in this mode.

1.4.2 Vacuum Ultraviolet Spectroscopy

The vacuum ultraviolet spectrophotometer (VUV) was developed and commercialized fairly recently by VUV Analytics, Inc.[15] This detector measures the absorption of a gaseous analyte in the range of 120-240 nm, where essentially all chemical compounds present a unique absorption spectra.[15] With the use of a deuterium lamp as a light source, photons in this area are able to excite the atomic species with any chemical bond, especially $\sigma \rightarrow \sigma^*$ and short wavelength high probability $\pi \rightarrow \pi^*$, which normally cannot be done in traditional UV/Vis absorption spectroscopy owing to the high absorption of most compounds in the lower UV range and instruments not operating under vacuum or being purge by an inert gas.[15-16] Quantitative analysis is governed by Beer-Lambert Law relationships.[17] Figure 1.2 provides a general depiction of the instrumental and operational principles of the GC-VUV.

The analytes eluting from the GC enter a heated transfer line (approximately 275°C typically), of uncoated deactivated glass capillary. A makeup flow carrier gas is introduced at the end of the transfer line. The makeup flow can be used to alter the residence time of the sample zone in the detector cell.[15] The analyte then reaches the 10 cm path length flow cell. The use of a specially coated reflective optic and a back-thinned charged coupled device (CCD) light path monitor to simultaneously asses absorption features across the spectrum for peaks eluting from the GC column is critical for the ability to obtain high quality VUV absorption data between 125-240 nm.[15] At the start of the run, a dark noise reading is taken for background subtraction. Gases such as He, N_2, Ar and H_2 provide a significantly reduced background due to their minimal absorption characteristics.[15, 18] The VUV detector is considered to act as both mass sensitive and a concentration sensitive detector.[15-17] In the case of a mass sensitive detector, the detector

response is proportional to the amount of analyte present per unit time.[15] In concentration sensitive detectors, the detector response is proportional to the concentration of the analyte per unit of volume at a particular point in time.[16] Due to the makeup flow and the pressure regulation of the makeup gas of the VUV detector, the detector response appear to be dependent on experimental conditions such as the makeup gas pressure.[16] Liu and colleagues showed that by keeping constant column flow and increasing the makeup gas pressure; peak heights and peak areas decreased; caused by the gas dilution in the flow cell and, thus performing as a concentration sensitive dector.[19] But for a constant gas rate exceeding that of the column flow rate, a concentration sensitive detector behaves as if it was a mass sensitive detector.[19-20] Following the analyte residence time in the flow cell, the analyte is swept out through the exit vent.

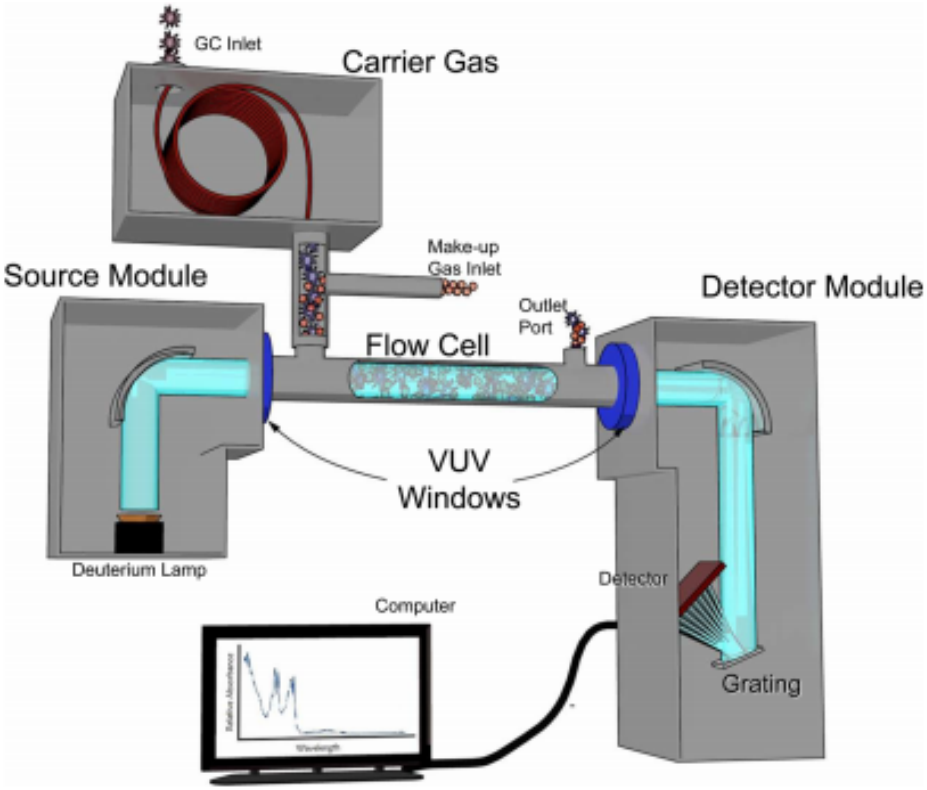

Figure 1.2: Schematic of the GC-VUV instrument. Reprinted with permission from (Schug, K. A.; Sawicki, I.; Carlton, D. D.; Fan, H.; McNair, H. M.; Nimmo, J. P.; Kroll, P.; Smuts, J.; Walsh, P.; Harrison, D., Vacuum Ultraviolet Detector for Gas Chromatography. *Analytical Chemistry* **2014,** *86* (16), 8329-8335).[15]

The VUV detector is a universal detector capable of providing qualitative and quantitative information. The VUV detector has a tremendous advantage over the MS detector when it comes to the discrimination of isomers like m-Xylene and p-Xylene and the deconvolution of co-eluting peaks see figure 1.3. Usually such discrimination is performed with the use of a specialty stationary phase to chromatographically resolve the analytes.

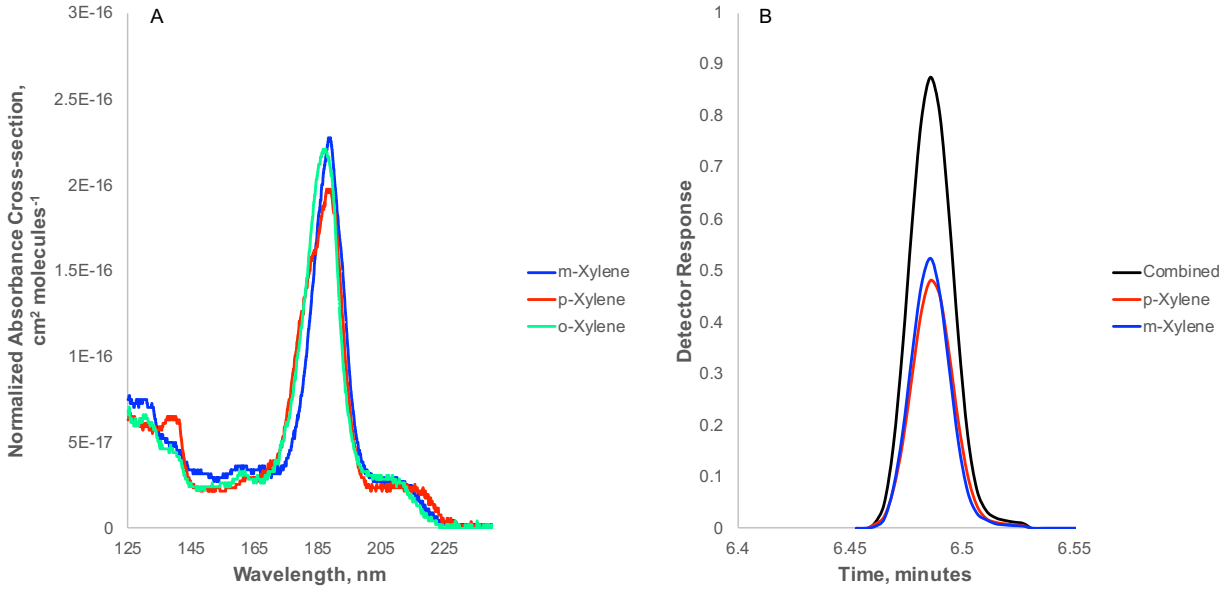

Figure 1.3: Normalized absorbance cross-sections for xylene isomers (A). Deconvolution of coeluting overlapping signals of m- and p- Xylene (B).

For qualitative analysis, a database library is used for the identification of unknown compounds by matching the analyte spectrum with the reference spectrum. The reference spectra depend only on the electronic and vibrational structure of the analyte molecule and not on the amount, thus allowing them to be used for identification of unknowns and for the deconvolution process.

One of the key features of the VUV detector is its ability to deconvolute co-eluting analytes. In the VUV detector, since absorption is additive, overlapping peaks give a spectrum that corresponds to the sum of the absorbance of each compound. If the cross-sections for both compounds are known, it is possible to determine the individual contribution of each compound.[15, 18] Other methods have been developed for when new unknown compounds and their VUV spectrum are unavailable.[21] By obtaining the mass spectrum of the unknown, and obtaining its possible chemical structure, quantum mechanical calculations are able to calculate electronic excitation energies (corresponding to absorption wavelength) as well as vibrational strength (corresponding to absorption intensity) for the unknown structure. Performing sum-squared residual analysis (SSR) to compare the theoretical spectrum to the VUV experimental spectrum. The smallest SSR value will correspond to the correct structure identification.[21]

As mentioned earlier, the VUV detector follows the Beer-Lambert Law, as given in equation 1.11.

$$A = \epsilon bc \quad \text{(Equation 1.11)}$$

Where A is the absorbance, ϵ is the molar absorptivity coefficient ($L\ mol^{-1}cm^{-1}$), b is the path length (cm), and c the analyte concentration ($mol\ L^{-1}$). The absorption cross-sections σ ($cm^2 molecule^{-1}$) via Avogadro's constant, can be used instead of the molar

absorptivity coefficient.[17-18] This allows for the VUV detector to quantify analytes without the need for a calibration, termed pseudo-absolute quantification.[17] When the cross-section of an analyte is known as well as the detector scan rate, the flow cell path length and carrier gas flow rate, the number of molecules that reached the detector can be determined as shown in equation 1.12.

$$PA = \frac{1}{\ln(10)} R \frac{d}{F} \Sigma N_{Det} \quad \text{(Equation 1.12)}$$

Where *PA* is actually a sum of chromatographic scans over the time region of the time region. N_{Det} is the total number of analyte molecules introduced to the detector, *R is the detector scan rate* ($scans\ min^{-1}$) *d* is the flow cell path length (cm), *F* is the sample flow rate ($mL\ min^{-1}$), Σ is the absorption cross-section integrated over the same wavelength region as the absorbance. The number of molecules determined in the detector would be theoretically equal to the amount in the sample if perfect transfer of the analyte was attained without any losses. Although, as it is known, loss of analyte may occur in sample preparation and injection procedures. It is then necessary to execute internal standardization or determination of sample losses or gains during injection to account for systematic errors. To this reason, this method is called pseudo-absolute quantitative method instead of absolute quantitative.[17]

1. References

1. Martin, A. J. The development of partition chromatography. NobelPrize.org/prizes/chemistry/1952/martin/lecture/.
2. Martin, A. J.; Synge, R. L., A new form of chromatogram employing two liquid phases: A theory of chromatography. 2. Application to the micro-determination of the higher monoamino-acids in proteins. *Biochem J* **1941,** *35* (12), 1358-1368.
3. Bartle, K. D.; Myers, P., History of gas chromatography. *TrAC Trends in Analytical Chemistry* **2002,** *21* (9), 547-557.
4. James, A. T.; Martin, A. J. P., Gas-liquid partition chromatography; the separation and micro-estimation of volatile fatty acids from formic acid to dodecanoic acid. *Biochem J* **1952,** *50* (5), 679-690.
5. Ettre, L. S., The Evolution of Gas Chromatographic Instrumentation at PerkinElmer. PerkinElmer, 2005; p. 16. (accessed 2021).
6. Buie, J. Evolution of Gas Chromatography. https://www.labmanager.com/lab-product/evolution-of-gas-chromatography-19883.
7. A.D. Mcnaught, A. W., IUPAC. Compendium of Chemical Terminology (the "Gold Book"). Blackwell Scientific Publications: Oxford, 1997; Vol. 2.
8. Schug, K. A., Back to Basics: The role of Thermodynamics in Chromatographic Separations. The LCGC Blog, 2013; Vol. 2021.
9. van Deemter, J. J.; Zuiderweg, F. J.; Klinkenberg, A., Longitudinal diffusion and resistance to mass transfer as causes of nonideality in chromatography. *Chemical Engineering Science* **1956,** *5* (6), 271-289.
10. Golay, M. J. E., Height Equivalent to a Theoretical Plate of Tubular Gas Chromatographic Columns lined with a Porous Layer. *Nature* **1963,** *199* (4891), 370-371.
11. Gary D. Christian, P. K. D., Kevin A. Schug, *Analytical Chemistry*. 7th ed.; Wiley.
12. Griffiths, J., A Brief History of Mass Spectrometry. *Analytical Chemistry* **2008,** *80* (15), 5678-5683.
13. Dass, C., *Fundamentals of Contemporary Mass Spectromery*. John Wiley & Sons: Wiley Interscience, 2007.
14. Dempster, A. J., A new Method of Positive Ray Analysis. *Physical Review* **1918,** *11* (4), 316-325.
15. Schug, K. A.; Sawicki, I.; Carlton, D. D.; Fan, H.; McNair, H. M.; Nimmo, J. P.; Kroll, P.; Smuts, J.; Walsh, P.; Harrison, D., Vacuum Ultraviolet Detector for Gas Chromatography. *Analytical Chemistry* **2014,** *86* (16), 8329-8335.
16. Lelevic, A.; Souchon, V.; Moreaud, M.; Lorentz, C.; Geantet, C., Gas chromatography vacuum ultraviolet spectroscopy: A review. *Journal of Separation Science* **2020,** *43* (1), 150-173.
17. Bai, L.; Smuts, J.; Walsh, P.; Qiu, C.; McNair, H. M.; Schug, K. A., Pseudo-absolute quantitative analysis using gas chromatography – Vacuum ultraviolet spectroscopy – A tutorial. *Analytica Chimica Acta* **2017,** *953*, 10-22.
18. Santos, I. C.; Schug, K. A., Recent advances and applications of gas chromatography vacuum ultraviolet spectroscopy. *Journal of Separation Science* **2017,** *40* (1), 138-151.
19. Liu, H.; Raffin, G.; Trutt, G.; Randon, J., Is vacuum ultraviolet detector a concentration or a mass dependent detector? *Journal of Chromatography A* **2017,** *1530*, 171-175.

20. Halasz, I., Concentration and Mass Flow Rate Sensitive Detectors in Gas Chromatography. *Analytical Chemistry* **1964,** *36* (8), 1428-1430.
21. Skultety, L.; Frycak, P.; Qiu, C.; Smuts, J.; Shear-Laude, L.; Lemr, K.; Mao, J. X.; Kroll, P.; Schug, K. A.; Szewczak, A.; Vaught, C.; Lurie, I.; Havlicek, V., Resolution of isomeric new designer stimulants using gas chromatography – Vacuum ultraviolet spectroscopy and theoretical computations. *Analytica Chimica Acta* **2017,** *971*, 55-67.

Chapter 2: Headspace Gas Chromatography (HS-GC)

2.1 Introduction

Headspace, in gas chromatography refers to the vapor phase in contact and in equilibrium with ideally a nonvolatile or less volatile sample in a sampling container and its investigation as headspace analysis. Gas extraction techniques have similarities to those of liquid extractions as they can be carried out by a single extraction step, thus, the purpose of the original sample (liquid or solid) being placed in a closed sampling container.[1] The technique usually involves the sample in the sealed vial to be heated to a pre-determined temperature in a thermostat oven. When equilibrium is reached between the sample and the gas phase, the volatile analyte in the sampling vial is said to be at equilibrium in the "sample phase". A defined amount of the gas phase is taken and carried to the column in the gas chromatograph (GC) for analysis. This technique only allows volatile substances to reach the GC and the nonvolatile substances to remain in the sampling vial. Headspace is considered the cleanest form of GC analysis, as no nonvolatile residues are introduced to the system.

Multifaceted matrices (liquid or solid) require extensive sample preparation and/ or are difficult to directly inject into the GC, are usually ideal candidates for headspace analysis since they can be placed in a sampling vial with minimal or no preparation. Headspace is widely employed for environmental, food and beverages, pharmaceutical, fragrance, and forensic analysis in laboratories around the world. [2-9] Headspace GC is widely used for the determination of volatile organic compounds (VOCs) in environmental analysis. Various forms of headspace GC can be employed: static headspace extraction (SHE), dynamic headspace extraction (DHE), multiple headspace extraction (MHE), and

solid phase micro extraction (SPME).[2-5, 10-11] Static headspace extraction will be discussed as it was the technique utilized in the chapters ahead.

The term headspace and headspace analysis in conjunction with GC first appeared in literature in 1960 by W.H.Stahl and colleagues.[12] Stahl and colleagues used headspace sampling for GC analysis of the gas in sealed cans and flexible packages for their oxygen content. Although, the first report of headspace analysis that could be found in literature is by R.N.Harger and colleagues from the Indiana University School of Medicine (Indianapolis, Indiana).[13-14] According to the abstract, this method dealt with the "aerometric method" for the rapid determination of alcohol in water and body fluids. The first report of the combination of headspace sampling with GC analysis was presented in 1958 at the Amsterdam Symposium by Bovijn and coworkers.[15] They used the technique to measure hydrogen at the 1 ppm level in water present in high pressure boilers.[13] The first automated instrument to carry out GC analysis of headspace samples was introduced in 1967 by PerkinElmer Model F-40.[1] The Model F-40 was the first automatic sample introduction system for GC even before the first liquid injection autosamplers were developed.[1]

2.2 Static Headspace Extraction (SHE)

In static headspace extraction (SHE)-GC, a sealed container (in this case a screw-cap vial) is placed in a heating oven in which it is heated until thermal equilibration of the volatile analytes is achieved inside the vial. A single headspace aliquot sample is obtained and injected into the GC. Thermostatting is the process of heating the vial to a set temperature and time with the intentions of achieving equilibrium in the vial. Equilibrium is considered to be achieved when the vapor concentration in the headspace and the

sample phase remain constant at a given temperature. The headspace aliquot can be obtained in various ways by using a gas-tight syringe operated manually or by automation, pressure-lock syringe (manual), pressure-loop (automation) or pressure-balanced systems (automation). Automated gas-tight syringe and the pressure loop systems are discussed in the following.

2.2.1 Automated Gas-Tight Syringe injection

Automated gas-tight syringe systems overcome various short comings of manual injection such as the lack of precision and risk of sample condensation among others. A heated gas-tight syringe typically ranging from 1-10 mL draws up a set volume of the sample. Typically, the syringe is maintained at a higher temperature than the vial to avoid possible sample. With the syringe being at a temperature above the sampling vial and the vapor pressure inside the vial will be at a higher pressure, there will be an expansion of the gas and loss through the needle when the syringe needle is withdrawn from vial and exposed to ambient pressure. Therefore the actual volume of headspace sample extracted and injected into the GC is less than the set syringe volume as seen in equation 2.1.[1, 16]

$$V_{Extracted} = V_{Syringe}\left(\frac{P_{Ambient}}{P_{Vial}}\right)\left(\frac{T_{Vial}}{T_{Syringe}}\right) \text{ (Equation 2.1)}$$

Where $V_{Extracted}$, is the volume of headspace vapor retained in the syringe after it is withdrawn from the sample vial. $V_{Syringe}$, is the sampling volume set in the method. P_{Vial}, is the absolute pressure of the headspace vapor inside the vial. $P_{Ambient}$, is the absolute ambient pressure. T_{Vial} and $T_{Syringe}$ is the absolute temperature of the vial and syringe respectively. As it is shown here (Eq. 2.1), the set syringe volume in the method is not an accurate representation of how much actual gas volume is injected into the GC. Other

considerations must be taken as well such as the column flow rate and flow rate at the split vent all in which contribute to the volume of sample actually injected.

2.2.2 Pressure loop System

The other headspace system that will be discussed is the pressure loop system or commonly referred to as the loop system. In this system, once equilibration of the sample is complete, a sampling needle pierces the vial septum and the vial is pressurized with an inert gas to a set amount usually 20-30 kPa above the native vial pressure at the set temperature. The pressurized vapor is then allowed to escape through a sample valve loop system. The sampling loop usually has a set capacity of 1 mL. It is usually kept above the vial heating temperature to prevent possible condensation. The pressure in the loop will be less than the pressure inside the sampling vial and will normally be at ambient pressure at the end of the sampling process. Figure 2.1 shows various diagrams of the various stages of the injection process in a loop system containing a 6-port 2 position valve.

During the pressurization stage, the sampling needle pierces the vial septum after the vial has me thermostated, and the pressurization gas, pressurizes the vial by maintaining a set flow rate into the vial until the pressure of the vial reaches the set pressure in the method. The HS then maintains this pressure during a set equilibration time typically 2 mins.[17]

Once the vial is pressurized and equilibrated, the sample loop filling mode initializes. The valve switches, thus allowing the pressurized sample to vent through the

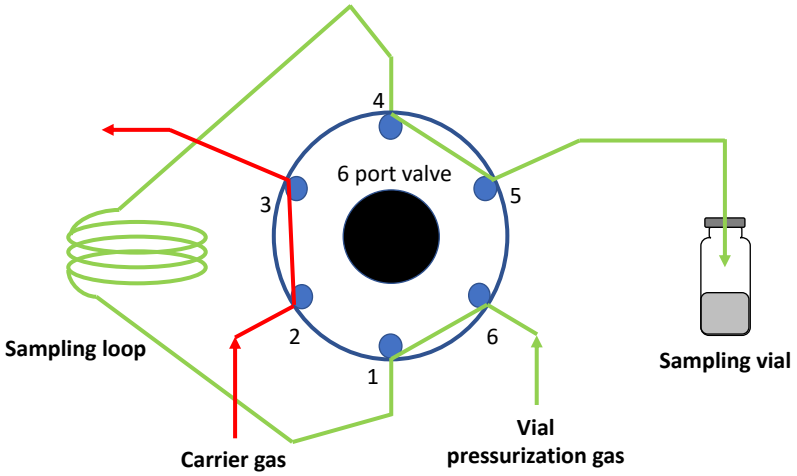

Vial pressurization

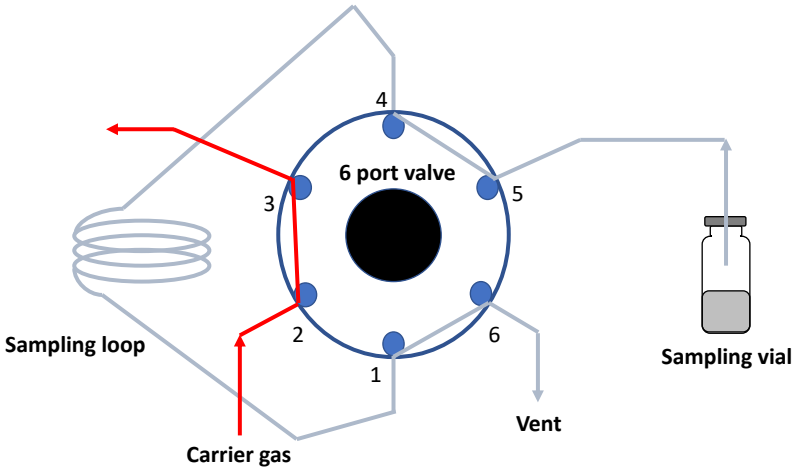

Sample loop filling

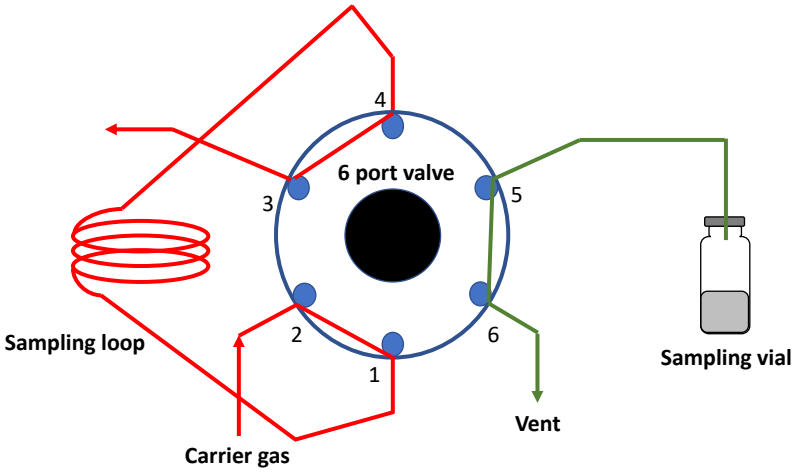

Injection

Figure 2.1. Schematic diagram of a 6-port 2-position pressure loop system at the vial pressurization stage, sample loop filling stage and injection stage.

sample loop for the allotted time specified in the method, usually 15-30 seconds the loop is considered filled.[17] The Injection mode initializes after the allotted time specified in the method for the loop equilibration is reached, usually 15-30 seconds.[17] In counter-clockwise fashion the HS 6-port valve rotates to the second position, the injection position. The carrier gas now flows through the sample loop and into the GC for the allotted time specified in the method. It is important to understand of how much headspace sample vapor is actually held in the loop shown in equation 2.2.

$$V_{Extracted} = V_{Loop}\left(\frac{P_{Loop}}{P_{Vial}}\right)\left(\frac{T_{Vial}}{T_{Loop}}\right) \text{ (Equation 2.2)}$$

Where $V_{Extracted}$, is the volume of headspace vapor removed from sample vial. V_{Loop}, is the volume of the sampling loop. P_{Vial}, is the absolute pressure of the headspace vapor inside the vial. P_{Loop}, is the absolute pressure inside the loop at the end of the sampling step. T_{Vial} and T_{Loop} is the absolute temperature of the vial and sampling loop respectively. As it is shown in equation 2.2, the capacity of the sample loop itself is not an accurate measure of how much sample is actually injected into the GC. Pressure and temperature changes along with other considerations such as, flow rates and time of injection, all have a direct effect on the volume of HS vapor sample that reaches the GC column. Unless all of the parameters are well understood and accurately measured it is nearly impossible to determine how much sample is actually injected in this system.[16]

2.3 Static Headspace Extraction (SHE) Theory

Static headspace theory was developed by both Bruno Kolb and Leslie S. Ettre and described in the text book "Static Headspace Gas Chromatogrphy".[1] It is of importance to understand the fundamental principles that govern the mass transfer of analytes in the headspace system for the design and optimization of sample preparation methods. In SHE at equilibrium, the system inside the vial can be characterized by conventional theoretical treatment. Figure 2.2 illustrates a static headspace vial, two-phase system.

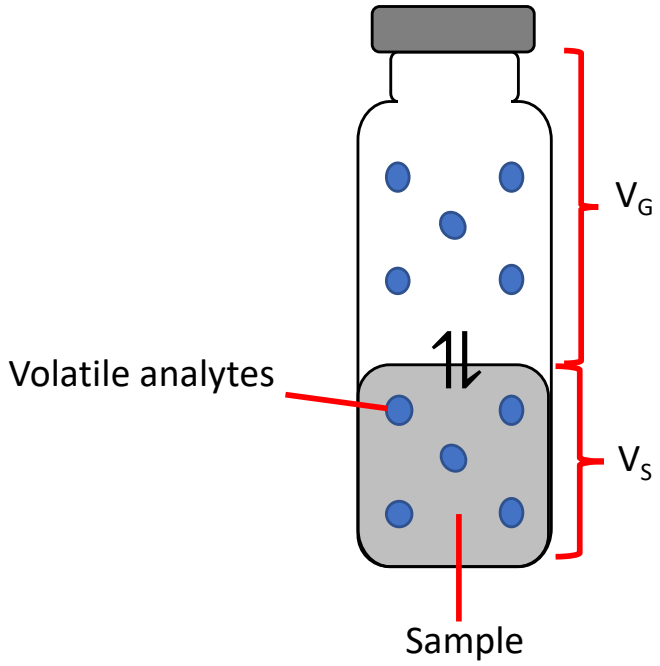

Figure 2.2. Headspace vial containing a sample: V_G, volume of the gas phase, V_s, volume of the sample phase.

The concentration of each analyte in the gas-phase ($[X]_G$) is the quantity that is measured by GC analysis, not the concentration in the sample phase. Two characteristics

determine the relationship between the measured gas-phase concentration and the original solute concentration in the sample. In order to determine the original analyte concentration ($[X]_0$), in the sample phase at equilibrium, one must consider the partition coefficient (Kp), which is the ratio of the analyte's concentration in the sample phase ($[X]_S$) to the concentration in the gas phase as shown in equation 2.3.

$$Kp = \frac{[X]_S}{[X]_G} \text{ (Equation 2.3)}$$

The partition coefficient, can be written in terms of amount of analyte in the gas phase and in the sample phase as W_G and W_S respectively, and the volume of the gas phase and sample phase as V_G and V_S, respectively shown in equation 2.4.

$$Kp = \frac{\left(\frac{W_S}{V_S}\right)}{\left(\frac{W_G}{V_G}\right)} \text{ (Equation 2.4)}$$

Rearranging equation 2.4 gives equation 2.5,

$$Kp = \left(\frac{W_S}{W_G}\right)\left(\frac{V_G}{V_S}\right) \text{ (Equation 2.5)}$$

Substituting the phase ratio β, for $\left(\frac{V_G}{V_S}\right)$ equation 2.5 can be written as equation 2.6.

$$Kp = \left(\frac{W_S}{W_G}\right)\beta \text{ (Equation 2.6)}$$

Thus, if the initial amount of the of analyte added to the solution before equilibration is taken as W_0, then the initial concentration can be obtained as shown in equation 2.7.

$$W_0 = V_S[X]_0 \text{ (Equation 2.7)}$$

After equilibration it can the amount of analyte can be written as equation 2.8 and 2.9 respectively.

$$W_S = V_S[X]_S \text{ (Equation 2.8)}$$

$$W_G = V_G[X]_G \text{ (Equation 2.9)}$$

Thus, W_0, after equilibration can be written as shown in equation 2.10.

$$W_0 = W_S + W_G \text{ (Equation 2.10)}$$

Substituting equations 2.7-2.9 into equation 2.10, one obtains the material balance as shown in equation 2.11.

$$V_S[X]_0 = (V_S[X]_S) + (V_G[X]_G) \text{ (Equation 2.11)}$$

Substituting $[X]_S = [X]_G Kp$, into equation 2.11 one derives to equation 2.12 in terms of $[X]_G$.

$$[X]_G = \frac{[X]_0}{Kp+\beta} \text{ (Equation 2.12)}$$

The peak area response (PA) for an analyte is directly proportional to the analytes concentration in the gas phase, $[X]_G$ as shown in equation 2.13.

$$PA \propto [X]_G = \frac{[X]_0}{Kp+\beta} \text{ (Equation 2.13)}$$

Equation 2.13 can be re-written to include the instrument response factor (RF) as shown in equation 2.14.[1]

$$PA = \frac{RF[X]_0}{Kp+\beta} \text{ (Equation 2.14)}$$

Equation 2.14 explains the key relationships in equilibrium headspace sampling.[18-20] Various conclusions can be made from equation 2.14. If V_S is increased, there will be a decrease in V_G, thus, β will decrease as of result. The decrease in β, leads to an increase $[X]_G$. If the Kp is decreased by increasing the temperature, this too will increase $[X]_G$. If both Kp and β are consistent between samples and calibration mixtures, then $[X]_G$ and

thus, PA, will be directly proportional to its concentration in the sample prior to analysis. Such conclusions help understand the impact of changing Kp and/ or β on the obtained chromatographic peak area.

2.3.2 Physicochemical Relationships

Within a system the value of the partition coefficient may be manipulated by varying analytical conditions. To understand such interactions further, the relationship between Kp and vapor pressures need to be considered. From here on in we will focus on three basic laws: Dalton's law, Raoult's law and Henry's law.

According to Dalton's law, the total amount of pressure exerted by a gaseous mixture (P_{Total}) is equal to the sum of partial pressures (P_i) of each analyte in the gas mixture.[1] Dalton's law is expressed as shown in equation 2.15.

$$P_{Total} = \Sigma P_i \quad \text{(Equation 2.15)}$$

Therefore, P_i for each individual analyte in the headspace is a fraction of its molecules in the total number of moles as shown in equation 2.16, where X_G is the mole fraction of the analyte in the headspace gas volume. It can be understood, that the concentration of the analyte in the gas phase is proportional to its partial pressure.

$$P_i = P_{Total} X_G \quad \text{(Equation 2.16)}$$

According to Raoult's law, the vapor pressure of a dissolved analyte (i.e P_i) over its solution is directly proportional to its mole fraction in the solution (X_S) as shown in equation 2.17.[1] Although, Raoult's law is only valid for ideal mixtures and in most cases there is a deviation. A factor was introduced to compensate for the deviation known at the activity coefficient (γ) as shown in equation 2.17. The activity coefficient relies on the

nature of the component and reflects the intermolecular interactions between the analyte and the other sample components, specifically the matrix (solvent).

$$P_i = P_{Total}\,\gamma\,X_G \text{ (Equation 2.17)}$$

It is important to note that at higher concentrations the activity coefficient become a function of concentrations while in dilute solutions it is constant and independent of the analyte's concentration. In dilute solutions with concentrations below 0.1%, an analytes molecular interaction will be almost exclusively with other molecules in the sample matrix and not with its self.[1, 16] This effect of making γ and thus, Kp essentially constant over a range of analytical conditions. Under such conditions Henry's law will apply. Henry's law states that in a dilute solution the amount of gas dissolved in a solvent is directly proportional to the partial pressure of that gas at equilibrium with that solvent. This is expressed mathematically in equation 2.18.

$$P_i = H\,X_S \text{ (Equation 2.18)}$$

2.3.3 Effect of Temperature

Partition coefficient and vapor pressures are all functions of temperature.[1, 16] The vapor pressure of an analyte is influenced by its temperature, and the relationship is exponential as seen in equation 2.19:

$$LogKp = \left(\frac{B'}{T}\right) - C' \text{ (Equation 2.19)}$$

where B' and C' are substance-specific constants while T, is the absolute temperature. With an increase in temperature, there is an increase in vapor pressure and the value for Kp will decrease leading to more analyte passing into the headspace phase.

2. References

1. Kolb, B., *Static Headspace-Gas Chromatography : Theory and Practice*. 2nd ed. ed.; John Wiley & Sons, Inc.: Hoboken, 2006.
2. USEPA *Method 5021A: volatile organic compounds by gaschromatography/mass spectrometry (GC/MS)*.
3. USEPA, Closed System Purge and Trap and Extraction for VOlatile Organics in Soil and Waste Samples. In Method 5035A.
4. Varona-Torres, E.; Carlton, D. D.; Hildenbrand, Z. L.; Schug, K. A., Matrix-effect-free determination of BTEX in variable soil compositions using room temperature ionic liquid co-solvents in static headspace gas chromatography mass spectrometry. *Analytica Chimica Acta* **2018**.
5. Varona-Torres, E.; Carlton, D. D.; Payne, B.; Hildenbrand, Z. L.; Schug, K. A., Chapter Twelve - The Characterization of BTEX in Variable Soil Compositions Near Unconventional Oil and Gas Development. In *Advances in Chemical Pollution, Environmental Management and Protection*, Schug, K. A.; Hildenbrand, Z. L., Eds. Elsevier: 2017; Vol. 1, pp 321-351.
6. Moshonas, M. G.; Shaw, P. E., Quantitation of Volatile Constituents in Mandarin Juices and Its Use for Comparison with Orange Juices by Multivariate Analysis. *Journal of Agricultural and Food Chemistry* **1997,** *45* (10), 3968-3972.
7. Frink, L. A.; Armstrong, D. W., Water Determination in Solid Pharmaceutical Products Utilizing Ionic Liquids and Headspace Gas Chromatography. *Journal of Pharmaceutical Sciences* **2016,** *105* (8), 2288-2292.
8. Holm, Y.; Galambosi, B.; Hiltunen, R., Variation of the main terpenes in dragonhead (Dracocephalum moldavica L.) during growth. *Flavour and Fragrance Journal* **1988,** *3* (3), 113-115.
9. Kordrostami, R.; Akhgari, M.; Ameri, M.; Ghadipasha, M.; Aghakhani, K., Forensic toxicology analysis of self-poisoning suicidal deaths in Tehran, Iran; trends between 2011-2015. *DARU Journal of Pharmaceutical Sciences* **2017,** *25* (1), 15.
10. Ezquerro, Ó.; Ortiz, G.; Pons, B.; Tena, M. a. T., Determination of benzene, toluene, ethylbenzene and xylenes in soils by multiple headspace solid-phase microextraction. *Journal of Chromatography A* **2004,** *1035* (1), 17-22.
11. Llompart, M.; Li, K.; Fingas, M., Headspace solid phase microextraction (HSSPME) for the determination of volatile and semivolatile pollutants in soils. *Talanta* **1999,** *48* (2), 451-459.
12. W.H. Stahl, W. A. V., J.H.Sullivan, A gas chromatographic method for determining gases in the headspace of cans and flexible packages. *Food Technol* **1960,** *14*, 14-16.
13. Ettre, L. S. The Beginnings of Headspace Analysis *LCGC North America* [Online], 2002.
14. R.N.Harger, E. G. B., B.B. Raney, *J. Biol. Chem* **1939,** *128*.
15. Symposium on Gas, C.; Desty, D. H.; Institute of, P.; Gas Chromatography Discussion, G. In *Gas chromatography, 1958; proceedings of the second symposium organized by the Gas Chromatography Discussion Group under the auspices of the Hydrocarbon Research Group of the Institute of Petroleum and the Koninklijke Nederlandse Chemische Vereniging held at the Royal Tropical Institute, Amsterdam, 19-23 May 1958*, New York, 1958; Academic Press: New York.
16. Tipler, A., An Introduction to Headspace Sampling in Gas Chromatography PerkinElmer, Ed. 2013. www.perkinelmer.com.

17. Head Space Sampler HS-20 Instruction Manual Shimadzu, Ed. 2013.
18. Ettre, L. S.; Welter, C.; Kolb, B., Determination of gas-liquid partition coefficients by automatic equilibrium headspace-gas chromatography utilizing the phase ratio variation method. *Chromatographia* **1993,** *35* (1), 73-84.
19. Kolb, B.; Welter, C.; Bichler, C., Determination of partition coefficients by automatic equilibrium headspace gas chromatography by vapor phase calibration. *Chromatographia* **1992,** *34* (5), 235-240.
20. Voice, T. C.; Kolb, B., Static and dynamic headspace analysis of volatile organic compounds in soils. *Environmental Science & Technology* **1993,** *27* (4), 709-713.

Chapter 3: The Characterization of BTEX in Variable Soil Compositions Near Unconventional Oil and Gas Development[55]

3.1 Introduction

As fossil fuel extraction development continues to increase in the United States and in other countries, it is expected to become more com- mon near residential and urban areas. This has increased the public's concern about the possible health and environmental implications associated with such industrial activities. As with any form of energy extraction, there is potential for: release of pollutants into the air, groundwater, and soil; development of physical and public safety hazards; and propagation of other psychosocial stressors. One relatively new form of fossil fuel extraction, known as unconventional oil and gas development (UD), has rapidly expanded across numerous international petroliferous basins, where oil and natural gas are extracted from shale and other previously unproductive low permeability strata. The potential risks associated with UD, and more specifically those associated with hydraulic fracturing, shale acidization, and horizontal drilling, are far more complex than those associated with conventional hydrocarbon development due to the scale and elaborate nature of the UD process.[1,2]

Various research groups have undertaken the task of evaluating the potential impacts that UD can have on the environment. Groundwater quality has been the most extensively studied, revealing methane[3] and stray thermogenic natural gas in groundwater near UD activities[4,5] and the natural occurrence of dissolved gases in areas away from active drilling.[6–8] Similarly, contamination of groundwater with inorganic metals and salts has been attributed to surface spills[9,10] and the transport of fluids through microscale fissures in UD gas wells.[11] More recent investigations have also found the presence of numerous alcohols, chlorinated compounds, BTEX (benzene, toluene, ethylbenzene, and

xylenes),[12,13] and aldehydes[14] in groundwater in the Barnett, Cline, and Eagle Ford shale formations in Texas. Moreover, Gross et al. investigated the potential impacts of surface spills on groundwater, discovering BTEX concentrations that exceeded the National Drinking Water maximum contaminant levels.[15]

A majority of the atmospheric studies performed near UD have focused primarily on the qualification and quantification of methane emissions.[16–19] For example, in the Bakken and Marcellus shale regions, methane emissions were detected from nonsputtering flares and unidentified venting practices.[20] In the Barnett shale region of northern Texas, numerous point sources have been identified as latent contributors to the emission of volatile organic compounds (VOCs). These include, with varying regularity and intensity, compressor units, engine exhausts, and condensate and oil tanks, in addition to production, well drilling, hydraulic fracturing, well completion, natural gas processing, and transmission lines.[21] Recent investigations in the Barnett and Eagle Ford shale regions detected notable emissions of VOCs, more specifically, aromatic compounds.[22,23] Ambient detections of benzene and toluene near UD gas flares, condensate tanks, compressor units, and hydrogen sulfide (H_2S) scavenger units were found to be as high as 1 and 5 ppm, respectively.[23] Hildenbrand and colleagues traveled along state highways and local country roads surrounded by producing UD oil wells and detected benzene and toluene levels up to 500 ppb and 2 ppm, respectively, using a mobile mass spectrometry system.[23]

Much less investigated are the possible environmental impacts that UD can have on soil quality. In conference proceedings in 1998, Zielinski and Otton presented a radiometric assessment of soils contacted by produced water.[24] They used ^{228}Ra–^{228}Th

disequilibrium to detect the age of contamination in soils and sediments near ponds storing produced water.[24] The ability to verify the age and source of contamination is imperative for linking contamination directly to oil and gas operations.[25] More so, distinguishing recent contamination related to hydraulic fracturing from older contamination related to conventional oil and gas operations is particularly important in petroliferous basins with both conventional and unconventional activities.[25] More recently, Lauer and Vengosh reported the use of isotopic dating methods to estimate the time since the accumulation of radium in impacted soil and sediments from UD wastewater spills.[25]

To our knowledge there is a lack of literature pertaining to VOCs contamination, such as BTEX, in soils related to UD activities. This may be due in part to the short-range variability in soils contaminated with VOCs. The natural variability of soil properties affects the spatial susceptibility of VOCs in the field and is worsened by the multiphase nature of VOCs.[26,27] In a study conducted at Superfund sites in Kent, Washington and Portland, Oregon, Schumacher and Minnich encountered significant variability in soil properties related to soil texture with concentrations of VOCs varying over distances as little as 15 cm.[26]

Soils can become contaminated with BTEX by an UD-related surface spill, or in the case of the work presented here, by the accumulation of atmospheric contaminants from emissions sources. BTEX compounds are natural constituents of crude petroleum and are also associated with hydraulic fracturing because they are common solvents used in fracking fluid, particularly when petroliferous strata are stimulated with diesel fuel.[28] BTEX is of particular concern due to the chronic toxicity associated with their aromatic ring structure and their solubility in water and other media.

Soil is a complex medium. It is a highly variable but nonrandom matrix of mineral and organic particles of various sizes that contains its own biological community and which, as a system, interacts with the surrounding ecological context. Consequently, the quantification of BTEX in soil poses a challenge. A convenient and functionally important descriptor of soils is soil texture, which parameterizes the sizes of particles that make up a soil in terms of the percentage of sand, silt, or clay. A soil texture triangle adapted for the samples collected in this study is illustrated figure 3.1. The triangle categorizes the soil depending on the proportions of sand, silt, and clay. Sand can differ in composition but usually is in the form of quartz (SiO_2) or calcite ($CaCO_3$).[30] The effective diameter of sand particles range from 0.05 to 2.0 mm.[30] The composition of silt can differ, quartz or feldspar ($KAlSi_3O_8$–$NaAlSi_3O_8$– $CaAl_2Si_2O_8$) being common.[30] Silt particles are typically granular, with a particle size from 0.002 to 0.05 mm, between sand and clay.[30] Clays are often composed of layered aluminosilicate minerals such as kaolins, micas, vermiculites, and montmorillonites.[30] Clays are the smallest particle size class, comprised of particles with effective diameters 0.002 mm or smaller.[30] Effective characterization of the texture of soil provides a basis for understanding soil sorption and interaction chemistry for BTEX.

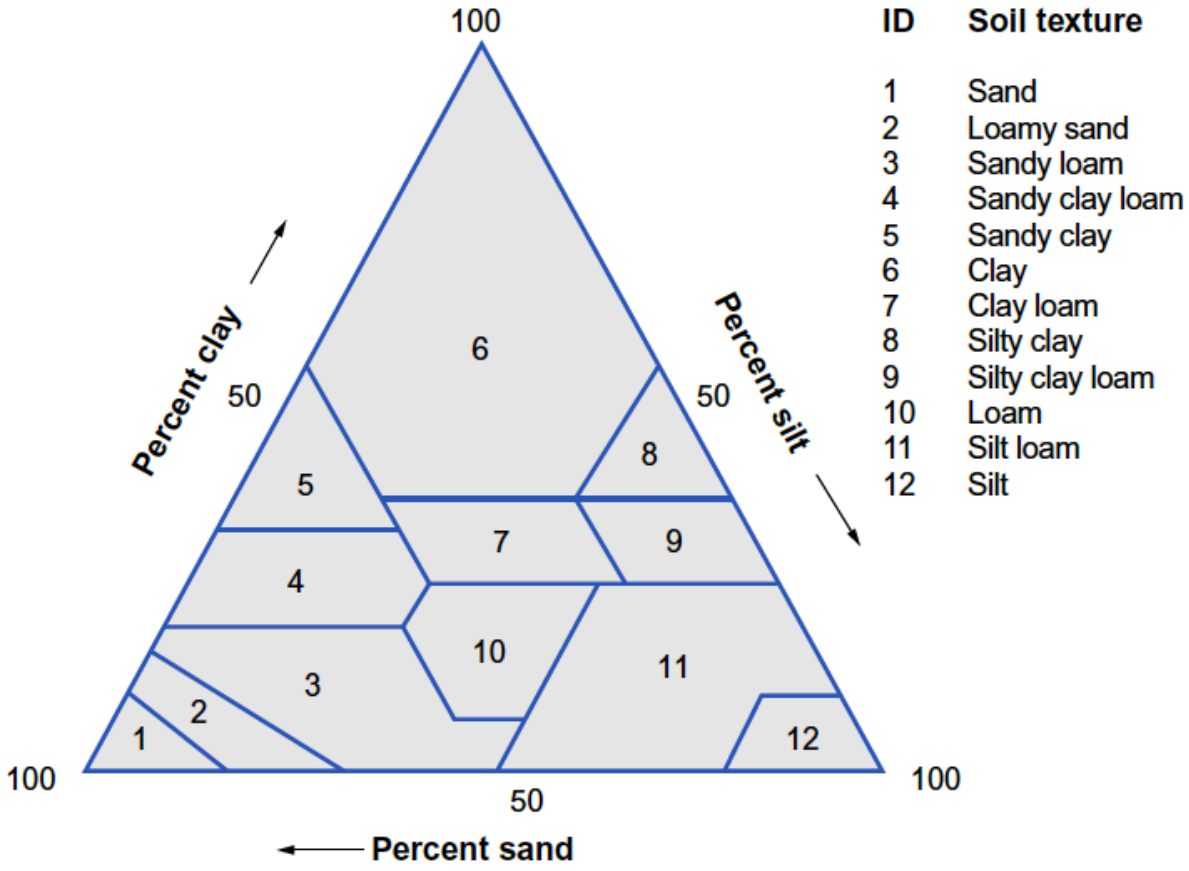

Figure 3.1. Soil texture is classified by the percent sand, silt, and clay in relation to the soil triangle.[29] (1) Sand, (2) loamy sand, (3) sandy loam, (9) silty clay loam, and (10) loam were all the varying soil textures obtained in this study.

In addition to soil texture (particle size distribution), the sorption of BTEX is affected by the abundance of organic carbon in the soil.[31] Nonpolar organic compounds such as BTEX have very high K_{OW} values. Commonly denoted K_{OW}, the octanol–water partition coefficient, is the ratio of the concentration of a chemical in the octanol phase relative to the concentration of the chemical in the water phase in a laboratory extraction procedure. High K_{OW} values indicate stronger attraction to soil organic matter than to mineral particles

or water. Soils with high organic matter can sorb and limit the potential migration of BTEX, including volatilization or extraction in analytical procedures. Consequently, soil texture/particle size and organic carbon context complicate and must be considered in attempts to quantify BTEX.[26.31]

The sorption of BTEX on clay, sand, and organic matter has been investigated.[32,33] In adsorption experiments, BTEX was observed to reach equilibrium faster in sand than in clay.[33] This was due to the higher bulk porosity and permeability of sand compared to clay.[32–34] Clay absorbed more BTEX than sand, suggesting that clay is a more potent sorbent for BTEX, presumably because of its larger surface area. In desorption experiments, BTEX was observed to reach equilibrium faster in sand than in clay; however, the desorption process was slow for both sediment textures. Collectively, these data indicate that organic chemicals are slowly released regardless of soil texture.[33,34] BTEX, like other organic compounds, has a strong tendency to bind with organic carbon, mineral surfaces, and within micropores and sub- micropores, which are most common in clays.[34,35] Therefore, slow desorption can be attributed to the absorptive effects of organic matter and hindered pore diffusion mechanisms.[33] In summary, soil texture can explain some of the variabilities as well as provides a means of accounting for the sorption and measurement of BTEX in soils.

The same soil properties and mechanisms complicate the remediation of contaminated soil. There are a variety of common approaches for remediation of VOCs in soil. Bioremediation usually involves supplementing natural, in situ microbial communities to increase microbial decay.[36–38] Soil vapor extraction (SVE) is another in situ approach, which utilizes vacuums inserted into the soil with the goal of creating a negative pressure

gradient that causes the desorption of VOCs.[39] Air sparging is generally used in conjunction with SVE and involves the injection of air into the soil to cause desorption of the VOCs from solids.[40] In 1994, Zytner reported the sorption of BTEX using various media: activated carbon (AC), peat moss, organic top soil, clay soil, and sandy loam soil.[41] Zytner discovered that both the sorption and retention potentials of BTEX increased with an increase in organic carbon content, with AC having the highest sorption preference for BTEX followed by peat moss, organic top soil, clay soil, and sandy loam soil, respectively.[41] He also demonstrated the order of preferential sorption on a component basis, consistent with the Log K_{OW} trend among toluene (2.73), xylenes (3.15–3.20), ethylbenzene (3.15), and benzene (2.13), respectively.[41–44] More recent literature demonstrates the use of AC for the remediation of various compounds and media. Denyes et al. performed an in situ application of AC on polychlorinated biphenyls contaminated soils.[45] Liang and Chen evaluated AC for remediating benzene contamination.[46] Additionally, Wan et al. found that coupling AC with biosurfactant- enhanced soil washing is a possible alternative to remove hydrophobic organic compounds from soil.[47] Collectively, these different remediation modalities show promise for extracting and sequestering BTEX and other hydrophobic organic compounds from soil.

In this chapter, we explore the relationship between BTEX emissions from production sites and BTEX detection in soil. During an 11-month time series analysis (June 2015–April 2016), soil samples were collected from contiguous cattle ranches in the Eagle Ford shale region of southern Texas, USA. The study area included 8 production sites with a total of 28 horizontal UD oil wells, and 7 putative sources of atmospheric BTEX contamination. We also evaluated the effectiveness of treating BTEX-contaminated soil

with AC.

3.2 Materials and Methods

3.2.1 Air Quality Analysis

In situ full mass scans from 0 to 200 *m*/*z* were performed of air on individual UD extraction sites (pads) with producing UD wells using a mobile mass spectrometer (MS) as described previously.[23,48] Briefly, the MS and residual gas analyzer were configured into an electric hybrid vehicle. Atmosphere is introduced into the system through a glass aperture that provides an inlet through which a diaphragm pump continuously pumps air.[48] Utilizing an atmospheric sampling tube, a smaller diaphragm pump allows a small quantity of air to pass through the tubular membrane inlet to the MS. The system repeatedly scans masses and tags each scan with associated latitude and longitude coordinates using a Python script and an Arduino-based microcontroller with global positioning system (GPS) capabilities. The postprocessing of data utilizes Google Earth to plot the acquired intensities for a given mass, which are represented by concentration-based colored circles on a map. Concentration determination is performed in conjunction with a Flexstream (KIN-TEK, Texas, USA) gas standards generator. The National Oceanic and Atmospheric Agency (NOAA) and the Environmental Protection Agency's Areal Locations of Hazardous Atmospheres (ALOHA) software were used in conjunction with local weather data to provide a theoretical interpretation of effluent plume diffusion, which enabled the rendering of heat map concentration gradients.

3.2.2 Soil Sampling

66 and 70 soils samples were collected during rounds 1 and 2–4, respectively, from a large ranching area in the Eagle Ford shale region of southern Texas as shown in figure

3.2. Core samples were collected using an AMS core sampler with slide hammer, a 2” X 6”-coring bit with AMS butyrate plastic replacement liners, and plastic end caps (Ben Meadows Company, Janesville, WI). GPS coordinates were used to mark location of the samples. Samples collected were wrapped in aluminum foil, transported on ice, and kept refrigerated/frozen until time of analysis to avoid loss of VOCs to volatilization or photodegradation. Soil texture was determined using a sedimentation rate method adapted from Bowman and Hutka.[49] Five different soil textures were found as shown in table 3.1. Slight adjustments to sampling locations changed from round 1 to 2–4, giving rise to the drastic change in soil composition populations. Sampling locations within the pad in round 1 were moved to the perimeter of the pad in rounds 2–4.

Figure 3.2. Sampling locations (gray dots) in relation to UD production sites (tan rectangles), and BTEX emission sources (red flame icons) in the study. The prevailing wind originates from the southeastern direction.

Table 3.1. Variable soils textures collected across sampling rounds 1-4.

Soil Classification	Round 1	Round 2–4
Sand	45	13
Loamy sand	6	27
Sandy loam	7	19
Loam	3	4
Silty clay loam	5	7

3.2.3 Remediation Plots

Replicate plots with 4, 10'x10' quadrants were established in areas near atmospheric contamination sources and where BTEX contaminants had been detected in soil previously. Samples were collected in triplicate from each quadrant, a total of 12 core samples per plot in March and again in April of 2016, before any treatment and after a 1-month incubation with the various conditions, respectively. The four experimental conditions in each plot corresponded to: (1) untreated and undisrupted soil (control), (2) disrupted soil where the top 6" of surface soil was perturbed by manual agitation with a hoe and pic axe, (3) undisrupted soil treated with a surface application of powdered activated carbon (PAC), and (4) disrupted soil treated with a surface application of PAC. Where used, the PAC was spread at a density of 0.1 lbs/sq. ft. (10 lbs/quadrant). The NORIT® SOILPURE (Cabot Corp; Marshall, TX) was utilized for its high adsorptive capacity and stated specificity to remove phenols and aromatic compounds.

3.2.4 Chemicals

Stock solutions were prepared in LC-MS grade analytical methanol (J.T. Baker; Phillipsburg, NJ) from a 2000-µg mL^{-1} BTEX calibration standard (Phenomenex Inc.;

Torrance, CA) and Fluorobenzene (≥99.7%) (Sigma Aldrich; St. Louis, MO), which was used as an internal standard (IS). Dilutions in methanol of 0.5–10 ng g^{-1} with 50 ng g^{-1} of IS were used for calibration. To reduce losses by volatilization, the BTEX solutions were stored at 4°C in sealed vials without free headspace [2], since BTEX can readily migrate from aqueous solution to the HS. Furthermore, fresh solutions were prepared on a weekly basis.

3.2.5 BTEX Analysis

The 6" core sleeve was cut open using a variable speed rotary tool. Any soil contacting the butyrate plastic was shaved off using a stainless-steel spatula to avoid contamination coming from the core sleeve. The stainless-steel spatula was rinsed with methanol followed by a rinse with 18.23MΩ purified water to avoid cross contamination between core samples. Aliquot samples were obtained from three 2" sequential depth sections of the 6-core sleeve. The sampling spatula was rinsed with methanol followed by 18.23MΩ purified water between aliquot sections to avoid cross contamination. The extraction of BTEX from soil samples was carried out following the EPA 5021A method, which recommended a triplicate set of 2g of soil in 10mL of water in a sealed 20-mL HS glass vial.[50] Each sample was matched with its corresponding soil texture calibration curve, to improve quantitation of the compounds of interest. A matrix sample used for the calibration curve was first dried under vacuum at approximately 120°C for 3 days to remove any organic trace and humidity.[51]

3.2.6 Instrumentation and Parameters

Various analytical methods for the determination of BTEX in environmental samples are based on gas chromatography mass spectrometry (GC-MS), using either

static or dynamic headspace [2], or HS solid-phase microextraction (HS-SPME) as sample introduction modules. Some other techniques, like liquid chromatography or near infrared, have also been used.[51–53] HS sampling has been used successfully in qualitative analysis of VOCs in soils. Difficulties arise when using HS methods for quantitative analysis of VOCs in soil because methods rely on equilibrium partitioning of the analyte of interest between the soil sample and the gas phase in the vial. In order to mitigate some of the soil matrix effects discussed previously, the EPA has a standardized method (EPA 5021A) that utilizes water as a HS solvent. This creates a hydrophilic environment, which is less favorable to BTEX, but which aids in homogenizing the sample medium in the HS vial.[50] When heated, the BTEX in the water/soil mixture reaches equilibrium faster with the HS than would be possible with an untreated soil. This method was chosen due to its relatively simple sample preparation protocol.

HS sampling was performed with an AOC-5000 Plus (Shimadzu Scientific Instruments, Inc., Columbia, MD) autosampler unit. Samples were incubated and agitated at 85.0°C for 50 min per EPA Method 5021A. A 2.5-mL HS syringe was utilized to sample 750µL with an injection speed of 500µL/s. A GC MS-TQ8040 (Shimadzu Scientific Instruments; Columbia, MD) gas chromatograph coupled to a triple quadrupole mass spectrometer was equipped with a Zebron ZB-WAXplus (30m x 0.25mm x 0.2µm) (Phenomenex, Inc., Torrance, CA) capillary column to carry out the separation and analysis following sample injection. The ZB-WAXplus polyethylene glycol stationary phase allowed for complete separation of all three xylene isomers, a separation not typically achieved in regulatory or standard methods. The injection port temperature was 200°C, and a 10:1 split ratio was set. The carrier gas was helium with a linear velocity of 50cm/s. The column oven

temperature program began with an initial temperature of 35°C for 4min, and then temperature was increased at a rate of 20°C/ min up to 240°C, and held for 4.75 min. The run time was 19min. The ion source was operated in the electron ionization mode (EI; 70 eV, 230°C). Full scan mass spectra (m/z 50–300), as well as optimized multiple reaction monitoring precursor-to-product ion transitions were recorded for the identification and determination of analytes as seen in table 3.2.

Table 3.2. MS-MRM parameters.

Compound Name	Start Time (min)	End Time (min)	Event Time (sec)	Channel 1 *m/z*	Channel 1 CE	Channel 2 *m/z*	Channel 2 CE
Benzene	2.00	3.60	0.050	78.00 > 52.10	16	78.00 > 63.10	22
Fluorobenzene	2.00	3.60	0.050	96.00 > 70.10	14	96.00 > 63.10	22
Toluene	3.60	5.00	0.050	91.00 > 65.10	14	92.00 > 65.10	24
Ethylbenzene/ *o*-Xylene	5.00	6.75	0.050	106.00 > 91.1	12	91.00 > 65.10	14
p-Xylene/ *m*-Xylene	5.00	6.75	0.050	106.00 > 91.2	14	91.00 > 65.11	14
Scan (q3 scan)	1.10	19.00	0.200				

3.2.7 Statistical Analysis

Nonparametric statistical analyses comparing two or more unpaired groups were performed using two-tailed Mann–Whitney and Kruskal–Wallis tests, respectively, in the GraphPad Prism Software suite.[54] Correlative analyses were also performed in Prism using the Spearman rank analysis. These data are not appropriate for multivariate ordination analyses, such as principal component analysis, because of the multiple

different scales and measurement techniques, as well as the uneven and somewhat small sample sizes, which would have made it difficult to detect multivariate differences.

3.2.8 Limitations in Data for Interpretation

The initial set of in situ air quality measurements were collected during round 1 in accordance with the rights afforded to the participating mineral rights lessors. However, due to discordance between the mineral rights lessors and the oil and gas operator at the time, opportunities for sampling during rounds 2–4, such as collecting additional soil samples from the extraction/production sites (pads), were restricted. Production data from the area UD wells were also not available. However, production began in 2010–2014 and it is well established that Eagle Ford shale wells experience a significant production decline (>50% reduction compared to initial output) within the first 20 months.[55] Given that these UD wells were not re-stimulated during the course of this surveillance effort (June 2015–April 2016), one might anticipate that the rates of BTEX emissions from the identified point sources would decline over time if no new mechanical or operational deficiencies were to arise. Other limitations of this study included the inabilities to monitor potential emissions sources from neighboring production sites and other anthropogenic sources of BTEX emissions (i.e., vehicles and motorized farming equipment).

3.3 Results and Discussion

3.3.1 Characterizing Atmospheric Contamination

The basic anatomy of the UD production sites (pads) in our study area was fairly consistent. The standard features include natural gas flaring stations, condensate tanks, compressor units, wellheads, heater-treaters, H2S scavengers, and additional auxiliary machinery. By quantifying ambient BTEX, we discovered that BTEX emissions were

highly variable across individual sites.[23] Heat map renderings were generated to illustrate the distribution of the atmospheric concentrations on each site to identify individual emission sources as shown in figures 3.3-3.6. These renderings take into account the distance between points and the number of points in an area, and prevent interpretation of an area as “hotter” (red) due to collection of more data in that area compared to neighbors. On the first pad site, elevated BTEX could be attributed to the gas flaring station and H2S scavenger on the south side of the site and condensate tanks and compressor unit located on the north side as seen in figure 3.3. Similarly, ambient BTEX detected on three other pad sites was associated with two flaring stations (pads 2 and 4), condensate tanks (pad 2), and a compressor unit (pad 3) as seen in figures 3.4 and 3.5. However, an analysis of pad 5 revealed very limited BTEX attributable to any of these processes, and a H2S scavenger was identified as the primary contributing source on pad 6 shown in figure 3.6. In total, seven-point sources were identified as BTEX emitters and were the subjects for the geospatial analyses described later in section 3.3.3.

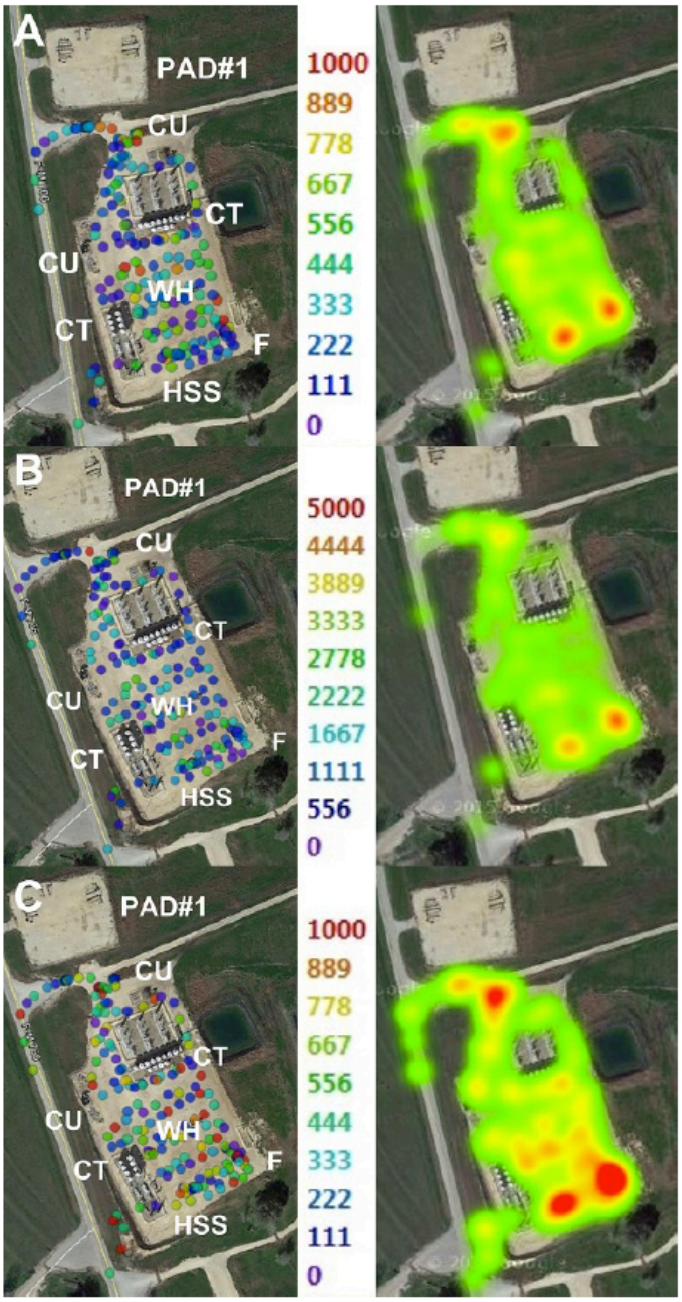

Figure 3.3. Ambient (A) benzene, (B) toluene, and (C) total xylene isomer concentrations and around pad site #1 in the study area. The components under investigation include wellheads (WH) condensate tanks (CT) compressor units [3] H_2S scavenger (HSS), and the gas flaring station (F). Individual measurements are represented in parts-per-billion. Reprinted with permission from (Hildenbrand ZL, Mach PM, McBride EM, Dorreyatim MN,

Taylor JT, Carlton DD, et al. Point source attribution of ambient contamination events near unconventional oil and gas development. Sci Total Environ 2016;573:382–8).[23]

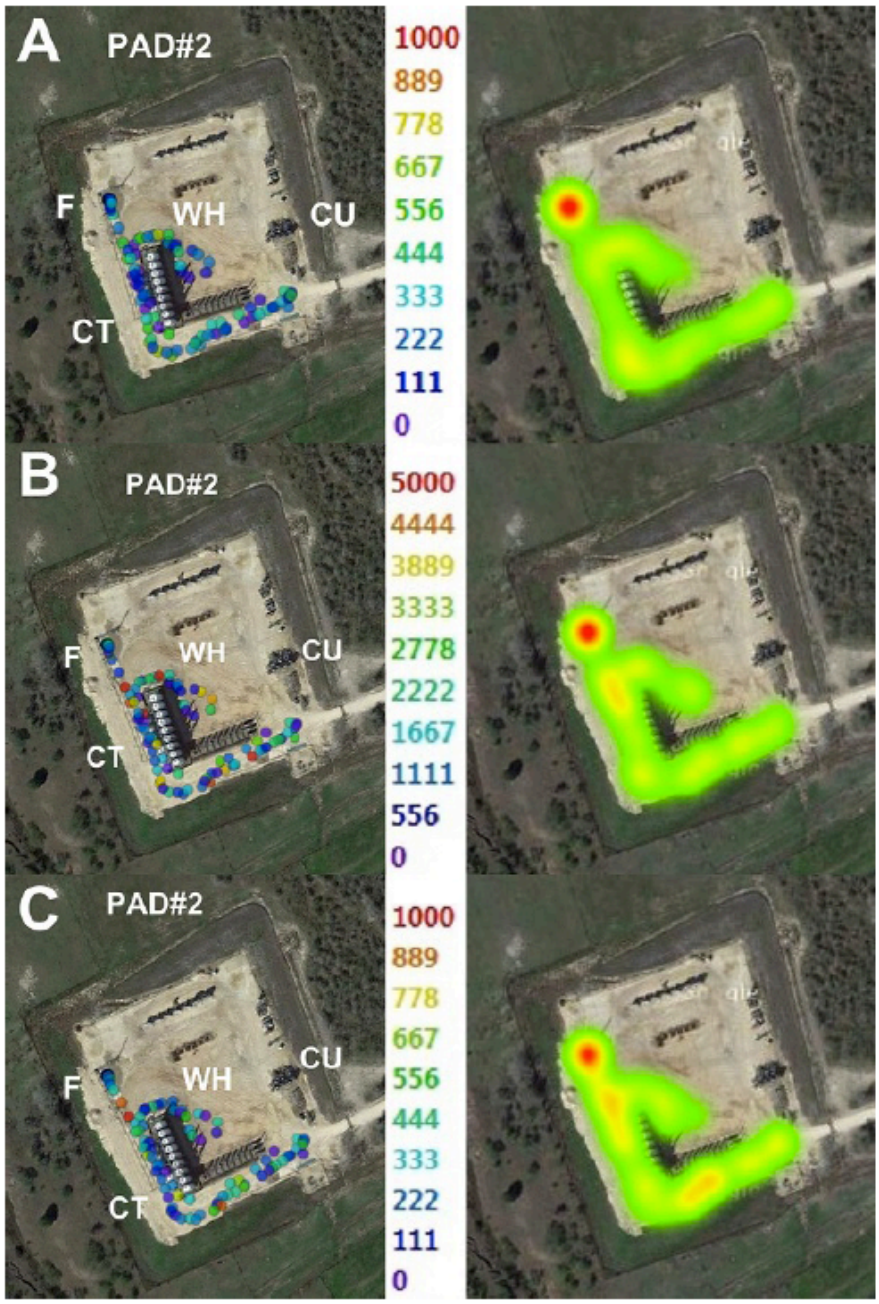

Figure 3.4. Ambient (A) benzene, (B) toluene, and (C) total xylene isomer concentrations and around pad site #2 in the study area. The components under investigation include wellheads (WH) condensate tanks (CT) compressor units [3] H_2S scavenger (HSS), and

the gas flaring station (F). Individual measurements are represented in parts-per-billion. Reprinted with permission from (Hildenbrand ZL, Mach PM, McBride EM, Dorreyatim MN, Taylor JT, Carlton DD, et al. Point source attribution of ambient contamination events near unconventional oil and gas development. Sci Total Environ 2016;573:382–8).[23]

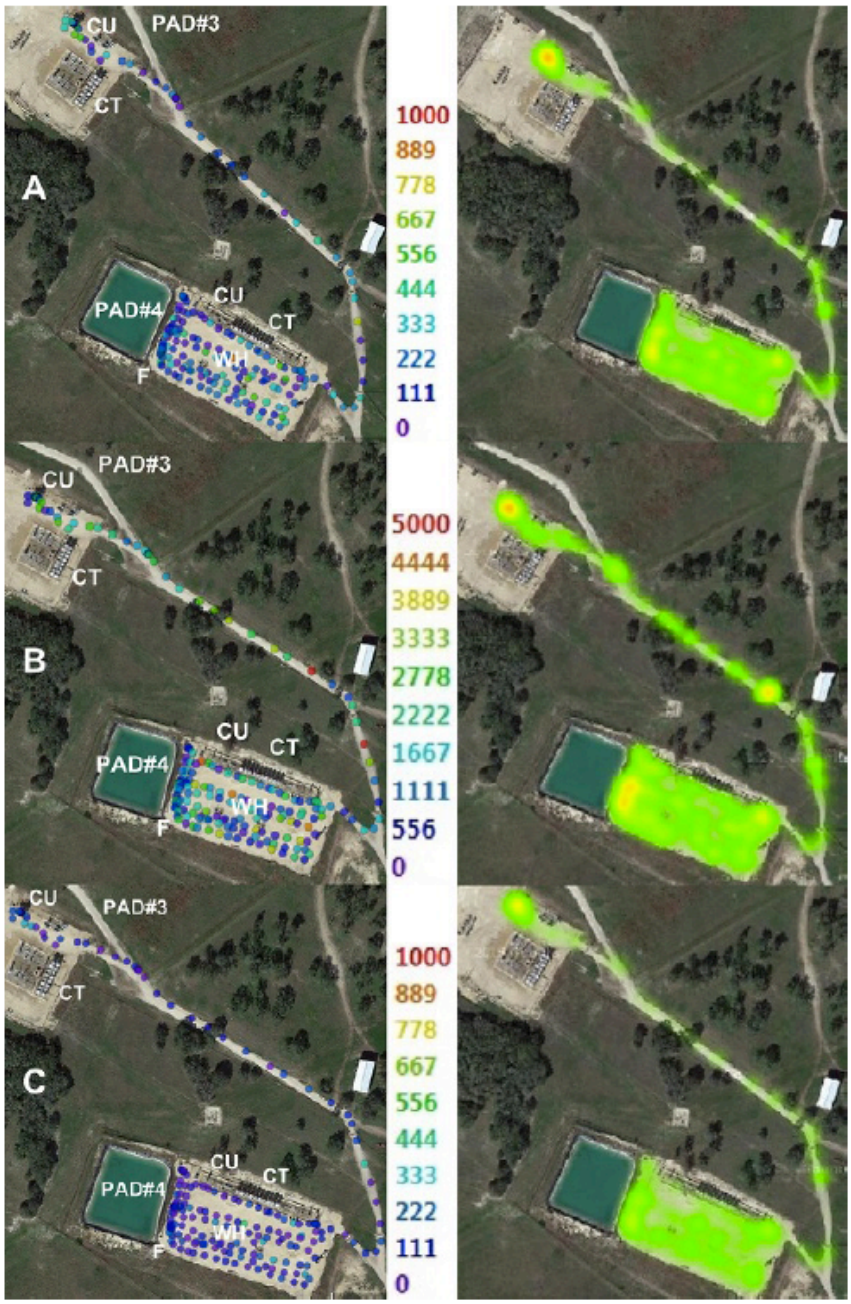

Figure 3.5. Ambient (A) benzene, (B) toluene, and (C) total xylene isomer concentrations

and around pad site #3 and #4 in the study area. The components under investigation include wellheads (WH) condensate tanks (CT) compressor units [3] H_2S scavenger (HSS), and the gas flaring station (F). Individual measurements are represented in parts-per-billion. Reprinted with permission from (Hildenbrand ZL, Mach PM, McBride EM, Dorreyatim MN, Taylor JT, Carlton DD, et al. Point source attribution of ambient contamination events near unconventional oil and gas development. Sci Total Environ 2016;573:382–8).[23]

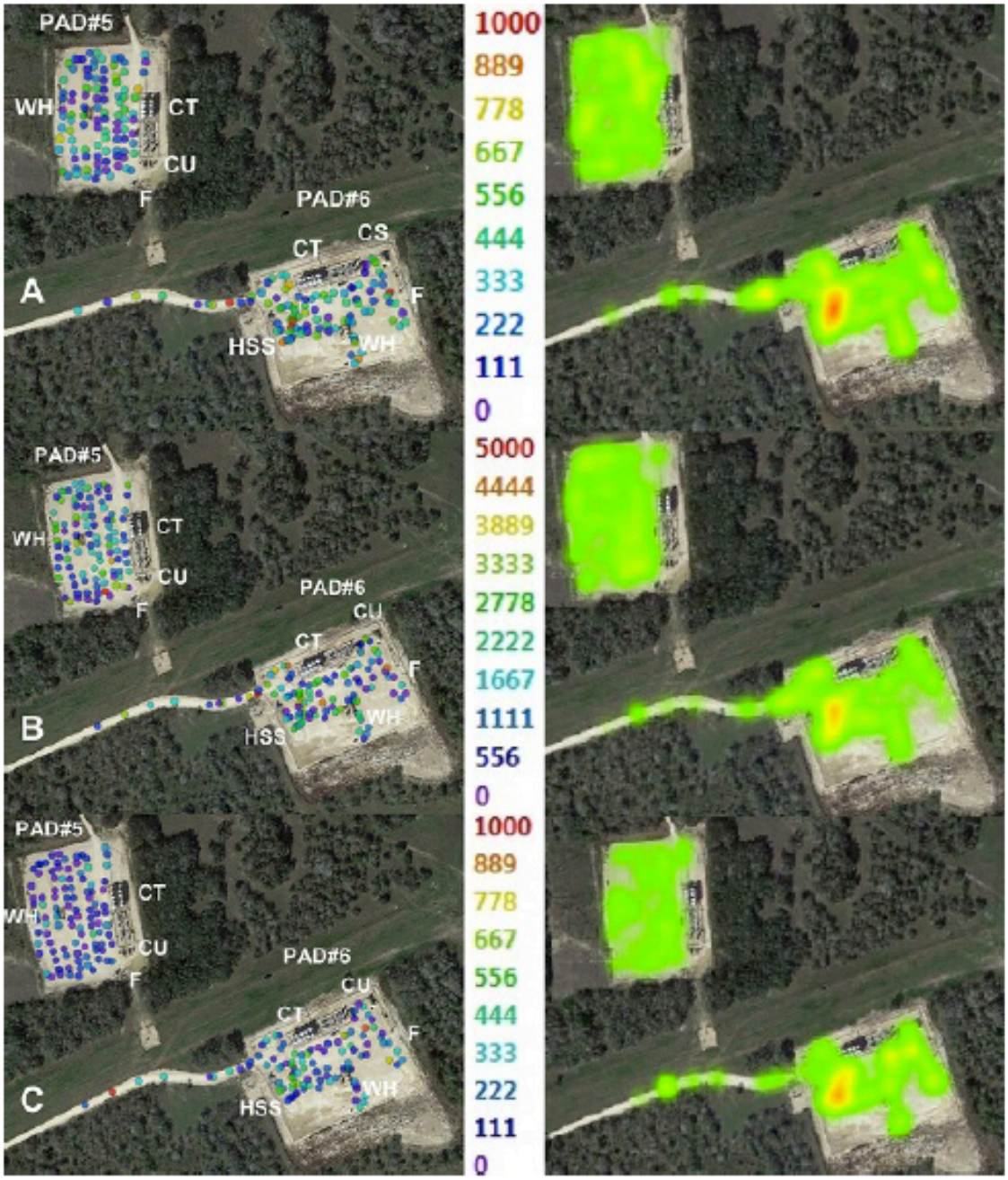

Figure 3.6. Ambient (A) benzene, (B) toluene, and (C) total xylene isomer concentrations and around pad site #5 in the study area. The components under investigation include wellheads (WH) condensate tanks (CT) compressor units [3] H_2S scavenger (HSS), and the gas flaring station (F). Individual measurements are represented in parts-per-billion. Reprinted with permission from (Hildenbrand ZL, Mach PM, McBride EM, Dorreyatim MN, Taylor

JT, Carlton DD, et al. Point source attribution of ambient contamination events near unconventional oil and gas development. Sci Total Environ 2016;573:382–8).[23]

3.3.2 Time Series Soil Analyses

Soil samples were collected on a quarterly basis starting in June of 2015 to assess soil BTEX concentrations over time. The R^2 values were greater than 0.99 for each BTEX constituent in each of the five soil matrices shown in table 3.3. Mean total BTEX concentrations varied from 0.64ppb (round 4) to 1.85ppb (round 2); however, the collective variation across the four rounds of sampling was not statistically significant (P= 0.13) shown in figure 3.7. Interround comparisons revealed that round 4 total BTEX concentrations were significantly lower than those observed in round 1 (0.64ppb mean vs 1.49ppbmean, P= 0.015) see figure 7A. This may be explained by the fact that the sampling sites were significantly closer to emission sources in round 1 compared to round 4 (276.4m mean vs 398.0m mean, P= 0.025). However, as will be discussed later in this text, geospatial metrics such as distance to the nearest emissions source and the number of emission sources within a 100- and 500-m radii of a given sampling site did not correlate with BTEX concentrations as shown in figure 3.8.

Table 3.3. R^2 values obtained from the calibration curves of each of the compound in the different soil matrices.

Compound	Sand (R^2)	Sandy Loam (R^2)	Loamy Sand (R^2)	Loam (R^2)	Silty Clay Loam (R^2)
Benzene	0.996	0.992	0.997	0.994	0.993
Toluene	0.998	0.991	0.995	0.995	0.993
Ethylbenzene	0.997	0.993	0.995	0.997	0.997
p-Xylene	0.996	0.995	0.996	0.995	0.998
m-Xylene	0.995	0.995	0.992	0.996	0.996
o-Xylene	0.997	0.992	0.993	0.996	0.997

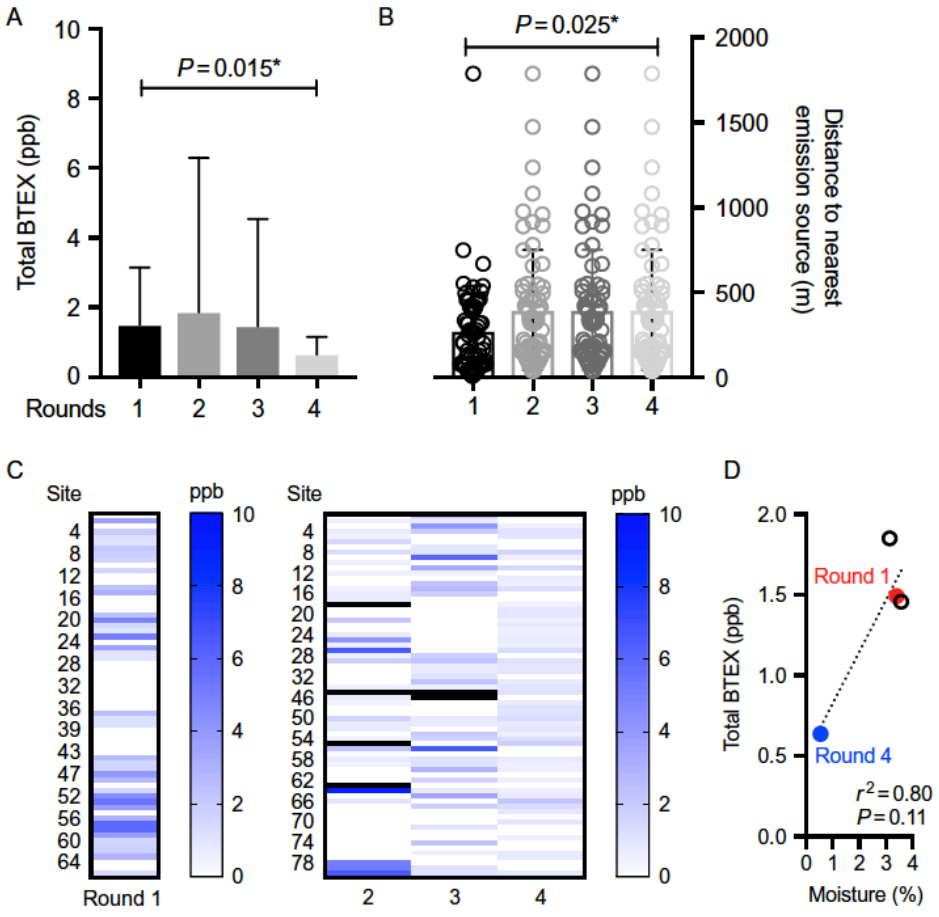

Figure 3.7. Total soil BTEX concentrations detected in rounds 1–4 as visualized cumulatively (A), with distances of the sampling sites to the nearest emissions source

illustrated across rounds 1–4 (B). Total soil BTEX concentrations detected in rounds 1–4 as visualized heat map renderings of individual sampling sites (C). Total BTEX concentrations (mean values) in relation to % moisture content (mean values) across rounds 1–4 (D). Statistically significant interround differences are denoted by an asterisk (*) when $P<0.05$. The error bars in the bar graphs represent the standard deviation.

The frequency of BTEX detections was also fairly consistent, with 58%, 53%, 54%, and 70% of the collected samples (rounds 1–4, respectively) testing positive for at least one of the BTEX constituents shown in figure 7C. Interestingly, round 4 displayed the highest frequency of total BTEX detections, yet exhibited the lowest maximum concentration (2.23 ppb) compared to the other rounds. The round 2 samples included the highest total BTEX detection (sample 45, 27.1 ppb) and cumulative BTEX signal (129.6 ppb). Sample 45 is of particular interest given that it exhibited the highest total BTEX levels in both rounds 2 and 3 (27.1 and 20.3 ppb, respectively), with a sharp decline to 1.09ppb observed in round 4, which is consistent with the general trend across the dataset.

Benzene was the most commonly detected soil contaminant in round 1(23/66 samples), whereas xylenes (24/70), toluene (35/70), and ethylbenzene (44/70) were the primary contaminants detected in rounds 2–4, respectively. It is plausible that either the composition of the emissions from the identified point sources varied over the time course of this investigation, and/or alterations in the structure of the soil microbiome occurred over time, which modulated the variable degradation of the individual BTEX constituents over time. Our investigation provided no data with respect to how soil microbes affected

BTEX contaminants over time. The rate of microbial degradation of BTEX and other hydrocarbons is influenced by various factors, such as contaminants present, temperature, oxygen availability, nutrient availability, pH, availability of the contaminants to the microbes, concentration of the contaminants, and the presence of substances toxic to the microbiome.[56] Furthermore, the availability of contaminants to microbes in soil is dependent on soil type. For example, clay-like soils will adsorb BTEX, making them less available for microbial degradation. If the concentration of BTEX present in soil is too high, it may also create a toxic environment in the microbiome, thus affecting microbial degradation.[56]

The variability observed throughout the time course may have also been attributed to meteorological conditions as shown in table 3.4. The increasing temperature in the 3 months prior to round 1 correlates with the seasonal changes, going from spring into the summer months. In the sampling month (June 2015), the average high temperature was approximately 92.0°F with an average low of 72.0°F and total precipitation of 3.40in. The average percent moisture content of the core samples collected was 3.40%. The higher temperature in the 2 months prior to round 2 correlates with what is expected in the summer months. In the sampling month of round 2 (September 2015), the average high temperature was approximately 93.7°F, with an average low of 68.5°F and total precipitation of 2.39in. The average percent moisture content of the core samples collected was 3.14%. The decreasing temperature in the 3 months prior to round 3 correlates with seasonal changes, going from fall into the winter months. In the sampling month of round 3 (January 2016), the average high temperature was approximately 64.5°F, with an average low of 37.0°F, and total precipitation of 2.01in. The average

percent moisture content of the core samples collected was 3.57%. The slight temperature increase between rounds 3 and 4 corresponds to the seasonal changes of entering into spring. In the sampling month of round 4 (March 2016), the average high temperature was approximately 77.8°F, with an average low of 52.8°F, and total precipitation of 2.72in. The average percent moisture content of the core samples collected was 0.55%, significantly drier than the previous 3 rounds.

With higher temperatures observed in round 1 and the relatively high volatility of BTEX, one would assume that the desorption of BTEX from the soils would increase. However, precipitation may be able to explain the variance observed between rounds 1 and 4. Three months prior to round 1, there was approximately 20in. of precipitation compared to approximately 4 in. the 3 months prior to round 4. The differences in the percent moisture content observed in the samples correlated with total BTEX concentrations (mean values, r^2= 0.80), albeit this relationship was not significant (P= 0.11) shown in figure 3.7D. Nonetheless, the relative solubility of BTEX in water allows for the contaminants to be retained longer in soils with a greater liquid phase (% moisture), as opposed to migrating downward and/or experiencing volatilization in drier soils.

Table 3.4. Meteorological conditions prior to and during the time of sampling.

Month	Average High Temperature (°F)	Average Low Temperature (°F)	Total Precipitation (inches)
March (2015)	69.7	50.0	9.04
April (2015)	81.4	63.2	6.98
May (2015)	86.7	68.6	10.4
June (2015)	92.0	72.0	3.40
July (2015)	97.3	73.7	1.57
August (2015)	100.4	72.6	3.06
September (2015)	93.7	68.5	2.39
October (2015)	89.3	60.1	6.10
November (2015)	74.4	52.8	2.29
December (2015)	70.4	45.4	1.97
January (2016)	64.5	37.0	2.01
February (2016)	64.7	42.6	1.66
March (2016)	77.8	52.8	2.72

Months in *bold lettering*, corresponds to when the core samples were collected.

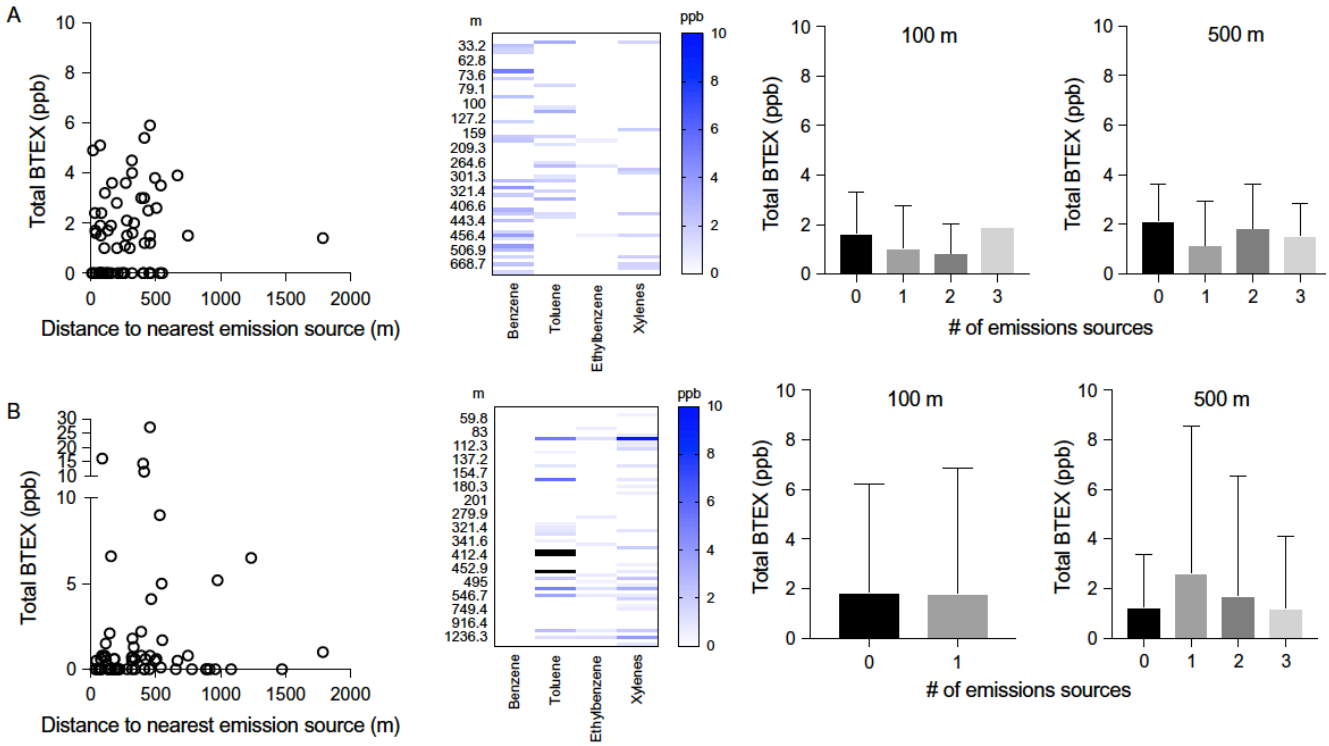

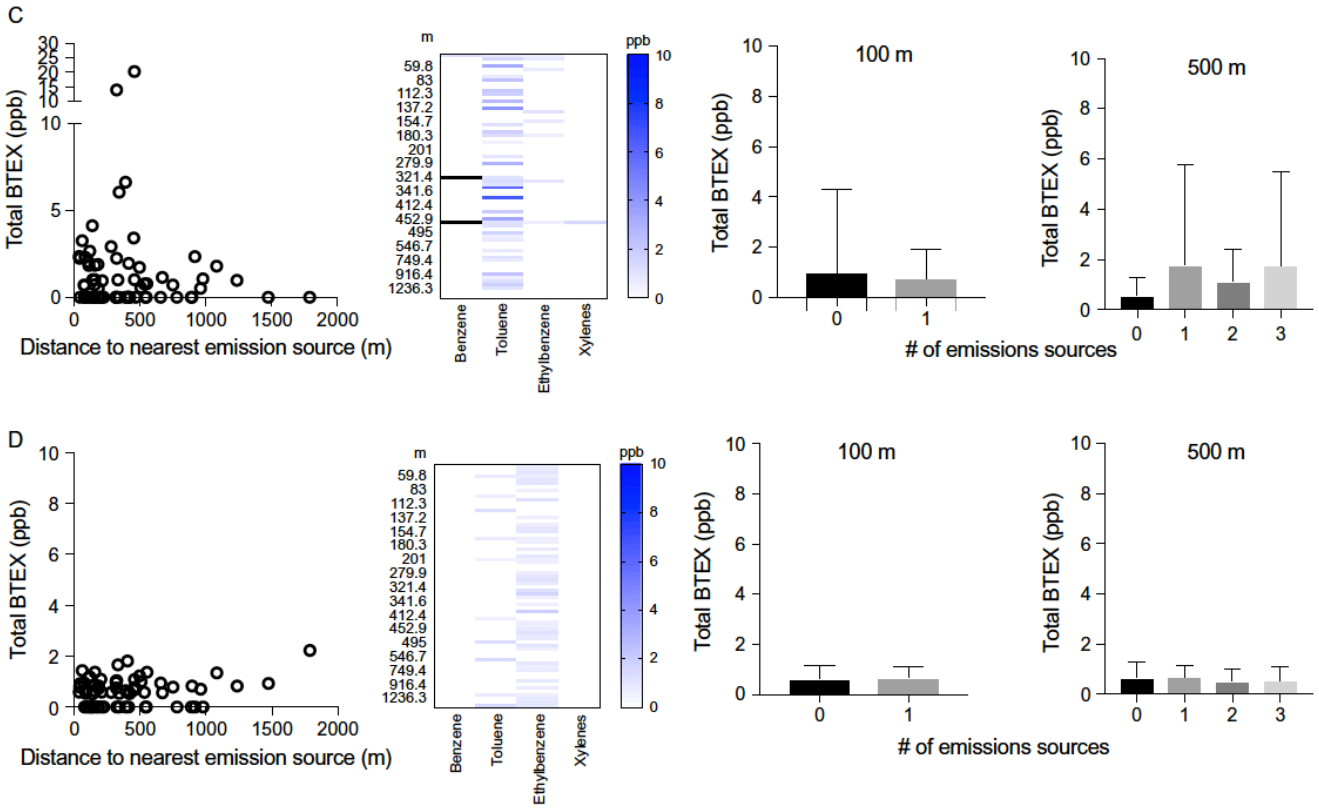

Figure 3.8. Geospatial analysis for the soil samples collected during rounds 1–4 (A–D). The relationships between total BTEX concentrations in soil, individual BTEX constituent concentration in soil, and the distance to the nearest BTEX emissions source are illustrated on left and left center, respectively. Total BTEX concentrations in relation to the number of emissions sources within 100 and 500m of the sampling sites are depicted on the right center and right, respectively. The error bars in the bar graphs represent the standard deviation.

3.3.3 Geospatial Analyses

To assess the relative impacts that the distance to a nearby emission source has on BTEX soil concentrations, a series of geospatial analyses were performed shown in figure 3.8. The “distance-to” analysis is a simple metric to assess whether a particular

anthropogenic process is contributing to the environmental contamination of test sites, assuming point sources in the anthropogenic processes are yielding contamination in a uniform fashion. This analysis has been used for comparisons of thermogenic methane levels[3] and heavy metal ions[57,58] in groundwater relative to the distances of the sampling sites to neighboring UD gas wells. Using the Spearman rank correlation, it was discovered that total BTEX concentrations did not correlate with the distances to the nearest emissions source for rounds 1–4 as seen in figure 8A-D. r-Values ranged from - 0.096 (round 3) to 0.21 (round 1), with P-values ranging from 0.083 (round 1) to 0.65 (round 4). Similarly, there were no discernible relationships between the concentrations of each of the BTEX constituents and the distance to the nearest emissions source in any of the sampling rounds as seen in figure 8A-D, left-center panels. We also examined soil BTEX concentrations with respect to the number of emissions sources within a 100- and 500-m radius of each sampling site. No relationships were observed between soil BTEX concentrations and the two emission source density metrics in any of the four sampling rounds (resulting Kruskal–Wallis P-values were all >0.16) shown in figure 7A-D, right panels. Even within the 500-m density metric analysis for round 3, which exhibited the highest variability among the eight different density analyses, no statistically significant intraround comparisons were observed (resulting Mann–Whitney P-values were all >0.36).

Next, we evaluated the relative impact of the prevailing wind direction on soil BTEX concentrations shown in figure 3.9. The hypothesis being, if the BTEX emission sources are contributing to the accumulation of BTEX in soil, then higher concentrations of BTEX should be observed in soil located downwind of the nearest emissions source compared

to soil samples collected upwind of the nearest emissions source.[19] No statistically significant differences were observed between the up- and downwind groups in rounds 1–4 as seen in figure 3.9A-D left axis, nor were there any differences in the average distances of the up- and downwind locations with respect to the nearest emissions source as shown in figure 3.9A-D right axis. Collectively these geospatial analyses indicate that the distance to an established point source of atmospheric contamination, the density of emission sources around a given sampling site, and the position of the sampling site with respect to the nearest point source and the prevailing wind had no significant influence on the accumulation of BTEX in soil. Based on these analyses alone, irrespective of soil structure and composition, one might postulate that the BTEX emission sources are not responsible for the BTEX detected in neighboring soils, or that the regional air quality or meteorological factors, or both, may be hindering the performance of a high spatial resolution, low time resolution analysis. In addition to the air quality measurements collected on the pad sites described here, we have also collected mobile measurements across 13 counties in the Eagle Ford shale region, revealing deteriorated air quality on a regional scale.[23] Consequently, it is possible that elevated atmospheric BTEX concentrations surrounding the study area imposed a background signal that masked detectable changes in our highly localized study.

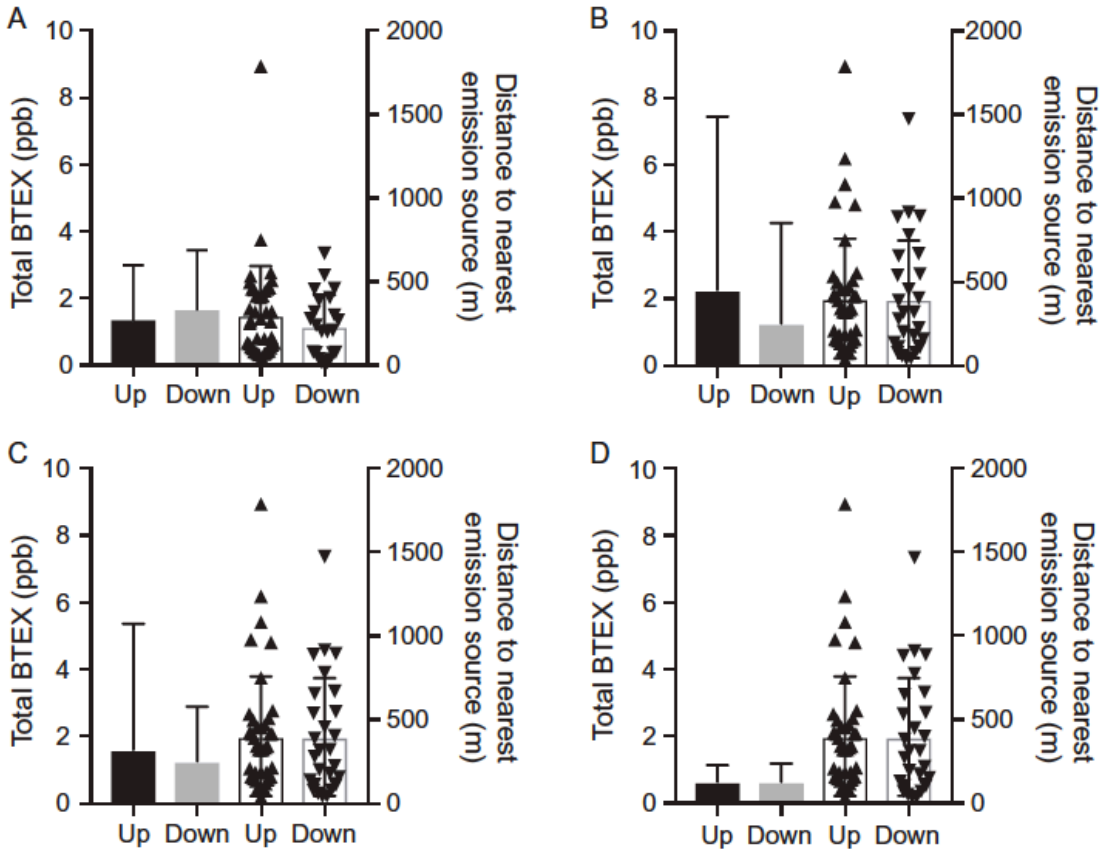

Figure 3.9. Total soil BTEX concentrations with respect to the prevailing wind position from the nearest BTEX emissions source for rounds 1–4 (A–D). Total BTEX concentrations for the up- and downwind groups are graphed in relation to the left y-axis, whereas the distances of the sampling sites to the nearest emissions source in both the up- and downwind groups are graphed against the right y-axis. The error bars represent the standard deviation.

3.3.4 Variable Soil composition

Of all the variables that were examined during the study, soil texture appeared to have the most influence on the total BTEX concentrations that were detected across rounds 1–4 shown in figure 3.10. Rounds 1, 2, and 4 each showed significant differences between the soil types (P-values of 0.044, 0.024, and 0.014, respectively). Assessing the data throughout the entirety of the time course, there was notable variation between the five soil types (P= 0.013) with sand-based soils exhibiting the lowest mean BTEX concentrations over the time course (0.91 ppb) and silty clay loam-based soils demonstrating the highest (3.26 ppb). The silty clay loam samples, that is the soils with the highest clay content, retained significantly more BTEX over time than sand and loamy sand soils seen in figure 3.10A. Silty clay loam-based samples exhibited the highest concentrations of BTEX in 2/4 sampling rounds (rounds 2 and 4), whereas sand-based samples had the lowest concentrations of BTEX in 2/4 sampling rounds (rounds 1 and 3) depicted in figure 3.10B-E. Collectively, these findings support the observations made by Owabor et al., where clay was found to be a better matrix for absorbing BTEX compared to sand.[33] Silty clay loam-based samples contain a higher percentage of clay and silt than sand. Due to the relatively small pore spaces of both clay and silt, the contaminant solutes remain adhered to the clay and silt particle surfaces. This variable life cycle and mobility of BTEX across soil compositions is important to note as it can confound point source investigations using traditional spatial correlations.

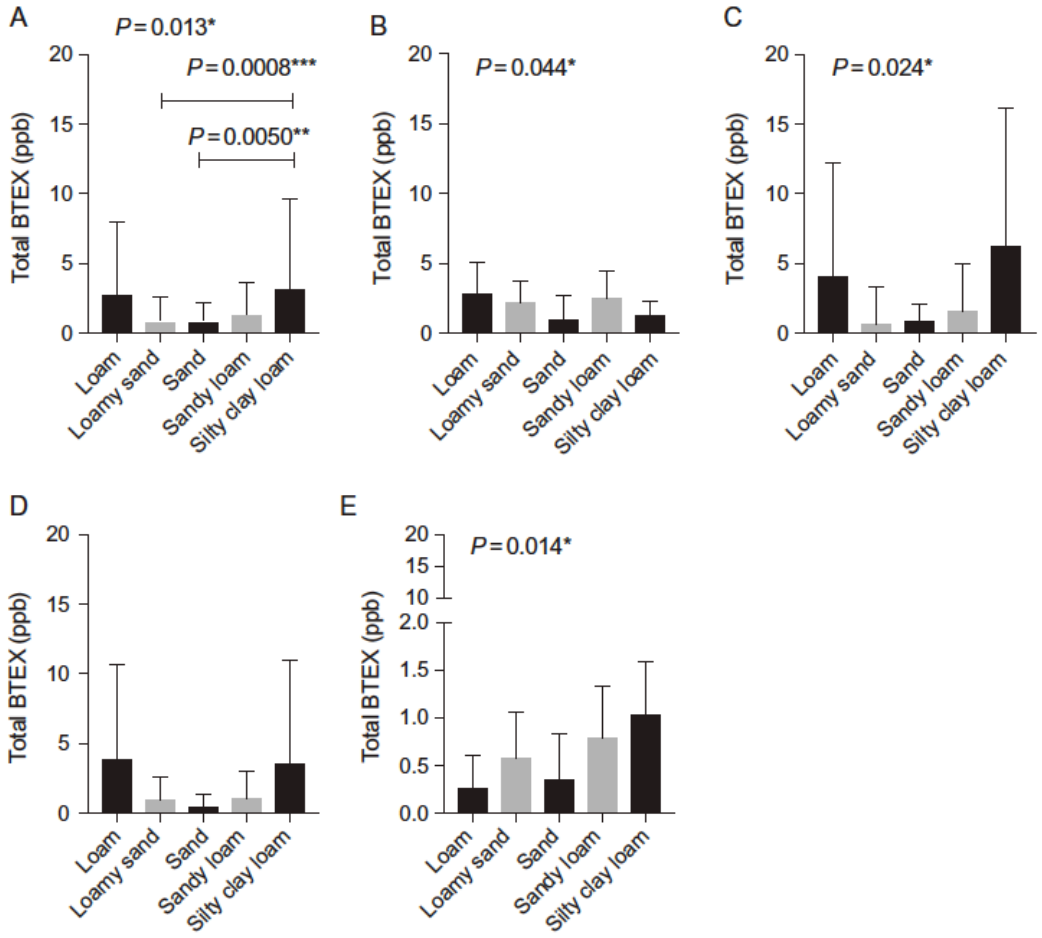

Figure 3.10. Total BTEX detected in the various soil types collected throughout the study (A) and in rounds 1–4 (B–E). Statistically significant (*) differences within each round across the various soil type were determined by Kruskal–Wallis ANOVA ($P<0.05$). Statistically significant (*) differences between individual soil types were determined by Mann–Whitney pairwise comparisons ($P<0.05$). The error bars represent the standard deviation.

3.3.5 BTEX Volatilization, Sequestration, and Remediation

As discussed earlier in this chapter, BTEX constituents are slightly soluble in water and have high K_{OW} values. Due to their physicochemical properties, BTEX is likely to dissolve in a water phase or evaporate into the air spaces (pores) of soil. The volatile behavior of BTEX is quite complex, differing for different matrices. Tong et al. studied the volatilization dynamics of BTEX in three matrices, water, sand, and a soil mixture, and found that the rate of volatilization of BTEX compounds and matrix mixture was benzene>toluene>xylenes>ethylbenzene for water, sand, and the soil mixture.[59]

We attempted in situ remediation of BTEX using soil disruption and PAC depicted in figure 3.11. In the untreated quadrant (q1) total BTEX concentration increased from time 0 (March 2016) to time 1 (April 2016) with 146% and 165% (relative change) for plots 1 and 2, respectively. The quadrant with disrupted soil (q2) showed an increase in total BTEX in both plots 1 and 2. Plot 1's increase was minimal with a percent change from time 0 to time 1 of 26%, while plot 2 had a percent change of 239%. The conflicting results of q2 generate uncertainty between the offsetting magnitude of increased volatility and increased sorption area after increasing the surface area of the soil. The PAC treatment quadrant (q3) had the greatest increase in total BTEX concentrations from time 0 to time 1 in both plots. The percent change for plots 1 and 2 was 45% and 544%, respectively. Overall q3 in plot 2 showed the greatest increase in total BTEX concentrations over the course of a month. It is hypothesized that treating with PAC without soil disruption did not present a mechanism for "mixing" the soil and the PAC merely created a "cap" to trap existing BTEX and strongly sequestered deposited BTEX. However, the soil disrupted+PAC treatment (q4) showed promising results as a possible remediation

technique. Plot 1 revealed a decrease of total BTEX concentration with a percent change of -16%. In plot 2 there was an increase of total BTEX concentration with a percent change of 15%, the smallest increase of all of the quadrants. Apparently, the tilling of soil and/or any other physical manipulation of soil, as performed in the “soil disruption” quadrant, enhances the volatilization of BTEX compounds. The physical manipulation disrupts the soil structure allowing for these compounds to become mobile and perhaps more accessible to photodegradation and digestion by microbes.[35] Physical manipulation along with PAC treatment allows the contaminants to volatilize as well as being sequestered by the PAC. The control quadrant, q1, for each replicate demonstrates there is active deposition occurring, confounding the ability to interpret the success of the three approaches. That said, all treated quadrants except q2 and q3 in plot 2 accumulated and/or retained less BTEX than the controls. Although in immediate vicinity to each other, and both in close proximity to established emission sources, plot 2 consistently had greater BTEX increase than plot 1.

Although, these remediation attempts showed promising results, it may not be practical in a larger scale. Physical manipulation with the addition of PAC allows for the liberation and sequestration of the contaminants by the PAC. As suggested by the results in q3, PAC may act as a cap, preventing volatilization of residual BTEX contaminants already present in the soil and also by reducing the rate of infiltration and leaching of surface deposited BTEX. Volatilization and sequestration of BTEX might be enhanced by recurring rounds of physical manipulation or both physical manipulation and PAC treatment.

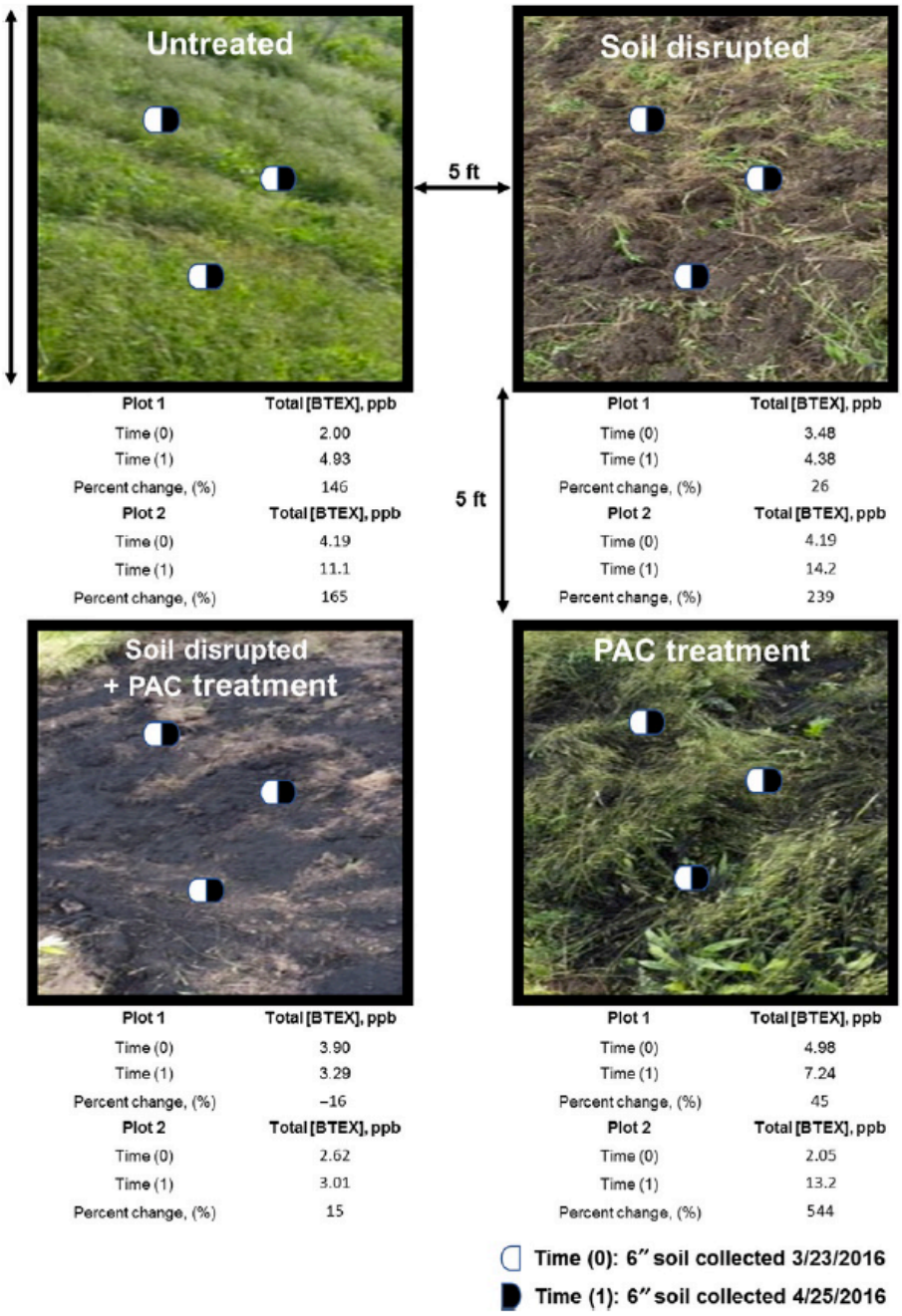

Plot 1	Total [BTEX], ppb
Time (0)	2.00
Time (1)	4.93
Percent change, (%)	146
Plot 2	**Total [BTEX], ppb**
Time (0)	4.19
Time (1)	11.1
Percent change, (%)	165

Plot 1	Total [BTEX], ppb
Time (0)	3.48
Time (1)	4.38
Percent change, (%)	26
Plot 2	**Total [BTEX], ppb**
Time (0)	4.19
Time (1)	14.2
Percent change, (%)	239

Plot 1	Total [BTEX], ppb
Time (0)	3.90
Time (1)	3.29
Percent change, (%)	−16
Plot 2	**Total [BTEX], ppb**
Time (0)	2.62
Time (1)	3.01
Percent change, (%)	15

Plot 1	Total [BTEX], ppb
Time (0)	4.98
Time (1)	7.24
Percent change, (%)	45
Plot 2	**Total [BTEX], ppb**
Time (0)	2.05
Time (1)	13.2
Percent change, (%)	544

Figure 3.11. Two plots with 4, 10’ x 10’ quadrants were constructed 5ft. apart from each other to evaluate remediation strategies in contaminated soils. Untreated (top left) quadrant (q1) was used as a control. In the second quadrant (q2, top right) the soil was physically disrupted by tilling. The third and fourth quadrants (q3, bottom right and q4, bottom left) correspond to soil treated with PAC and disrupted soil treated with PAC,

respectively. Three core samples were collected from each quadrant in each plot immediately before treatment (0) and after a 1-month incubation under the respective conditions (1).

3.4 Conclusion

As fossil fuel extraction development continues to increase in petroliferous basins all across the United States, it is of the utmost importance to investigate all of the environmental systems (soil, air, and water) for occurrences and mechanisms of contamination. As discussed, characteristics of the soil matrix play a key role in the sorption of BTEX and make the analysis a challenge.

In this chapter, we explored the relationship between BTEX emissions from production sites and BTEX detection in soil during an 11-month time series analysis in the Eagle Ford shale region of southern Texas, USA. The distance of sampling sites to a nearby source of atmospheric contamination, and the density of these emissions sources surrounding the sampling sites, appeared to have little impact on the accumulation of BTEX in soils. Soil composition/texture was the only factor affecting soil BTEX concentrations in the study area. These findings corroborated data from previous soil investigations, in that higher total BTEX concentrations were observed in samples with higher percentages of clay than sand. Aside from the variable soil matrix, it is also important to take into account variables, such as weather conditions and moisture content, as they may help further explain the rates of BTEX accumulation in soils. Further examination of BTEX contamination in field based and experimental research will continue to increase our understanding of the environmental effects of UD.

3. References

1. Adgate JL, Goldstein BD, McKenzie LM. Potential public health hazards, exposures and health effects from unconventional natural gas development. Environ Sci Technol 2014;48(15):8307–20.
2. Goldstein BD, Kriesky J, Pavliakova B. Missing from the table: role of the environmental public health community in governmental advisory commissions related to Marcellus Shale drilling. Environ Health Perspect 2012;120(4):483–6.
3. Osborn SG, Vengosh A, Warner NR, Jackson RB. Methane contamination of drinking water accompanying gas-well drilling and hydraulic fracturing. Proc Natl Acad Sci USA 2011;108(20):8172–6.
4. Darrah TH, Vengosh A, Jackson RB, Warner NR, Poreda RJ. Noble gases identify the mechanisms of fugitive gas contamination in drinking-water wells overlying the Marcellus and Barnett Shales. Proc Natl Acad Sci USA 2014;111(39):14076–81.
5. Jackson RB, Vengosh A, Darrah TH, Warner NR, Down A, Poreda RJ, et al. Increased stray gas abundance in a subset of drinking water wells near Marcellus shale gas extraction.
Proc Natl Acad Sci USA 2013;110(28):11250–5.
6. Molofsky LJ, Connor JA, Wylie AS, Wagner T, Farhat SK. Evaluation of methane sources in groundwater in northeastern Pennsylvania. Ground Water 2013;51(3):333–49.
7. Siegel DI, Azzolina NA, Smith BJ, Perry AE, Bothun RL. Methane concentrations in water wells unrelated to proximity to existing oil and gas wells in northeastern Pennsylvania. Environ Sci Technol 2015;49(7):4106–12.
8. Baldassare FJ, McCaffrey MA, Harper JA. A geochemical context for stray gas investigations in the northern Appalachian Basin: implications of analyses of natural gases from Neogene-through Devonian-age strata. AAPG Bull 2014;98(2):341–72.
9. Lauer NE, Harkness JS, Vengosh A. Brine spills associated with unconventional oil development in North Dakota. Environ Sci Technol 2016;50(10):5389–97.
10. Warner NR, Christie CA, Jackson RB, Vengosh A. Impacts of shale gas wastewater disposal on water quality in western Pennsylvania. Environ Sci Technol 2013;47(20): 11849–57.
11. Burton TG, Rifai HS, Hildenbrand ZL, Carlton Jr DD, Fontenot BE, Schug KA. Elucidating hydraulic fracturing impacts on groundwater quality using a regional geospatial statistical modeling approach. Sci Total Environ 2016;545–546:114–26.
12. Hildenbrand ZL, Carlton Jr DD, Meik JM, Taylor JT, Fontenot BE, Walton JL, et al. A reconnaissance analysis of groundwater quality in the Eagle Ford shale region reveals two distinct bromide/chloride populations. Sci Total Environ 2017;575:672–80.
13. Hildenbrand ZL, Carlton DD, Fontenot BE, Meik JM, Walton JL, Taylor JT, et al. A comprehensive analysis of groundwater quality in the Barnett Shale region. Environ Sci Technol 2015;49(13):8254–62.
14. Hildenbrand ZL, Carlton Jr DD, Fontenot BE, Meik JM, Walton JL, Thacker JB, et al. Temporal variation in groundwater quality in the Permian Basin of Texas, a region of increasing unconventional oil and gas development. Sci Total Environ 2016;562:906–13.
15. Gross SA, Avens HJ, Banducci AM, Sahmel J, Panko JM, Tvermoes BE. Analysis of BTEX groundwater concentrations from surface spills associated with hydraulic fracturing operations. J Air Waste Manag Assoc 2013;63(4):424–32.

16. Allen DT, Torres VM, Thomas J, Sullivan DW, Harrison M, Hendler A, et al. Measurements of methane emissions at natural gas production sites in the United States. Proc Natl Acad Sci USA 2013;110(44):17768–73.
17. Harriss R, Alvarez RA, Lyon D, Zavala-Araiza D, Nelson D, Hamburg SP. Using multiscale measurements to improve methane emission estimates from oil and gas operations in the Barnett Shale region, Texas. Environ Sci Technol 2015;49(13):7524–6.
18. Yacovitch TI, Herndon SC, P_etron G, Kofler J, Lyon D, Zahniser MS, et al. Mobile laboratory observations of methane emissions in the Barnett Shale region. Environ Sci Technol 2015;49(13):7889–95.
19. Payne BF, Ackley R, Paige Wicker A, Hildenbrand ZL, Carlton DD, Schug KA. Characterization of methane plumes downwind of natural gas compressor stations in Pennsylvania and New York. Sci Total Environ 2017;580:1214–21.
20. Caulton DR, Shepson PB, Cambaliza MOL, McCabe D, Baum E, Stirm BH. Methane destruction efficiency of natural gas flares associated with shale formation wells. Environ Sci Technol 2014;48(16):9548–54.
21. Armendariz A. Emissions from natural gas productions in the Barnett Shale area and opportunities for cost-effective improvements. New York, NY: Southern Methodist University: Environmental Defense Fund; 2009.
22. Bunch AG, Perry CS, Abraham L, Wikoff DS, Tachovsky JA, Hixon JG, et al. Evaluation of impact of shale gas operations in the Barnett Shale region on volatile organic compounds in air and potential human health risks. Sci Total Environ 2014;468–469:832–42.
23. Hildenbrand ZL, Mach PM, McBride EM, Dorreyatim MN, Taylor JT, Carlton DD, et al. Point source attribution of ambient contamination events near unconventional oil and gas development. Sci Total Environ 2016;573:382–8.
24. White GJ. In: Zielinski RW, Otton JK, editors. Chemical and radiometric assessment of NORM in soils and sediments' contacted by produced water. Proceedings of the 5th international petroleum environmental conference; 1998 October 20–23; Albuquerque, NM; 1998.
25. Lauer N, Vengosh A. Age dating oil and gas wastewater spills using radium isotopes and their decay products in impacted soil and sediment. Environ Sci Technol Lett 2016;3(5):205–9.
26. Schumacher BA, Minnich MM. Extreme short-range variability in VOC-contaminated soils. Environ Sci Technol 2000;34(17):3611–6.
27. Minnich MM. Behavior and determination of volatile organic compounds in soil: a literature review. College Park, MD: Agency USEPA; 1993.
28. Hendler A, Nunn J, Lundeen J, McKaskle R. VOC emissions from oil and condensate storage tanks. Texas: Agency TCEQ; 2009.
29. Soil classification United States Department of Agriculture, Washington, DC; 2017 [Available from: http://www.nrcs.usda.gov/].
30. Canada A. Glossary of terms in soil science: minister of supply and services Canada. Ottawa: Canada Department of Agriculture; 1976.
31. Ryan P. Environmental and low temperature geochemistry. New York: Wiley; 2014.
32. Serrano A, Gallego M. Sorption study of 25 volatile organic compounds in several Mediterranean soils using headspace–gas chromatography–mass spectrometry. J Chromatogr A 2006;1118(2):261–70.

33. Owabor NC, Agarry ES, Ayodele VB, Udeh SI, Ehiousun E. Comparative study of the adsorption and desorption behavior of single and multi-ring aromatics in sediment fractions. Adv Chem Eng Sci 2013;3:67–73.
34. Lima DLD, Schneider RJ, Scherer HW, Duarte AC, Santos EBH, Esteves VI. Sorption– desorption behavior of atrazine on soils subjected to different organic long-term amendments. J Agric Food Chem 2010;58(5):3101–6.
35. Pignatello JJ, Xing B. Mechanisms of slow sorption of organic chemicals to natural particles. Environ Sci Technol 1996;30(1):1–11.
36. Prenafeta-Boldu´ FX, Ballerstedt H, Gerritse J, Grotenhuis JTC. Bioremediation of BTEX hydrocarbons: effect of soil inoculation with the toluene-growing fungus Cladophialophora Sp. strain T1. Biodegradation 2004;15(1):59–65.
37. Salanitro JP, Dorn PB, Huesemann MH, Moore KO, Rhodes IA, Rice Jackson LM, et al. Crude oil hydrocarbon bioremediation and soil ecotoxicity assessment. Environ Sci Technol 1997;31(6):1769–76.
38. Margesin R, Schinner F. Biodegradation and bioremediation of hydrocarbons in extreme environments. Appl Microbiol Biotechnol 2001;56(5):650–63.
39. Frank U, Barkley N. Remediation of low permeability subsurface formations by fracturing enhancement of soil vapor extraction. J Hazard Mater 1995;40(2):191–201.
40. Kirtland BC, Aelion CM. Petroleum mass removal from low permeability sediment using air sparging/soil vapor extraction: impact of continuous or pulsed operation. J Contam Hydrol 2000;41(3):367–83.
41. Zytner RG. Sorption of benzene, toluene, ethylbenzene and xylenes to various media. J Hazard Mater 1994;38(1):113–26.
42. Hansch C, Quinlan JE, Lawrence GL. Linear free-energy relationship between partition coefficients and the aqueous solubility of organic liquids. J Org Chem 1968;33(1):347–50.
43. Karickhoff SW, Brown DS, Scott TA. Sorption of hydrophobic pollutants on natural sediments. Water Res 1979;13(3):241–8.
44. Banerjee S, Howard PH. Improved estimation of solubility and partitioning through correction of UNIFAC-derived activity coefficients. Environ Sci Technol 1988;22(7): 839–41.
45. Denyes MJ, Rutter A, Zeeb BA. In situ application of activated carbon and biochar to PCB-contaminated soil and the effects of mixing regime. Environ Pollut 2013;182:201–8.
46. Liang C, Chen Y-J. Evaluation of activated carbon for remediating benzene contamination: adsorption and oxidative regeneration. J Hazard Mater 2010;182(1):544 51.
47. Wan J, Chai L, Lu X, Lin Y, Zhang S. Remediation of hexachlorobenzene contaminated soils by rhamnolipid enhanced soil washing coupled with activated carbon selective adsorption. J Hazard Mater 2011;189(1):458–64.
48. Mach PM, McBride EM, Sasiene ZJ, Brigance KR, Kennard SK, Wright KC, et al. Vehicle-mounted portable mass spectrometry system for the covert detection via spatial analysis of clandestine methamphetamine laboratories. Anal Chem 2015;87(22):11501 8.
49. Bowman GM, Hutka J. Particle size analysis. In: McKenzie N, Coughlan K, Cresswell H, editors. Soil physical measurement and interpretations for land evaluation. Australia: CSIRO Publishing; 2002.

50. USEPA.n.d. Test methods for evaluating solid waste—physical/chemical methods EPA/SW-846. Method 5021A: volatile organic compounds by gas chromatography/ mass spectrometry (GC/MS).
51. Ezquerro O ´ , Ortiz G, Pons B, Tena MAT. Determination of benzene, toluene, ethylbenzene and xylenes in soils by multiple headspace solid-phase microextraction. J Chromatogr A 2004;1035(1):17–22.
52. Buerck J, Roth S, Kraemer K, Scholz M, Klaas N. Application of a fiber-optic NIR-EFA sensor system for in situ monitoring of aromatic hydrocarbons in contaminated groundwater. J Hazard Mater 2001;83(1):11–28.
53. Yang Y, Jones AD, Eaton CD. Retention behavior of phenols, anilines, and alkylbenzenes in liquid chromatographic separations using subcritical water as the mobile phase. Anal Chem 1999;71(17):3808–13.
54. suite GPS, One-way ANOVA followed by Dunnett's multiple comparisons test was performed using GraphPad Prism version 7.00 for Windows: GraphPad Software, Inc., LaJolla, CA; 2017 [Available from: www.graphpad.com].
55. Varona-Torres, E.; Carlton, D. D.; Payne, B.; Hildenbrand, Z. L.; Schug, K. A., Chapter Twelve - The Characterization of BTEX in Variable Soil Compositions Near Unconventional Oil and Gas Development. In *Advances in Chemical Pollution, Environmental Management and Protection*, Schug, K. A.; Hildenbrand, Z. L., Eds. Elsevier: 2017; Vol. 1, pp 321-351.

Chapter 4: Room Temperature Ionic Liquids (RTILs)

4.1 Introduction

Ionic liquids are liquid organic, molten or fused salts; a class of nonmolecular ionic solvents with melting points below 100 ℃ .[1-6] Room temperature ionic liquids (RTILs) a class of ILs, is defined as any salt that has a melting point lower than ambient temperature.[1, 7] Most ILs are composed of an organic cation, commonly a quaternary amine and an organic or inorganic anion as shown in figure 4.1. The range of possible cation and anion variations could provide up to 10^{18} different ILs.[1, 8] The first RTIL to be reported was by John S. Wilkes and colleagues in 1982 on an 1-alkyl-3-methylimidazolium based cation.[6] Due to their physiochemical properties: negligible vapor pressure, wide liquid range, tunable viscosity, and tunable thermal stabilities, RTILs have garnered significant attention for their use in general analytical chemistry, in separation techniques, and in sample preparation methodologies.[1-2, 5, 9-14]

Ionic liquids' appealing physiochemical properties are due to poor ion coordination.[7] The combination of a large asymmetrical organic cation and a symmetrical anion prevents the formation of crystal lattices, thus lowering the melting point and resulting in an ionic liquid.[15] The strong Coulombic interactions within the RTILs result in the negligible vapor pressure. Thus, making RTILs a great candidate to be used in headspace analyses.

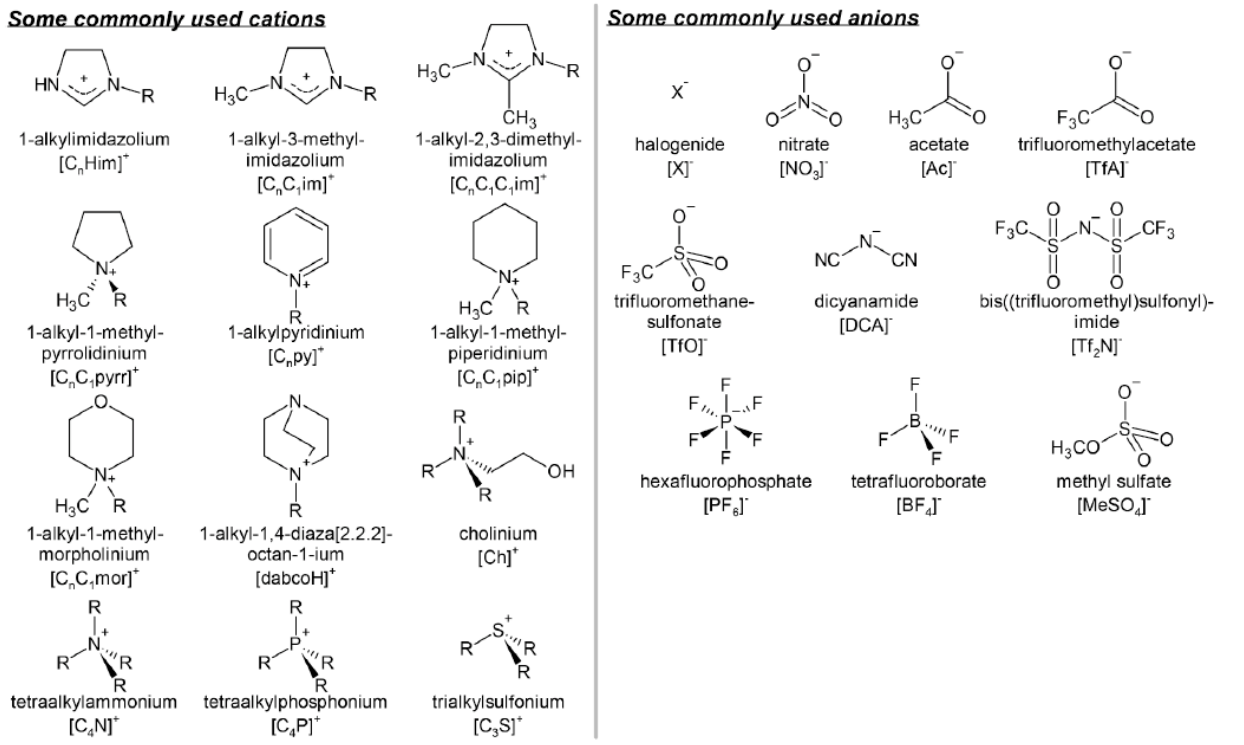

Figure 4.1. Commonly used cations and anions for the synthesis of RTILs. Reprinted from Płotka-Wasylka, J.; de la Guardia, M.; Andruch, V.; Vilková, M., Deep eutectic solvents vs ionic liquids: Similarities and differences. *Microchemical Journal* **2020,** *159*, 105539 with permision from Elsevier.[16]

4.2 Room Temperature Ionic Liquids as co-Solvent in Headspace Analysis

Headspace (HS) analysis is commonly used for volatile organic compounds (VOCs) and residual solvents in the environmental and pharmaceutical laboratories.[11, 17-20] Per discussion in chapter 2, static headspace extraction gas chromatography (SHE-GC), only the volatile components are introduced into the GC system. Co-solvents in HS have shown to increase the sensitivity of compounds of interest.[13] Equilibration temperature and type of co-solvent used, can significantly impact the sensitivity of the

analytes. Water is a common co-solvent used in the analysis of VOCs in environmental samples.[18, 21]

Although, using conventional co-solvents such as water and dimethyl sulfoxide (DMSO) in HS-GC, pose great advantages, it also has disadvantages. The main disadvantage for using such co-solvents is the increased vapor pressure at elevated temperatures, which causes flooding of the co-solvent into the GC. Flooding causes broad solvent peaks on the chromatogram. This limits the equilibrium temperatures used and usually leads to lengthy equilibration times.

Room temperature ionic liquids and their unique physiochemical properties such as negligible vapor pressure, tunable thermal stabilities, wide liquid range, and tunable viscosities present a great alternative to conventional co-solvents in HS-GC. The use of RTILs as co-solvents in HS-GC have been reported in various publications.[3-4, 10-11, 20] RTILs have shown the capability of dissolving both polar and non-polar molecules.[1, 11] A disadvantage of using an RTIL as a co-solvent, is the volatile impurities that can exist within them, which can potentially interfere with the peak of interest. This can be overcome by heating while purging with an inert gas such as nitrogen.[22]

In the following chapters, the application of RTILs were investigated for the potential use in HS-GC analysis of benzene, toluene, ethylbenzene, and xylenes (BTEX) from soil. The thermodynamic properties associated with such environmental contaminants in commercially available RTILs were investigate as well. The four RTILs investigated were 1-ethyl-3-methylimidazolium ethylsulfate ([EMIM][ESO_4]), 1-ethyl-3-methylimidazolium diethyl phosphate ([EMIM][DEP]), tris(2-hydroxyethyl)methylammonium methylsulfate ([MTEOA][$MeOSO_3$]) and (1-ethyl-

3-methylimidazolium bis(trisfluoromethanesulfonyl)imide ([EMIM] [NTf2]), the structures for which are shown in Figure 4.2. [EMIM][ESO_4], [EMIM][DEP] and [MTEOA][$MeOSO_3$] were chosen as they are characterized as being hydrophilic and [EMIM][NTF2], which is characterized as being hydrophobic in nature and their ability to homogenize various sample matrices.

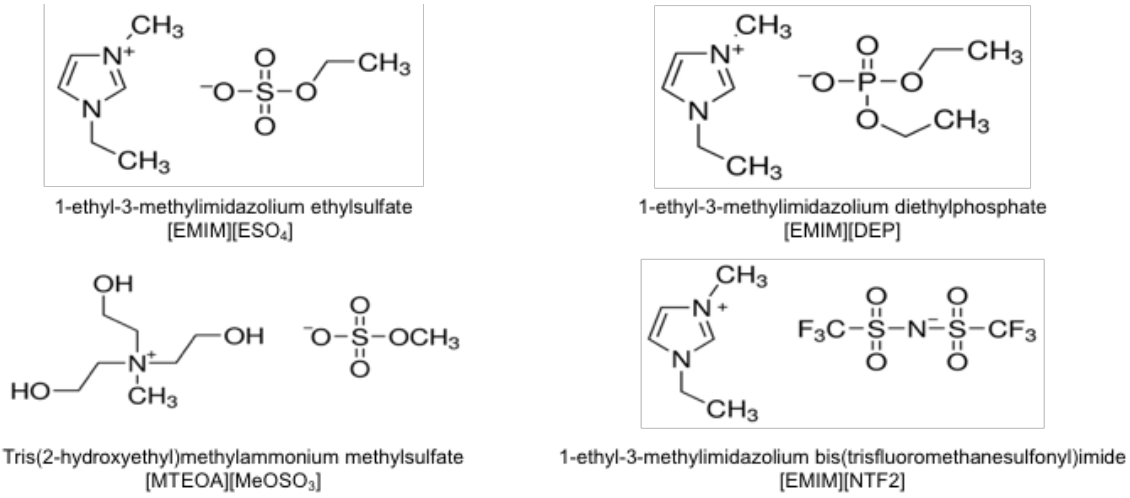

Figure 4.2. Structure of RTILs being investigated. 1-ethyl-3-methylimidazolium ethylsulfate ([EMIM][ESO_4]), 1-ethyl-3-methylimidazolium diethylphosphate ([EMIM][DEP]), tris(2-hydroxyethyl)methylammonium methylsulfate ([MTEOA][$MeOSO_3$]) and 1-ethyl-3-methylimidazolium bis(trisfluoromethanesulfonyl)imide ([EMIM] [NTf2]).

4. References

1. Anderson, J. L.; Armstrong, D. W.; Wei, G.-T., Ionic Liquids in Analytical Chemistry. *Analytical Chemistry* **2006,** *78* (9), 2892-2902.
2. Feng, J.; Loussala, H. M.; Han, S.; Ji, X.; Li, C.; Sun, M., Recent advances of ionic liquids in sample preparation. *TrAC Trends in Analytical Chemistry* **2020,** *125*, 115833.
3. Laus, G.; Andre, M.; Bentivoglio, G.; Schottenberger, H., Ionic liquids as superior solvents for headspace gas chromatography of residual solvents with very low vapor pressure, relevant for pharmaceutical final dosage forms. *Journal of Chromatography A* **2009,** *1216* (32), 6020-6023.
4. Liu, F.-h.; Jiang, Y., Room temperature ionic liquid as matrix medium for the determination of residual solvents in pharmaceuticals by static headspace gas chromatography. *Journal of Chromatography A* **2007,** *1167* (1), 116-119.
5. Liu, R.; Liu, J.-f.; Yin, Y.-g.; Hu, X.-l.; Jiang, G.-b., Ionic liquids in sample preparation. *Analytical and Bioanalytical Chemistry* **2009,** *393* (3), 871-883.
6. Wilkes, J. S.; Levisky, J. A.; Wilson, R. A.; Hussey, C. L., Dialkylimidazolium chloroaluminate melts: a new class of room-temperature ionic liquids for electrochemistry, spectroscopy and synthesis. *Inorganic Chemistry* **1982,** *21* (3), 1263-1264.
7. Welton, T., Room-Temperature Ionic Liquids. Solvents for Synthesis and Catalysis. *Chemical Reviews* **1999,** *99* (8), 2071-2033.
8. Carmichael, A. J.; Seddon, K. R., Polarity study of some 1-alkyl-3-methylimidazolium ambient-temperature ionic liquids with the solvatochromic dye, Nile Red. *Journal of Physical Organic Chemistry* **2000,** *13* (10), 591-595.
9. Poole, C. F.; Poole, S. K., Extraction of organic compounds with room temperature ionic liquids. *Journal of Chromatography A* **2010,** *1217* (16), 2268-2286.
10. Varona-Torres, E.; Carlton, D. D.; Hildenbrand, Z. L.; Schug, K. A., Matrix-effect-free determination of BTEX in variable soil compositions using room temperature ionic liquid co-solvents in static headspace gas chromatography mass spectrometry. *Analytica Chimica Acta* **2018**.
11. Frink, L. A.; Armstrong, D. W., Water Determination in Solid Pharmaceutical Products Utilizing Ionic Liquids and Headspace Gas Chromatography. *Journal of Pharmaceutical Sciences* **2016,** *105* (8), 2288-2292.
12. Baltazar, Q. Q.; Leininger, S. K.; Anderson, J. L., Binary ionic liquid mixtures as gas chromatography stationary phases for improving the separation selectivity of alcohols and aromatic compounds. *Journal of Chromatography A* **2008,** *1182* (1), 119-127.
13. Kolb, B., *Static Headspace-Gas Chromatography : Theory and Practice*. 2nd ed. ed.; John Wiley & Sons, Inc.: Hoboken, 2006.
14. Voice, T. C.; Kolb, B., Static and dynamic headspace analysis of volatile organic compounds in soils. *Environmental Science & Technology* **1993,** *27* (4), 709-713.
15. Keskin, S.; Kayrak-Talay, D.; Akman, U.; Hortaçsu, Ö., A review of ionic liquids towards supercritical fluid applications. *The Journal of Supercritical Fluids* **2007,** *43* (1), 150-180.
16. Płotka-Wasylka, J.; de la Guardia, M.; Andruch, V.; Vilková, M., Deep eutectic solvents vs ionic liquids: Similarities and differences. *Microchemical Journal* **2020,** *159*, 105539.

17. Esteve-Turrillas, F. A.; Armenta, S.; Garrigues, S.; Pastor, A.; de la Guardia, M., Headspace–mass spectrometry determination of benzene, toluene and the mixture of ethylbenzene and xylene isomers in soil samples using chemometrics. *Analytica Chimica Acta* **2007,** *587* (1), 89-96.
18. USEPA *Method 5021A: volatile organic compounds by gaschromatography/mass spectrometry (GC/MS)*.
19. USEPA, Closed System Purge and Trap and Extraction for VOlatile Organics in Soil and Waste Samples. In Method 5035A.
20. Nacham, O.; Ho, T. D.; Anderson, J. L.; Webster, G. K., Use of ionic liquids as headspace gas chromatography diluents for the analysis of residual solvents in pharmaceuticals. *Journal of Pharmaceutical and Biomedical Analysis* **2017,** *145*, 879-886.
21. Varona-Torres, E.; Carlton, D. D.; Payne, B.; Hildenbrand, Z. L.; Schug, K. A., Chapter Twelve - The Characterization of BTEX in Variable Soil Compositions Near Unconventional Oil and Gas Development. In *Advances in Chemical Pollution, Environmental Management and Protection*, Schug, K. A.; Hildenbrand, Z. L., Eds. Elsevier: 2017; Vol. 1, pp 321-351.
22. Von Wald, G.; Albers, D.; Cortes, H.; McCabe, T., Background vapor from six ionic liquids and the partition coefficients and limits of detection for 10 different analytes in those ionic liquids measured using headspace gas chromatography. *Journal of Chromatography A* **2008,** *1201* (1), 15-20.

Chapter 5: Matrix-effect-free determination of BTEX in variable soil compositions using room temperature ionic liquids co-solvents in static headspace gas chromatography mass spectrometry.[1]

5.1 Introduction

Due to the continued growth of hydrocarbon extraction in the United States and in other countries, unconventional oil and gas development (UD) is expected to become more common near residential and urban areas. This growth has increased public concern about the human health and environmental implications associated with such industrial activities. The potential for the release of pollutants into the air,[2-3] groundwater,[4-6] and soil[7] exists within many phases of the hydrocarbon extraction process. More specifically, soil can become contaminated by hazardous volatile organic compounds (VOCs), such as benzene, toluene, ethylbenzene, and xylene isomers (BTEX) as a result of spills and pipeline leaks. BTEX compounds have a high pollution potential, attributed to their solubility in water and other matrices.

Soil, as a matrix, is very complex. It is an extremely variable mixture of mineral and organic particles of various sizes that also carry diverse microbial communities, which collectively interact with the surrounding ecological frame work.[8-9] An important descriptor of soils is soil texture, which parameterizes the different sizes of particles that make up a soil in terms of the percentage of sand, silt, or clay, as shown in figure 5.1. Soil texture and the abundance of organic carbon are the primary contributing factors to the relative sorption of VOCs like BTEX.[10] Furthermore, soils with high organic matter can affect the sorption and limit the extraction efficiency of target analytes in analytical procedures, in this case, such

that the accurate quantification of BTEX in soil can be a significant challenge.

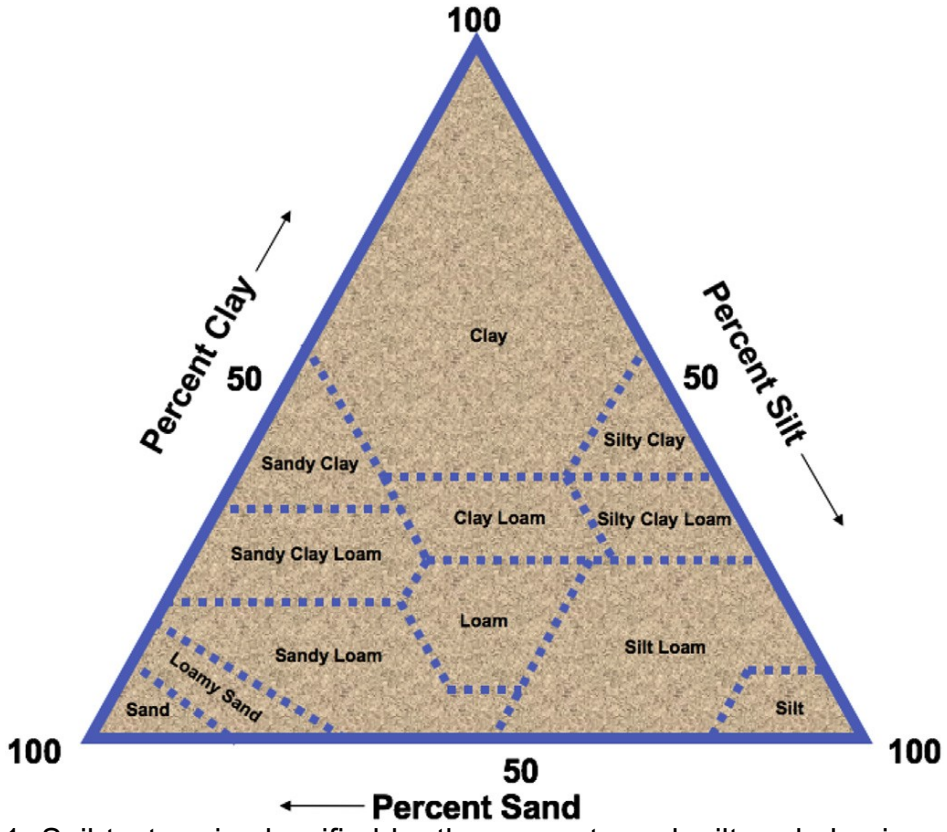

Figure 5.1. Soil texture is classified by the percent sand, silt and clay in relation to the soil texture triangle.[7, 11]

Various analytical methods for the determination of VOCs in multiple environmental matrices have been based on gas chromatography mass spectrometry (GC-MS), using either static or dynamic headspace [12], or HS solid phase microextraction (HS- SPME), as sample introduction modules.[10, 13-16] Other techniques, like liquid chromatography, supercritical fluid extraction or near infrared spectroscopy, have also been used.[17-20] HS sampling has been used successfully in qualitative and quantitative analysis of VOCs in soils. However, difficulties arise when using HS methods for quantitative analysis of VOCs in soil, because these methods rely on equilibrium partitioning of the analyte of interest

between the soil sample and the gas phase in the vial. Many studies have shown that the equilibrium partitioning can be altered by changing the heating temperature, time, and co-solvents used. These are indicated as possible approaches to overcome matrix dependency in HS analysis of soils.[13-14, 21]

Here, we explore the use of room temperature ionic liquids (RTILs) as solvents for HS-GC-MS quantification of BTEX from contaminated soils. RTILs are liquid organic, molten, or fused salts; they are a class of molecular ionic solvents with low melting points.[22] Ionic liquids [23] have garnered significant attention for their use in general analytical chemistry, in separation techniques, and in sample preparation methodologies.[24-28] RTILs can be ideal HS solvents due to their physiochemical properties, including negligible vapor pressure, wide liquid range, high viscosity, and tunable thermal stabilities.

The aim of this work was to evaluate the use of three hydrophilic RTILs (1-ethyl-3-methylimidazolium ethylsulfate ([EMIM][ESO_4]), 1-ethyl-3-methylimidazolium diethyl phosphate ([EMIM][DEP]), and tris(2-hydroxyethyl) methylammonium methylsulfate ([MTEOA][$MeOSO_3$])) and one hydrophobic RTIL (1-ethyl-3- methylimidazolium bis(trisfluoromethanesulfonyl)imide ([EMIM] [NTf2]), as solvents for homogenization of soil samples prior to HS sampling and GC-MS analysis. To the authors knowledge, this is the first time RTILs are utilized in HS analysis with soil being the environmental matrix. The RTILs were chosen in an attempt to increase sensitivity, improve measured accuracy, and normalize matrix effects caused by different soils, a problem pervasive in current standard methods. In comparison to current standard method USEPA 5021A,

BTEX response in varying certified reference soil compositions using RTILs was demonstrated to be statistically similar. Five samples with varying soil composition were collected and analyzed using the RTIL-based method from areas associated with UD activity.

5.2 Materials and Methods

5.2.1 Standards and Chemicals

Stock solutions were prepared in LC-MS grade analytical methanol (J.T. Baker; Phillipsburg, NJ) from a 2000 mg mL^{-1} BTEX calibration standard (Phenomenex, Inc.; Torrance, CA) and fluorobenzene (≥ 99.7%) (Sigma-Aldrich; St. Louis, MO), which was used as an internal standard (IS). Dilutions in methanol with 50 ng g^{-1} were used for calibration. To reduce losses by evaporation, the BTEX solutions were stored at 4℃ in sealed vials without free headspace. RTILs 1-ethyl-3-methylimidazolium ethyl sulfate ([EMIM][ESO_4]) (≥ 95%), 1-ethyl-3-methylimidazolium diethyl phosphate ([EMIM][DEP]) (≥ 95%), tris(2-hydroxyethyl) methylammonium methylsulfate ([MTEOA][$MeOSO_3$]) (≥ 95%) (Sigma-Aldrich; St. Louis, MO) and 1-ethyl-3-methylimidazolium bis(trisfluoromethanesulfonyl)imide ([EMIM][NTF2]) (99.9%) (Solvionic; France) were utilized as HS solvents. Certified reference material (CRM) soils clean sand #4, clean clay #5, clean sediment #2 (loam) and BTEX loamy sand #1 (Sigma-Aldrich; St. Louis, MO) were used as sample matrix.

5.2.2 Instrumentation and Parameters

Headspace sampling was performed with an AOC-5000 Plus (Shimadzu Scientific Instruments, Inc.; Columbia, MD) autosampler unit. Samples were

incubated and agitated at 100 ^{O}C for 30 min. A 2.5 mL SGE Diamond Headspace Syringe (Trajan Scientific and Medical; Victoria, Australia) was used to sample 750 mL with an injection speed of 500 mL s^{-1}. A GCMS TQ8040 (Shimadzu) gas chromatograph coupled to a triple quadrupole mass spectrometer was equipped with a Zebron ZB WAXplus (30 m x 0.25 mm x 0.2 mm) (Phenomenex) capillary column to carry out the separation and analysis following sample injection. The ZB WAXplus polyethylene glycol stationary phase allowed for complete separation of all 3 xylene isomers. The injection port temperature was 200 ℃ and a 10:1 split ratio was set. The carrier gas was helium with a constant linear velocity of 50 cm s^{-1}. The column oven temperature program began with an initial temperature of 35 ^{O}C for 2 min, and then temperature was increased at a rate of 20 ℃ min^{-1} up to 200 ℃, and held for 2 min. The run time was 12.25 min with BTEX eluting within 6 min, as depicted in figure 5.2. The ion source was operated in the electron ionization mode (EI; 70 eV, 230℃). Optimized multiple reaction monitoring (MRM) precursor-to-product ion transitions were recorded for the identification and determination of analytes, as delineated in table 5.1.

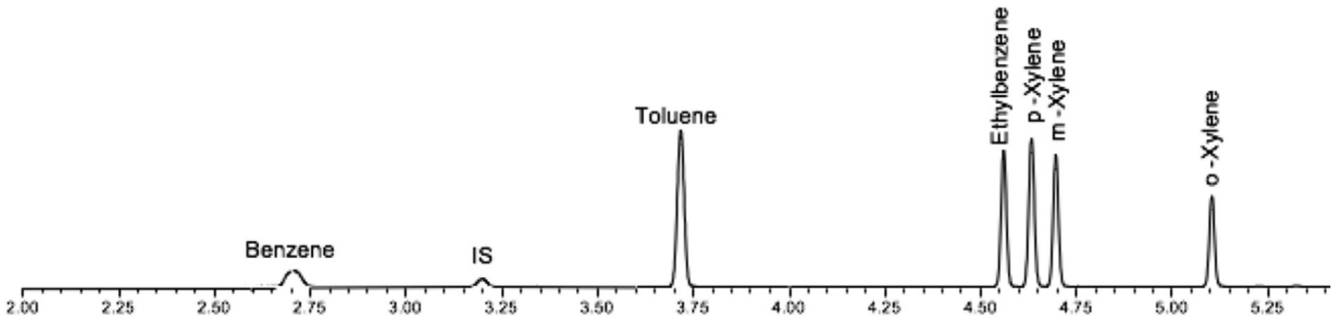

Figure 5.2. Chromatogram of sample 5, with complete separation of xylene isomers.

Table 5.1. Multiple reaction monitoring mode transition and settings for BTEX detection.

Compound Name	Start Time (min)	End Time (min)	Event Time (sec)	Ch1 *m/z*	Ch 1 CE	Ch 2 *m/z*	Ch 2 CE
Benzene	2.00	3.60	0.050	78 > 52	16	78 > 63	22
Fluorobenzene	2.00	3.60	0.050	96 > 70	14	96 > 63	22
Toluene	3.60	4.00	0.050	91 > 65	14	92 > 65	24
Ethylbenzene/*o*-Xylene	4.00	6.75	0.050	106 > 91	12	91 > 65	14
p- Xylene/*m*- Xylene	4.00	6.75	0.050	106 > 91	14	91 > 65	14

5.2.3 Preparation of Spiked Samples

250 mL (approximately 330 mg) of RTIL was pipetted into a 10 mL HS vial (Restek Corp.; Bellefonte, PA). 1.00 g of soil was placed in the HS vial, along with 50 mL total volume pipetted of BTEX standards with 50 ng g^{-1} of IS. The HS vial was immediately capped using a magnetic screw and

PTFE/silicone septa-based cap (Restek Corp.). The sample was vortexed for approximately 10 s or until the soil was fully wetted with RTIL. Each sample was left to equilibrate at room temperature for at least 30 min prior to analysis. Samples were prepared in triplicate.

5.2.4 Statistical Analysis

Non-parametric statistical analyses comparing two or more unpaired groups were performed using two-tailed Mann-Whitney and Kruskal-Wallis tests, respectively, in the GraphPad Prism Software suite.[29]

5.2.5 Soil Samples

Five soil samples were obtained from areas engaged in oilfield activities in the Permian Basin of west Texas, USA. Samples 1, 2, and 3, were soils obtained from a salt water disposal (SWD) facility. Sample descriptions include: Soil collecting runoff water from a truck discharge dock (Soil 1); soil from directly underneath a leaking fitting between produced water holding tanks (Soil 2); and from soil mixed with spilled solids from the sock filter onsite (Soil 3). Soil 4 was from an area near a decommissioned produced water retention pond. Soil 5 was comprised of soil obtained from a decommissioned produced water retention pond.

5.3 Results and Discussion

5.3.1 Exploratory Experiments

The three hydrophilic RTILs, [EMIM][ESO_4], [EMIM][DEP], and [MTEOA][$MeOSO_3$], were evaluated using sandy loam and sandy clay loam soils. Taking advantage of the thermal stabilities and negligible vapor pressures of the

RTILs, the samples were heated at 100 ℃ for 10 min and seven-point calibrations curves were obtained. In figure 5.3, it shows that significant variance between the sensitivity for BTEX compound determinations was not observed amongst the 3 ILs in sandy loam and sandy clay loam (p-values ranged between 0.900 and 0.979), which illustrates the normalization of BTEX response in different soil types.

5.3.2 Optimization of HS Equilibration time

Common soil HS methods that are deployed tend to have long heating equilibration times, averaging approximately 85 ℃ for nearly 45 min.[10, 14-15, 30] This is partially attributable to the boiling points of solvents commonly used in HS; higher temperatures cannot typically be used to shorten HS equilibration times. A two- step optimization process should be considered. The extraction conditions must be modified to establish that analytes of interest are not being retained by the matrix and establish a swift mass transfer.[19] In order to attain desired sensitivity, the time to reach HS equilibrium at 100 ℃ was optimized. [EMIM][ESO_4] was used as the HS solvent in CRM sand with spiked BTEX and IS. Samples were prepared in triplicate. In figure 5, it is shown that similar profiles were observed for all BTEX compounds with the maximum normalized response obtained in 20 min. After 30 min, normalized response for all BTEX compounds leveled out, which is a strong indication that HS equilibrium is being reached. Therefore, 30-min was selected as the optimal heating time, having relatively good efficiencies for all analytes of interest.

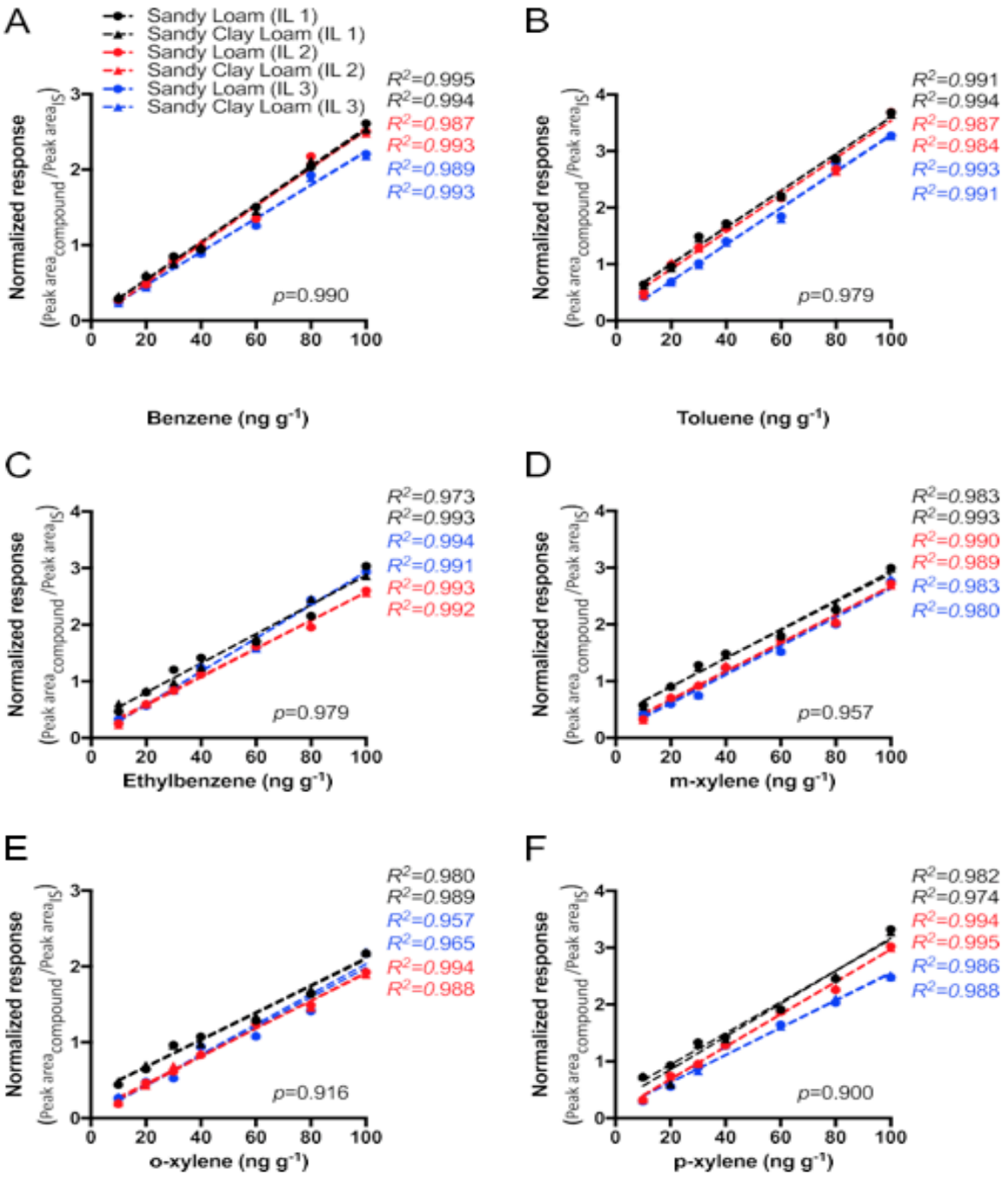

Figure 5.3. Calibration curves for benzene, toluene, ethylbenzene and xylene isomers utilizing [EMIM][ESO_4] (IL1), [EMIM][DEP] (IL2), and [MTEOA][$MeOSO_3$] (IL3) as a HS solvent in sandy loam and sandy clay loam soils.

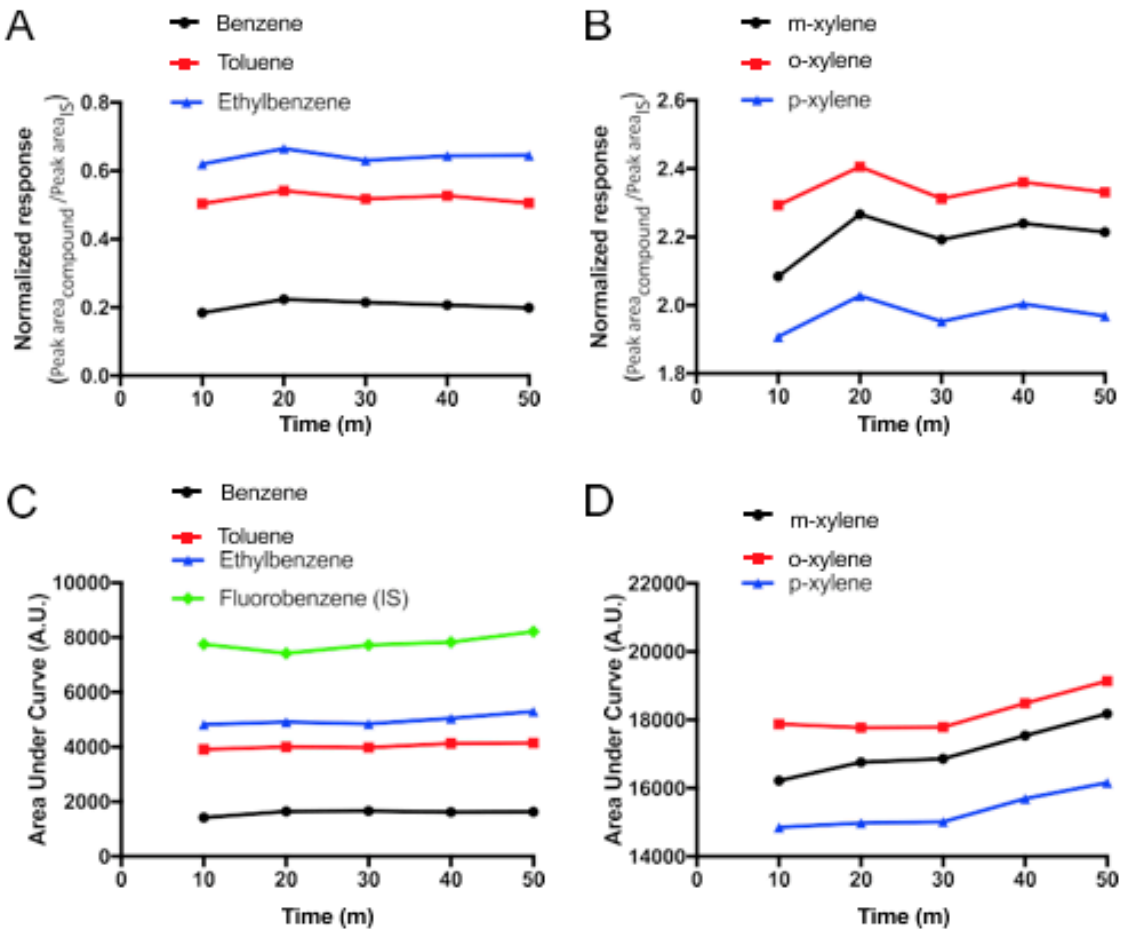

Figure 5.4 HS heating time optimization for benzene, toluene, ethylbenzene, and xylene isomers utilizing [EMIM][ESO_4] (IL1) as the HS in CRM sand, as illustrated by IS-normalized (A&B) and non-normalized (C&D) responses.

5.3.3 EPA Method with CRM Soils

The United States Environmental Protection Agency (USEPA) has various standard methods for analyzing VOCs in soil.[30-32] Utilizing USEPA method 5021A, 5-point calibration curves with CRM soils (sand, clay, and loam) were prepared in triplicate, in an effort to evaluate the statistical difference between calibration curves generated for BTEX in soils dissimilar in profile, shown in figure 5.5. The low concentration range was chosen to emulate concentrations of real life samples as observed by Varona-Torres and colleagues.[7] Significant variation was observed for sensitivity amongst the three soil types for *o*-xylene (p= 0.038), where the most notable pairwise difference was observed between the clay and sand soil textures (p= 0.032). This phenomenon was also observed with *m*- xylene (p= 0.0079), in addition to a significant difference between loam and sand (p= 0.016). The statistical difference between the different soil types using this method leads to a composition- specific response, which ultimately can affect both precision and accuracy in the quantification of BTEX. The decrease in linearity observed between BTEX and the differ types of soils can be attributed but not necessarily limited to, the absorption potential, biological activity, and actual composition of the soil.[30] USEPA method 5021A suggests modifying the pH of the HS solvent but also acknowledges that this approach varies by sample and that matrix effects are difficult, if not impossible, to overcome.[30]

With such a method, there is a higher dependence on compositional information, such as soil texture, to guide the accuracy of quantification (i.e.,

for the preparation of matrix-matched calibration standards). In a recent study, Varona-Torres and colleagues accounted for this when they analyzed a library of contaminated soils exhibiting highly variable textures. Using USEPA method 5021A, they matrix-matched each sample to a calibration curve with the corresponding soil texture.[7] However, this is a decidedly laborious process.

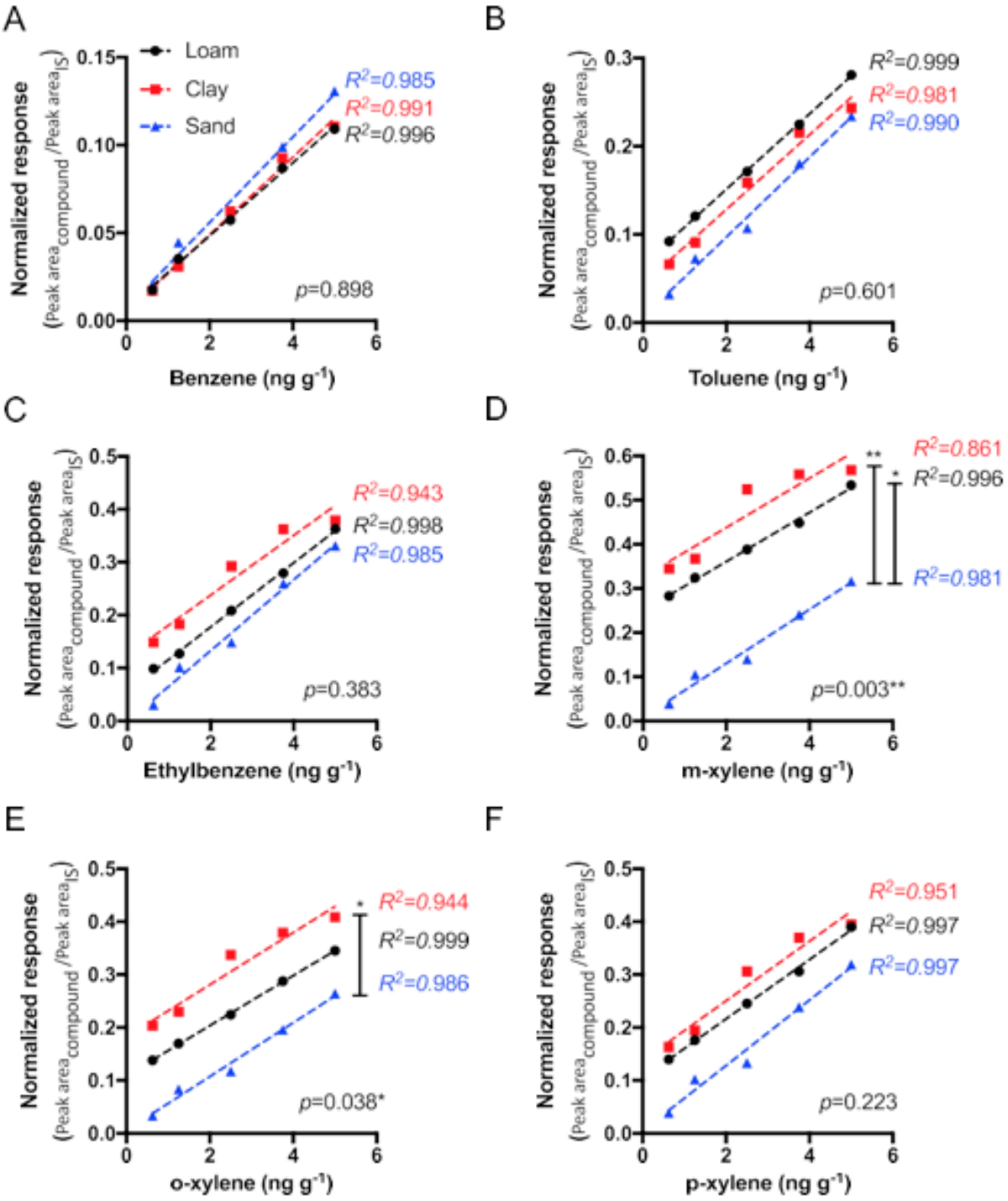

Figure 5.5. Low concentration calibration curves for benzene, toluene, ethylbenzene, and xylene isomers utilizing EPA 5021A in sand, clay and loam soils. *p*-values < 0.05*, <0.01**.

5.3.4 Optimized Method with CRM Soils

Calibration curves with CRM soils: Sand, clay, and loam were utilized in an effort to evaluate the normalization of matrix effects observed previously in soils dissimilar in profile. [MTEOA] [$MeOSO_3$] was used as the HS solvent because it was the most hydrophilic of the RTILs investigated in this study, based on its structure. Two 5- point calibration curve ranges were prepared in triplicate: a series of low-end concentrations (0.625 - 10 ng g^{-1}), shown in figure 5.6, and a series of broad range concentrations (0.700 - 10,000 ng g^{-1}) to show linearity was still observed at higher concentrations, as shown in figure 5.7. Significant variance was not observed amongst the three soil types with both concentration r ranges (*p*-values ranged between 0.725 and > 0.999). Along with creating a hydrophilic environment unfavorable to BTEX, the RTIL provides a salting-out effect that facilitates the extraction of VOCs from water and soil samples.[13, 16, 30, 32-33] Statistical similarities of BTEX response between the varying soils allow for better precision and accuracy in quantification. To demonstrate that hydrophilicity, and not just the physiochemical properties of RTILs, contribute to the normalization of matrix effects between soils, a hydrophobic RTIL [EMIM][NTf2] was evaluated shown in figure 5.8. [EMIM][NTf2] created a hydrophobic environment, which supported the interactions between BTEX and the soil, thus lowering the response and efficiency to liberate compounds into the headspace for analysis.

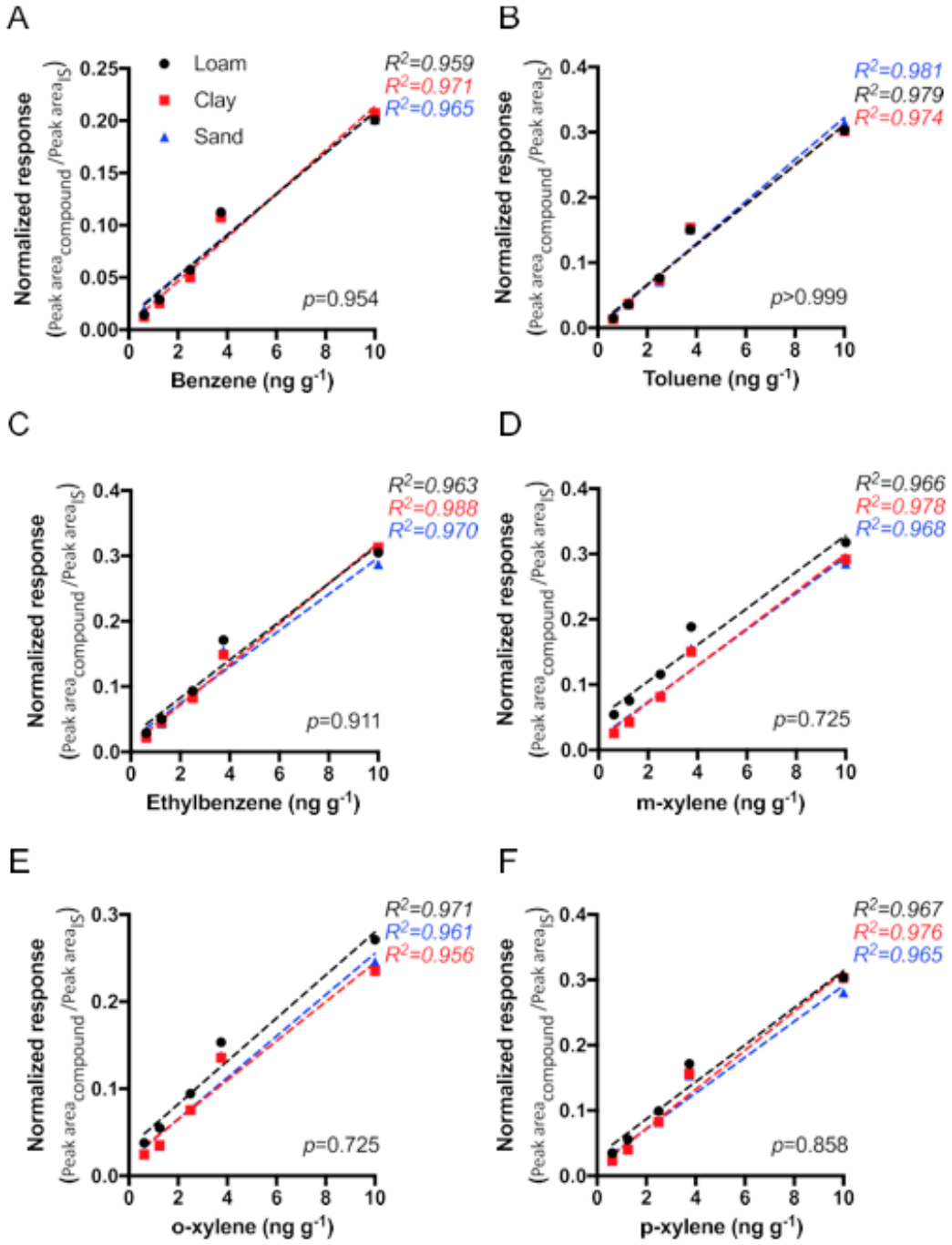

Figure 5.6. Low concentration calibration curves for benzene, toluene, ethylbenzene, and xylene isomers utilizing [MTEOA][$MeOSO_3$] as a HS solvent in sand, clay and loam soils.

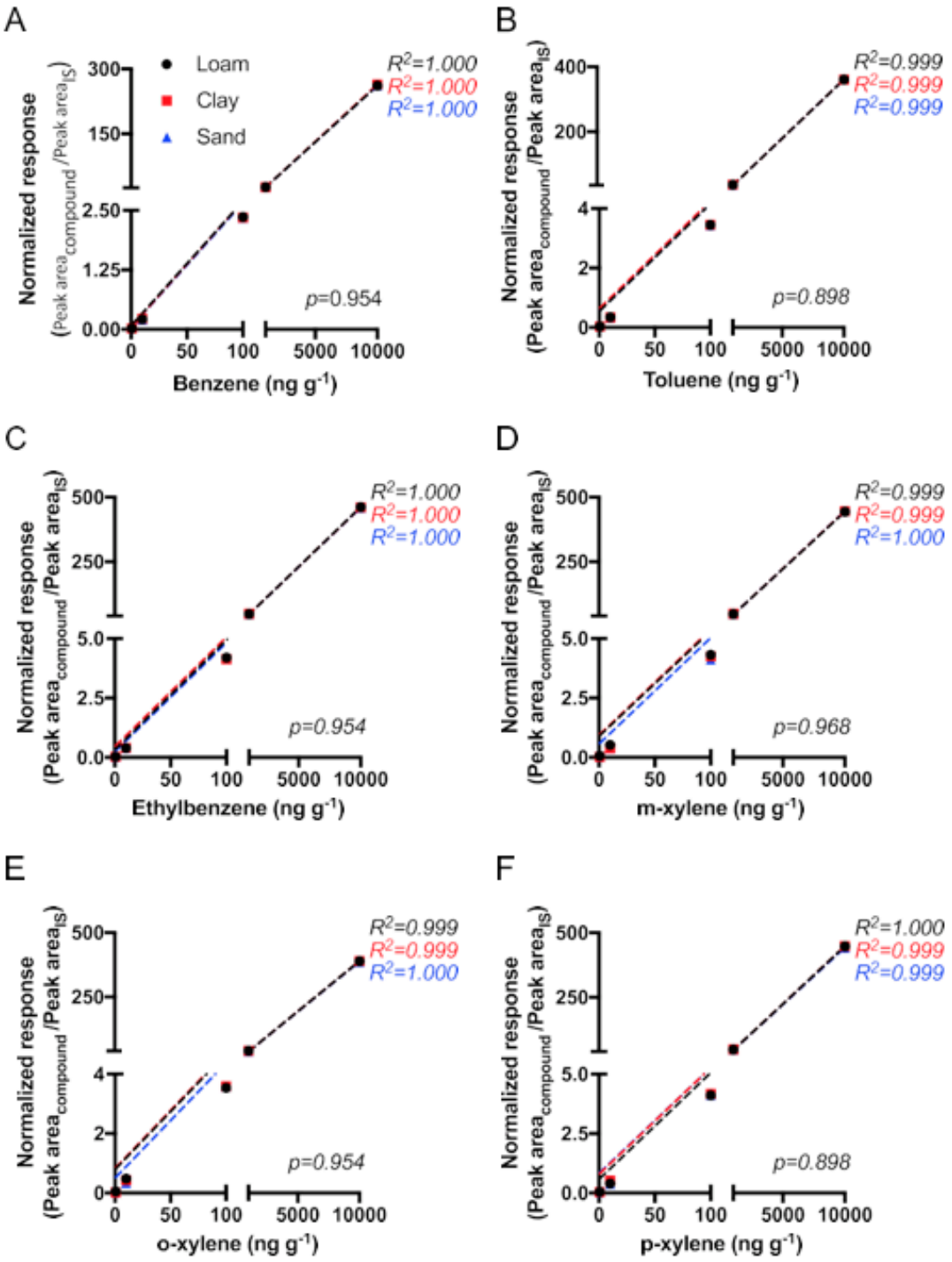

Figure 5.7 Broad concentration calibration curves for benzene, toluene, ethylbenzene, and xylene isomers utilizing [MTEOA][$MeOSO_3$] as a HS solvent in sand, clay and loam soils.

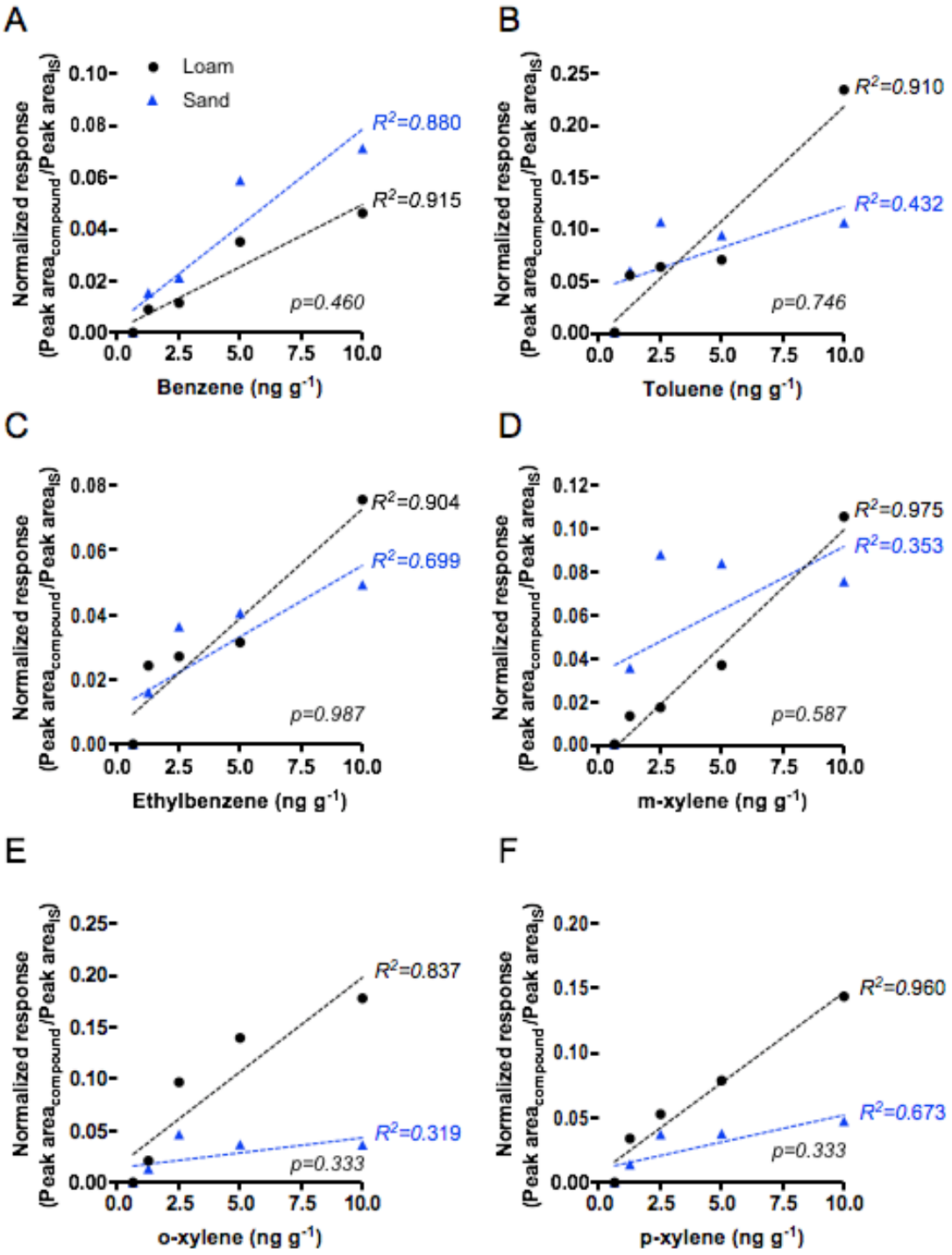

Figure 5.8. Calibration curves for benzene, toluene, ethylbenzene and xylenes isomers utilizing [EMIM][NTF2] as a HS solvent in sand and loam soils.

5.3.5 Method Validation (*LOQ, LOD, Linearity, Percent Recovery and RSD*)

Limit of quantification (LOQ) of the method was estimated from the analyte chromatogram with signal-to-noise ratio of 10. LOQ obtained were in the mid pg g^{-1} level in soil, as shown in table 5.2. LOQ observed are comparable to USEPA method 5021A of 500 pg g^{-1}.[30] Limit of detection (LOD) was determined experimentally and found to be 75 pg g^{-1} for all BTEX compounds. All 3 soils demonstrated r^2 values of above 0.99 for all BTEX compounds. To determine percent recovery and percent relative standard deviation (RSD), a CRM BTEX loamy sand #1 soil was used. The certified concentrations were as follows: 1520 ± 238, 3740 ± 794, 6420 ± 1,080, 9320 ± 1880 ng g^{-1} for BTEX, respectively along with other contaminants such as methyl *tert*-butyl ether, naphthalene, 1,2,4-trimethylbenzene, 1,3,5- trimethylbenzene. Weight-to- weight (w w^{-1}) dilutions were performed with CRM sand to obtain lower concentrations. Each sample was prepared in triplicate. The percent recovery ranged from 15 - 20%, 103 - 105%, 86 - 104%, and 82 - 99% for benzene, toluene, ethylbenzene and xylenes, respectively shown in table 5.2. The variations observed in the percent recoveries and percent RSDs, specifically for benzene, can be attributed to the samples not being prepared at 4 ℃ to minimize volatilization and a sample minimum of 5 g per recommendations of the certificate of analysis. EPA 5021A gives no recovery recommendations for BTEX, but the authors deemed recoveries (and the reproducibility of the recoveries) of all compounds besides benzene to be acceptable.[30]

Table 5.2 LOQ and % recovery determination using BTEX CRM soil Wt Wt^{-1} dilution with CRM sand. Concentrations are in pg g^{-1}

LOQ	[Benzene]	[Toluene]	[Ethylbenzene]	[Xylenes]
	575	300	500	300–550
	[Benzene]	[Toluene]	[Ethylbenzene]	[Xylenes]
BTEX CRM soil (x 10^6)	1.56 ± 0.05	3.85 ± 0.10	6.61 ± 0.20	9623 ± 300
Sand	0.24 ± 0.04	3.98 ± 0.40	5.75 ± 0.40	8164 ± 800
% Recovery	15	103	87	85
% RSD	17	10	7	10
Clay	0.24 ± 0.04	3.98 ± .40	5.88 ± 0.40	7909 ± 600
% Recovery	15	103	96	82
% RSD	17	10	7	8
Loam	0.24 ± 0.04	3.98 ± 0.40	5.71 ± 0.40	8.01 ± 0.60
% Recovery	15	103	86	83
% RSD	17	10	7	7
	[Benzene]	[Toluene]	[Ethylbenzene]	[Xylenes]
BTEX CRM soil (x 10^6)	0.75 ± 0.04	1.85 ± 0.09	3.19 ± 0.20	4.63 ± 0.20
Sand	0.15 ± 0.04	1.91 ± 0.40	3.25 ± 0.50	4.61 ± 0.80
% Recovery	20	103	102	99
% RSD	26	21	15	17
Clay	0.15 ± 0.03	1.96 ± 0.50	3.31 ± 0.60	4.52 ± 0.80
% Recovery	20	105	104	98
% RSD	20	25	18	18
Loam	0.15 ± 0.04	1.91 ± 0.40	3.22 ± 0.50	4.57 ± 0.50
% Recovery	20	103	101	99
% RSD	26	21	15	11

5.3.6 Soil Sample Analysis

Soil samples taken near unconventional oil and gas wastewater disposal sites were prepared in triplicate and spiked with IS. Samples were not dried prior to HS analysis, as this would promote the volatilization of the compounds of interest. The percent moisture content of the samples was found to be 2.02, 0.6, 0.87, 1.97, and 1.21% for samples 1 - 5, respectively. The soil texture classification for the samples was determined to be clay loam, sand, clay loam, clay, and loam for samples 1 - 5, respectively. Samples 3 and 5 were the only samples with quantifiable amounts of all BTEX compounds. Samples 1 and 4 exhibited BTEX below the LOQ, and no BTEX compounds were detectable in sample 2. Table 5.3, shows the quantitative data of the samples in relation to the calibration curves made with the CRM soils. It is important to

note that for calibration curves performed using CRM soils, the analytes were incorporated by adsorption (30 min of interaction prior to analysis), a mechanism in which dispersion, hydrogen-bond and Π- / n- electrons interactions prevail.[34] Thus, the desorption process of BTEX in the CRM soil with RITL may be different from that of long term contaminated soil where the analytes are incorporated by sequestration.

Table 5.3 Quantitative data of samples (3 and 5) utilizing all 3 CRM calibration curves.

ng g^{-1}

Soil 3	Sand CRM	Sediment (loam) CRM	Clay CRM
Benzene	68 ± 30	67 ± 30	67 ± 29
Toluene	210 ± 71	210 ± 71	208 ± 71
Ethylbenzene	114 ± 28	112 ± 28	102 ± 29
p- Xylene	61 ± 21	66 ± 21	60 ± 21
m- Xylene	39 ± 14	38 ± 14	38 ± 14
o- Xylene	635 ± 200	624 ± 200	615 ± 200
Soil 5	**Sand CRM**	**Sediment (loam) CRM**	**Clay CRM**
Benzene	71 ± 8	70 ± 8	70 ± 8
Toluene	330 ± 40	330 ± 40	327 ± 40
Ethylbenzene	155 ± 25	153 ± 25	144 ± 26
p- Xylene	176 ± 26	179 ± 26	174 ± 26
m- Xylene	152 ± 23	146 ± 23	142 ± 23

5.4 Conclusions

The use of hydrophilic RTILs in HS-GC-MS is a suitable method to normalize the matrix effects from BTEX determination in contaminated soils. Matrix-matching soil composition is no longer a critical variable affecting sample preparation, or the accuracy of quantification of BTEX when using RTILs as a headspace solvent. The sample preparation is less exhaustive and reasonably inexpensive; that offers an alternative to

other extractions techniques, such as multiple HS-SPME and purge and trap. The decreased vapor pressure of RTILs and GC separation using a polyethylene glycol phase are two components of this method that drastically reduce analysis time. Additional monitoring information is gleaned by the resolution of m- and p-xylene isomers by this stationary phase.

The results obtained under equilibrium conditions using RTILs were statistically similar between the different soil textures. This allows for less dependence on sample information, i.e. the determination of soil texture, moisture content, and pH, prior to analysis. Measured BTEX concentration values in the varying certified soils were statistically equivalent and accurate according to the specifications of the CRM. This helped demonstrate that the matrix effects caused by the different soils had been normalized across soil textures.

5. References

1. Varona-Torres, E.; Carlton, D. D.; Hildenbrand, Z. L.; Schug, K. A., Matrix-effect-free determination of BTEX in variable soil compositions using room temperature ionic liquid co-solvents in static headspace gas chromatography mass spectrometry. *Analytica Chimica Acta* **2018,** *1021*, 41-50.
2. Hildenbrand, Z. L.; Mach, P. M.; McBride, E. M.; Dorreyatim, M. N.; Taylor, J. T.; Carlton, D. D.; Meik, J. M.; Fontenot, B. E.; Wright, K. C.; Schug, K. A.; Verbeck, G. F., Point source attribution of ambient contamination events near unconventional oil and gas development. *Science of The Total Environment* **2016,** *573*, 382-388.
3. Payne, B. F.; Ackley, R.; Paige Wicker, A.; Hildenbrand, Z. L.; Carlton, D. D.; Schug, K. A., Characterization of methane plumes downwind of natural gas compressor stations in Pennsylvania and New York. *Science of The Total Environment* **2017,** *580*, 1214-1221.
4. Hildenbrand, Z. L.; Carlton, D. D.; Fontenot, B. E.; Meik, J. M.; Walton, J. L.; Taylor, J. T.; Thacker, J. B.; Korlie, S.; Shelor, C. P.; Henderson, D.; Kadjo, A. F.; Roelke, C. E.; Hudak, P. F.; Burton, T.; Rifai, H. S.; Schug, K. A., A Comprehensive Analysis of Groundwater Quality in The Barnett Shale Region. *Environmental Science & Technology* **2015,** *49* (13), 8254-8262.
5. Hildenbrand, Z. L.; Carlton, D. D.; Fontenot, B. E.; Meik, J. M.; Walton, J. L.; Thacker, J. B.; Korlie, S.; Shelor, C. P.; Kadjo, A. F.; Clark, A.; Usenko, S.; Hamilton, J. S.; Mach, P. M.; Verbeck, G. F.; Hudak, P.; Schug, K. A., Temporal variation in groundwater quality in the Permian Basin of Texas, a region of increasing unconventional oil and gas development. *Science of The Total Environment* **2016,** *562*, 906-913.
6. Burton, T. G.; Rifai, H. S.; Hildenbrand, Z. L.; Carlton, D. D.; Fontenot, B. E.; Schug, K. A., Elucidating hydraulic fracturing impacts on groundwater quality using a regional geospatial statistical modeling approach. *Science of The Total Environment* **2016,** *545-546*, 114-126.
7. Varona-Torres, E.; Carlton, D. D.; Payne, B.; Hildenbrand, Z. L.; Schug, K. A., Chapter Twelve - The Characterization of BTEX in Variable Soil Compositions Near Unconventional Oil and Gas Development. In *Advances in Chemical Pollution, Environmental Management and Protection*, Schug, K. A.; Hildenbrand, Z. L., Eds. Elsevier: 2017; Vol. 1, pp 321-351.
8. Acosta-Martínez, V.; Dowd, S.; Sun, Y.; Allen, V., Tag-encoded pyrosequencing analysis of bacterial diversity in a single soil type as affected by management and land use. *Soil Biology and Biochemistry* **2008,** *40* (11), 2762-2770.
9. Mendes, L. W.; Tsai, S. M.; Navarrete, A. A.; de Hollander, M.; van Veen, J. A.; Kuramae, E. E., Soil-Borne Microbiome: Linking Diversity to Function. *Microbial Ecology* **2015,** *70* (1), 255-265.
10. Ezquerro, Ó.; Ortiz, G.; Pons, B.; Tena, M. a. T., Determination of benzene, toluene, ethylbenzene and xylenes in soils by multiple headspace solid-phase microextraction. *Journal of Chromatography A* **2004,** *1035* (1), 17-22.
11. Soil classification United States Department of Agriculture. http://www.nrcs.usda.gov/.
12. Griffiths, J., A Brief History of Mass Spectrometry. *Analytical Chemistry* **2008,** *80* (15), 5678-5683.
13. Shin, H.-S., Determination of MTBE, TBA and BTEX in soil by headspace gas chromatography-mass spectrometry. *Bulletin of the Korean Chemical Society* **2012,** *33*.

14. Voice, T. C.; Kolb, B., Static and dynamic headspace analysis of volatile organic compounds in soils. *Environmental Science & Technology* **1993,** *27* (4), 709-713.
15. Esteve-Turrillas, F. A.; Armenta, S.; Garrigues, S.; Pastor, A.; de la Guardia, M., Headspace–mass spectrometry determination of benzene, toluene and the mixture of ethylbenzene and xylene isomers in soil samples using chemometrics. *Analytica Chimica Acta* **2007,** *587* (1), 89-96.
16. Llompart, M.; Li, K.; Fingas, M., Headspace solid phase microextraction (HSSPME) for the determination of volatile and semivolatile pollutants in soils. *Talanta* **1999,** *48* (2), 451-459.
17. Yang, Y.; Jones, A. D.; Eaton, C. D., Retention Behavior of Phenols, Anilines, and Alkylbenzenes in Liquid Chromatographic Separations Using Subcritical Water as the Mobile Phase. *Analytical Chemistry* **1999,** *71* (17), 3808-3813.
18. Buerck, J.; Roth, S.; Kraemer, K.; Scholz, M.; Klaas, N., Application of a fiber-optic NIR-EFA sensor system for in situ monitoring of aromatic hydrocarbons in contaminated groundwater. *Journal of Hazardous Materials* **2001,** *83* (1), 11-28.
19. Pawliszyn, J., Kinetic Model of Supercritical Fluid Extraction. *Journal of Chromatographic Science* **1993,** *31* (1), 31-37.
20. Langenfeld, J. J.; Hawthorne, S. B.; Miller, D. J.; Pawliszyn, J., Effects of temperature and pressure on supercritical fluid extraction efficiencies of polycyclic aromatic hydrocarbons and polychlorinated biphenyls. *Analytical Chemistry* **1993,** *65* (4), 338-344.
21. Kolb, B.; Welter, C.; Bichler, C., Determination of partition coefficients by automatic equilibrium headspace gas chromatography by vapor phase calibration. *Chromatographia* **1992,** *34* (5), 235-240.
22. Anderson, J. L.; Armstrong, D. W.; Wei, G.-T., Ionic Liquids in Analytical Chemistry. *Analytical Chemistry* **2006,** *78* (9), 2892-2902.
23. Wilkes, J. S.; Levisky, J. A.; Wilson, R. A.; Hussey, C. L., Dialkylimidazolium chloroaluminate melts: a new class of room-temperature ionic liquids for electrochemistry, spectroscopy and synthesis. *Inorganic Chemistry* **1982,** *21* (3), 1263-1264.
24. Liu, F.-h.; Jiang, Y., Room temperature ionic liquid as matrix medium for the determination of residual solvents in pharmaceuticals by static headspace gas chromatography. *Journal of Chromatography A* **2007,** *1167* (1), 116-119.
25. Liu, R.; Liu, J.-f.; Yin, Y.-g.; Hu, X.-l.; Jiang, G.-b., Ionic liquids in sample preparation. *Analytical and Bioanalytical Chemistry* **2009,** *393* (3), 871-883.
26. Poole, C. F.; Poole, S. K., Extraction of organic compounds with room temperature ionic liquids. *Journal of Chromatography A* **2010,** *1217* (16), 2268-2286.
27. Laus, G.; Andre, M.; Bentivoglio, G.; Schottenberger, H., Ionic liquids as superior solvents for headspace gas chromatography of residual solvents with very low vapor pressure, relevant for pharmaceutical final dosage forms. *Journal of Chromatography A* **2009,** *1216* (32), 6020-6023.
28. Baltazar, Q. Q.; Leininger, S. K.; Anderson, J. L., Binary ionic liquid mixtures as gas chromatography stationary phases for improving the separation selectivity of alcohols and aromatic compounds. *Journal of Chromatography A* **2008,** *1182* (1), 119-127.
29. suite GPS, One-way ANOVA followed by Dunnett's multiple comparisons test was performed using GraphPad Prism version 7.00 for Windows. . www. graphpad.com.
30. USEPA *Method 5021A: volatile organic compounds by gaschromatography/mass spectrometry (GC/MS)*.

31. USEPA, Volatile Organic Compounds by Gas Chromatography/Mass Spectrometry in Method 8260B.
32. USEPA, Closed System Purge and Trap and Extraction for VOlatile Organics in Soil and Waste Samples. In Method 5035A.
33. Alonso, M.; Castellanos, M.; Besalú, E.; Sanchez, J. M., A headspace needle-trap method for the analysis of volatile organic compounds in whole blood. *Journal of Chromatography A* **2012,** *1252*, 23-30.
34. Serrano, A.; Gallego, M., Sorption study of 25 volatile organic compounds in several Mediterranean soils using headspace–gas chromatography–mass spectrometry. *Journal of Chromatography A* **2006,** *1118* (2), 261-270.

Chapter 6: Thermodynamic Characterization of interactions between Environmental Contaminants and RTILs by Static Headspace Gas Chromatography Vacuum Ultraviolet Detection

6.1 Introduction

Understanding the thermodynamics associated with interactions between an analyte and a solvent can improve the selection of a solvent for a specific task. Here, is investigated the interactions between a room temperature ionic liquid (RTIL) and analytes for the headspace analysis of environmental contaminants. Measurement of a partition coefficient (Kp), the ratio between the analyte concentration in the sample phase ($[X]_S$) and the analyte concentration in the gas phase ($[X]_G$) at equilibrium, under various temperatures allows for the determination of thermodynamic properties, such as the entropy (ΔS) and enthalpy (ΔH), through the creation of van't Hoff plots, as discussed in chapter 1 section 1.3.1. In static headspace gas chromatography (SHS-GC), Kp determinations are performed by two methods: vapor phase calibration (VPC) and phase ratio variation (PRV).[1-2] The experiments discussed within this chapter are based on the VPC method.

The vapor phase calibration (VPC) method was developed by Kolb and colleagues in 1992.[2] The VPC method relies on two sets of conditions. The first is an external calibration curve where a known concentration of the pure analyte is completely vaporized into the headspace and analyzed under the established experimental conditions. Alone, this technique is referred to as the total vaporization technique (TVT).[3] In the second set of conditions, the same amount of analyte used in TVT is added to the vials containing a known constant volume of the sample phase. This is referred to as the sample set. Peak area response is then plotted against concentration or amount added for both conditions,

and a linear regression analysis is performed. By knowing experimental conditions, such as vial volume (V_V), sample phase volume (V_S) and volume of the gas phase (V_G), the Kp can be determined as shown in equation 6.1, where $A_{Vap}\ and\ A_S$ are the slope of the regression line for the analyte in the vapor standard and sample set respectively.

$$Kp = \frac{A_{Vap}V_V - A_S V_G}{A_S V_S} \text{ (Equation 6.1)}$$

The phase ratio variation (PRV) method was introduced by Ettre and colleagues in 1993.[1] The PRV method utilizes the a standard solution containing a known concentration of the analyte, and the phase ratio (β) between the condensed phase and the headspace is varied. This method is based on the relationship between the reciprocal of the peak area (1/PA) and the β of the sample phase in the vial. The determination of the partition coefficient is derived from linear regression analysis of the 1/PA vs. β, as shown in equation 6.2 where A' and B', are the slope and the intercept of the linear regression analysis. Accuracy of this method diminishes with analytes with larger Kp values, as the absolute differences in peak areas are minimal, as the β is varied.[4]

$$Kp = \frac{B'}{A'} \text{ (Equation 6.2)}$$

The objective of this study is to determine the thermodynamic properties of environmental contaminants in 3 hydrophilic RTILs, specifically 1-ethyl-3-methylimidazolium ethylsulfate ([EMIM][ESO_4]), 1-ethyl-3-methylimidazolium diethylphosphate ([EMIM][DEP]), tris(2-hydroxyethyl)methylammonium methylsulfate ([MTEOA][$MeOSO_3$]), and one hydrophobic RTIL, (1-ethyl-3-methylimidazolium bis(trisfluoromethanesulfonyl)imide ([EMIM] [NTf2]). The structures of these RTILs is given in figure 6.1. The pseudo-absolute quantitative

capabilities of the vacuum ultraviolet detector (VUV) (discussed in chapter 1 section 1.4.2) were utilized to perform the PRV method, and the results were compared to those obtained by the widely accepted VPC method.

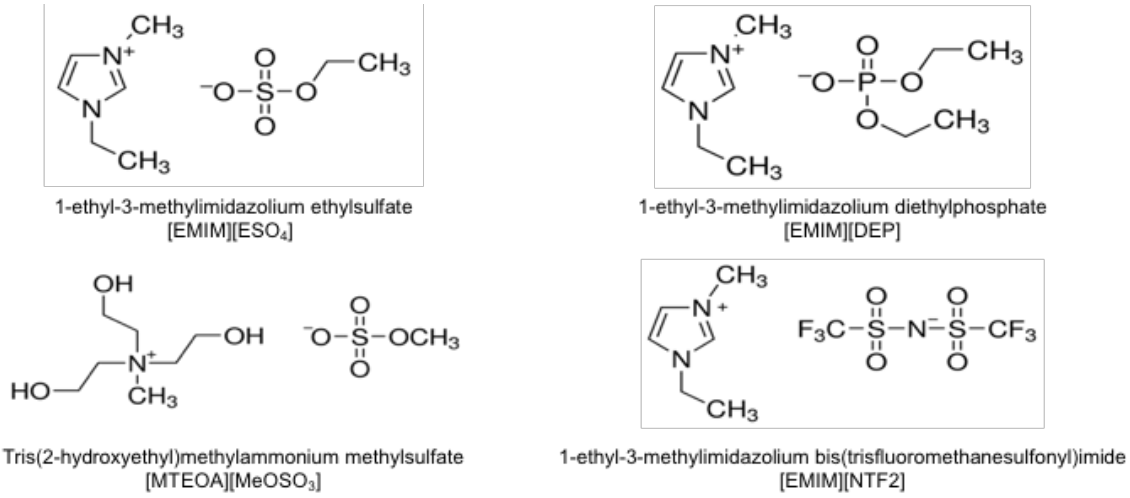

Figure 6.1. Chemical structures of RTILs being investigated.

6.2 Materials and Methods

6.2.1 Standards and Chemicals

Stock solutions were prepared in ACS-Grade (≥ 99.5%) dichloromethane (MilliporeSigma; St.Louis MO) with analytical standards (≥ 99.9%): benzene, toluene, ethylbenzene, m-xylene, p-xylene, o-xylene, octane, chlorobenzene (MilliporeSigma) and cyclohexane (≥ 99 %) (MilliporeSigma). To reduce losses by evaporation, the standards were stored at 4 ℃ in sealed vials without free headspace. Fresh standards were prepared weekly. RTILs 1-ethyl-3-methylimidazolium ethylsulfate ([EMIM][ESO_4]) (≥ 95%), 1-ethyl-3-methylimidazolium diethylphosphate ([EMIM][DEP]) (≥ 95%), tris(2-hydroxyethyl)methylammonium methylsulfate ([MTEOA][$MeOSO_3$]) (≥ 95%) (MilliporeSigma) and 1-ethyl-3-methylimidazolium

bis(trisfluoromethanesulfonyl)imide ([EMIM][NTF2]) (99.9%) (Solvionic; France) and 18.23 $M\Omega$ purified water were used as HS solvents.

6.2.2 Instrumentation and Parameters

Headspace (HS) sampling was performed with the HS-20 (Shimadzu Scientific Instruments, Inc.; Columbia, MD), a pressure loop autosampler unit. Samples were incubated and agitated for 30 min at varying temperatures (70-100 ℃). Both the sample loop and transfer line temperature matched the incubation temperature. All of the HS vials were pressurized with Ar gas to 55 kPa for 2 mins and equilibrated for 2 mins. The sample loop was opened for 15 sec and left to equilibrate for 15 sec. Injection time was set to 3 sec. Chromatographic analysis and detection were performed using a GC 2010Plus (Shimadzu) gas chromatograph coupled to a VGA-100 (VUV Analytics, Inc., Cedar Park, TX) vacuum ultraviolet spectrophotometer (125-240 nm). The VGA Model & Analyze software was used; this software has features for deconvolution of co-eluting analytes and pseudo-absolute quantitation. The GC was equipped with a Rtx-VMS (30 m x 0.32 mm x 1.80 μm) (Restek Corp. Bellefonte, PA) capillary column to carry out the separation and analysis following sample injection. Chromatographic separation was established using the Pro EZGC Chromatogram Modeler by Restek.[5] The injection port temperature was 200 ℃, operated in spitless mode, with a hold time of 60 sec. The carrier gas was hydrogen with a constant linear velocity of 50 cm s^{-1}. The column oven temperature program began with an initial temperature of 35 ℃ for 2 min, and

then temperature was increased 25 ℃ min^{-1} up to 225 ℃, and held for 2 min, as shown in Figure 6.2. The VUV detector spectral acquisition rate was set to 4 Hz, the make-up gas (N_2) was set to 1.00 psi, and the transfer line and flow cell were set to 275 ℃. A ProFLOW 6000 electronic flowmeter (Restek Corp.) was used to record the exit port flow rate.

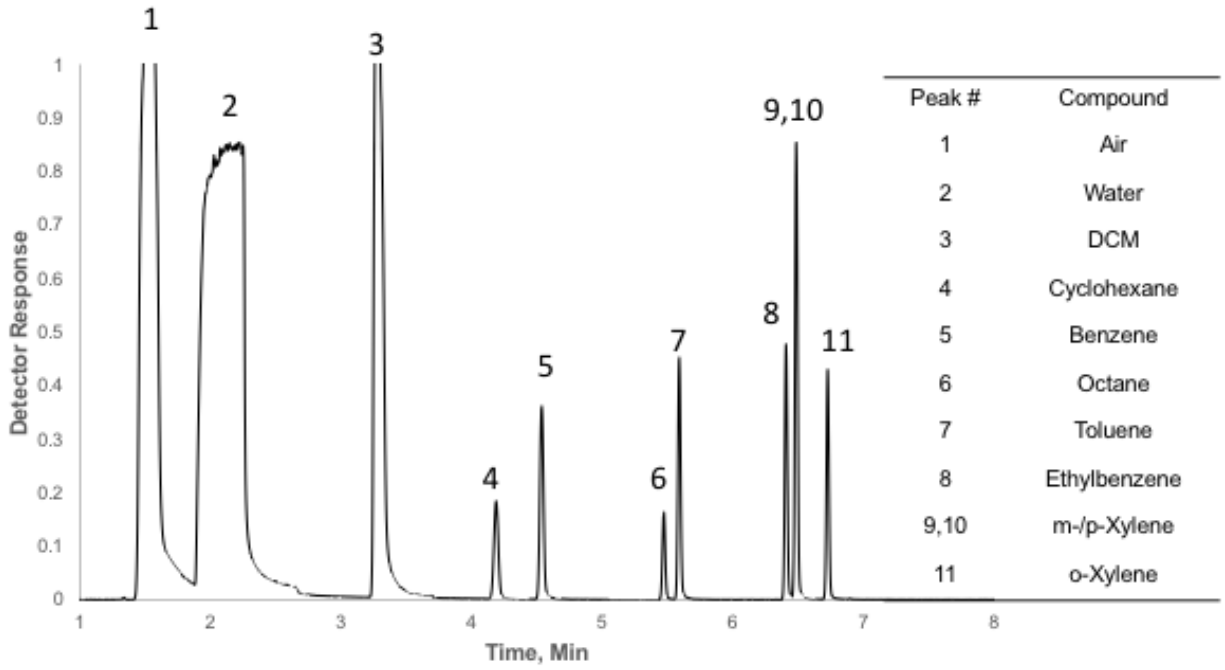

Figure 6.2. Chromatogram of analytes of interest with water as the HS solvent.

6.2.3 Headspace Vial Volume Determination

In order to determine the actual vial volume of the 10 mL headspace sample vial (Restek), 5 empty headspace vials were individually weighed on an analytical balance. The Vials were then filled with water completely and reweighed. The volume of the vial

was determined using the density of value of water 0.998 g ml^{-1} at 20 ℃. The results are tabulated on table 6.1. The actual volume of the 10 mL headspace vial was determined to be 11.1 ± 0.1 mL, and this value was used throughout the study.

Table 6.1. Determination of headspace vial volume (V_V).

10 mL HS Vial	Empty Weight (g)	Full Weight (g)	Weight Differnce (g)	Actual Vial Volume (mL)
1	10.07762	21.20945	11.13183	11.15413828
2	10.12103	21.21373	11.0927	11.11492986
3	10.1035	21.0219	10.9184	10.94028056
4	10.18016	21.21138	11.03122	11.05332665
5	10.17567	21.26907	11.0934	11.11563126
			Avg.	11.1
			Stdev.	0.1

6.2.4 Sample Preparation

Standard solutions of the analytes were prepared at approximately 5000, 10,000, 15,000, 20,000 and 30,000 $\mu g\ ml^{-1}$ concentration in DCM using a 5 mL grade A volumetric flask. A volume of 1 μL of these solutions was added to individual empty headspace vials using the Merlin MicroShot Injector from Restek Corp. and immediately capped; creating a 5-point calibration curve. This resulted in a known ng mL^{-1} of the analyte in the headspace that can be used for calibration. Sample vials were prepared by adding 1 mL of the RTIL using a the MICROMAN E M1000, positive dispensing pipette (Gilson Inc., Middleton WI) followed by 1 μL of the standard solution and immediately capped. β was 10.1. All samples were prepared in triplicate. Blank and control samples were prepared to contain just ionic liquid, just the calibration mix, and an empty vial with nothing added.

6.2.5 Background Measurements of RTILs

In order to measure background vapor (i.e. impurities) above the RTILs, 1 mL of the RTIL was dispensed into the HS vial with a positive dispensing pipette and capped. The HS vial was then analyzed at the highest temperature utilized in the experiment (110 ℃). The chromatograms of the background vapor from RTILs can be seen in figure 6.3. Analyte identification was performed by matching the absorbance spectrum to the VUV library database. To rid the RTILs of background vapors, approximately 100 g of the RTIL was placed into a double neck, 250 mL round bottom flask and placed in an oil bath at 70 ℃ with N_2 vigorously bubbling through the RTIL for approximately 24 hours. The result of this treatment is shown in figure 6.4. This cleaning treatment was sufficient to rid of the excess vapors in the RTILs.

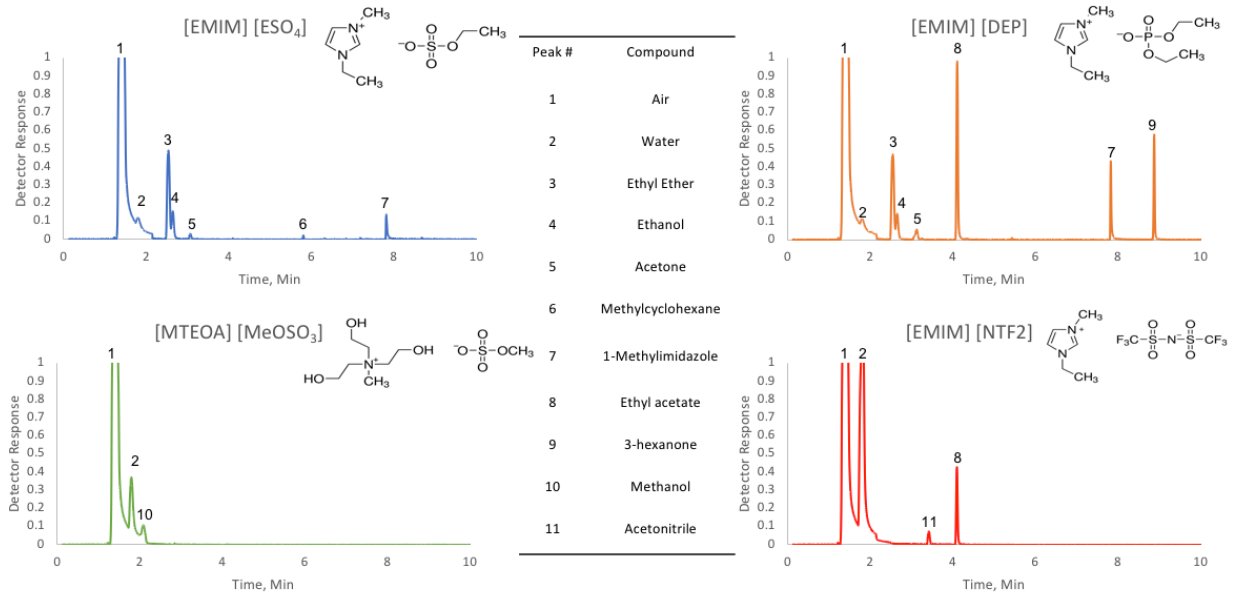

Figure 6.3. Chromatograms and peak identification of background vapor in RTILs.

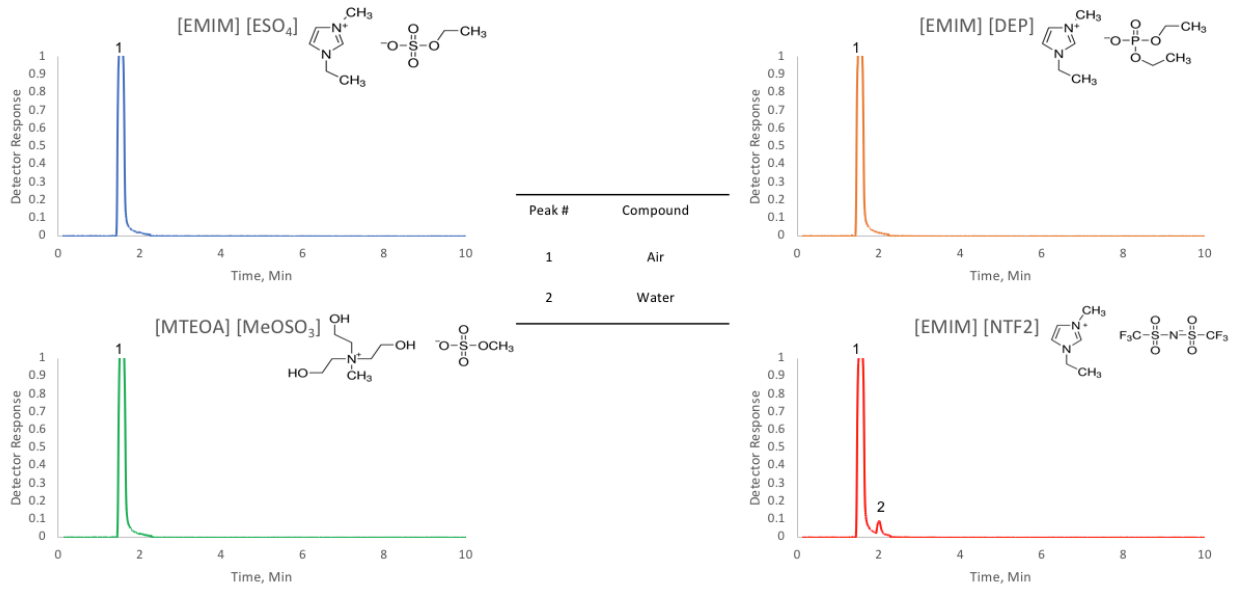

Figure 6.4. Chromatograms and peak identification of clean RTILs.

6.2.6 Pseudo-Absolute Quantification

In headspace pressure-loop systems, it is considered nearly impossible to determine how much sample volume actually made it to the GC system due to the various pressures, temperature, and flow rates the gaseous sample experiences, as discussed in chapter 2 section 2.2.2. Thus, the determination of the concentration of the analyte in the gas phase ($[X]_G$) depends on calibration curves.

The GC-VUV has the ability to quantify and identify analytes based on their known absorption cross-section of the gas phase molecules within the spectral regime (125-240 nm), as discussed in chapter 1 section 1.4.2. The measured absorbance spectra for the analytes were compared to their respective cross-sections to confirm identification. Figure 6.5 and table 6.2, show the recorded normalized cross-sections of the analytes investigated in this study (octane, cyclohexane, benzene, toluene, ethylbenzene,

chlorobenzene, and xylene isomers) and the average cross-sections used in the study. Chemical structures of the analytes being investigated are shown in figure 6.6. When the cross-section of an analyte is known along with the detector scan rate, the flow cell path length and carrier gas flow rate at the exit port, the number of molecules that reached the detector can be determined directly from the peak area as shown in equation 6.3:

$$PA = \frac{1}{\ln(10)} R \frac{d}{F} \Sigma N_{Det} \quad \text{(Equation 6.3)}$$

where *PA* is the sum of chromatographic scans over the time region of the time region (i.e., peak area), N_{Det} is the total number of analyte molecules introduced to the detector, *R* is the detector scan rate $(scans\ min^{-1})$, *d* is the flow cell path length (cm), *F* is the sample flow rate $(mL\ min^{-1})$, and Σ is the absorption cross-section over the same wavelength region as the measured absorbance. The number of molecules determined in the detector would be theoretically equal to the amount in the sample if perfect transfer of the analyte was attained without any losses.[7]

Spiking an empty vial with a known concentration of the analyte into an empty HS vial with a known volume, results in a known concentration of the gas phase. The utilization of a pressure-loop HS system, allows one to set a constant pressurization of the vial and thus, ideally leading to the same constant "unknown volume" to reach the GC. With the use of VUV detection and equation 6.3, the determination of N_{Det} can be used to determine the "actual volume" of analyte sample that made it to the GC. This, in turn, allows for determination of the analyte gas phase concentration in a sample vial and the direct determination of Kp via rearrangement of the HS equation, shown in equation 6.4:

$$[X]_G = \frac{[X]_0}{Kp+\beta}$$ (Equation 6.4)

where $[X]_0$ is the original analyte concentration in the solution, $[X]_G$ is the concentration of the analyte in the gas phase at equilibrium, and β is the phase ratio.

Table 6.2. Average cross-sections of analytes in the 125 – 240 nm range.

Compound	$\boldsymbol{\Sigma_{125-240\,nm},\ cm^2\ molecules^{-1}}$
Octane	1.47E-17
Cyclohexane	9.89E-18
Benzene	3.67E-17
Chlorobenzene	3.92E-17
Ethylbenzene	4.21E-17
Toluene	3.91E-17
m-Xylene	4.97E-17
p-Xylene	4.86E-17
o-Xylene	4.78E-17

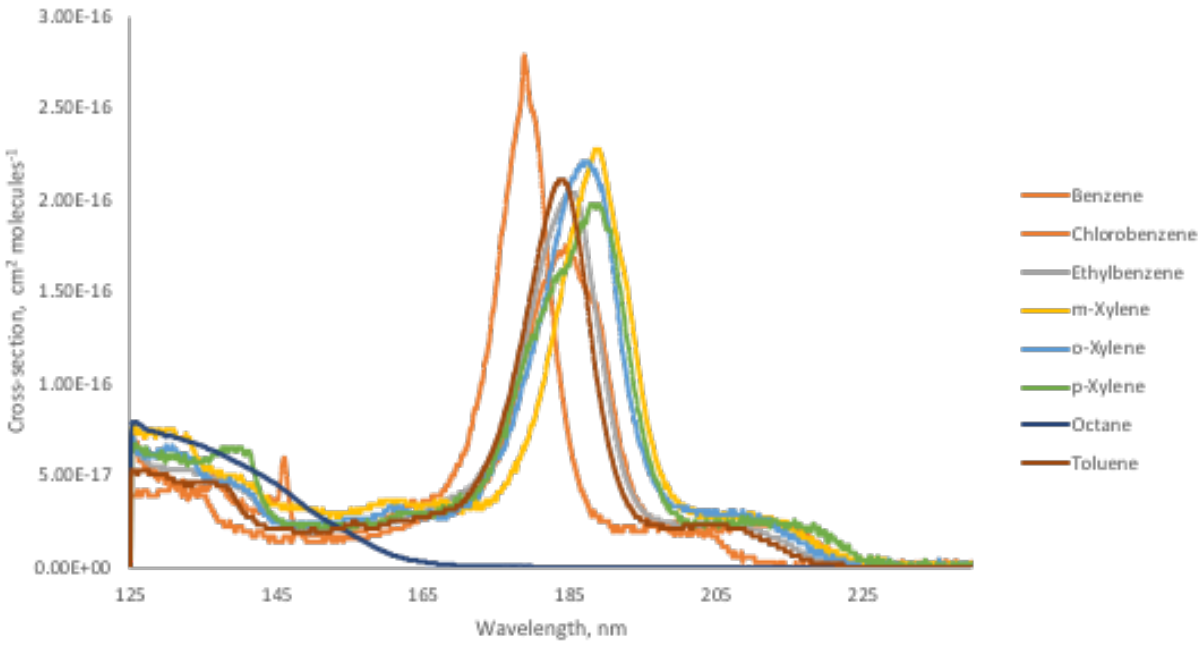

Figure 6.5. Recorded cross-sections for octane, cyclohexane, benzene, toluene, ethylbenzene, chlorobenzene, and xylene isomers.

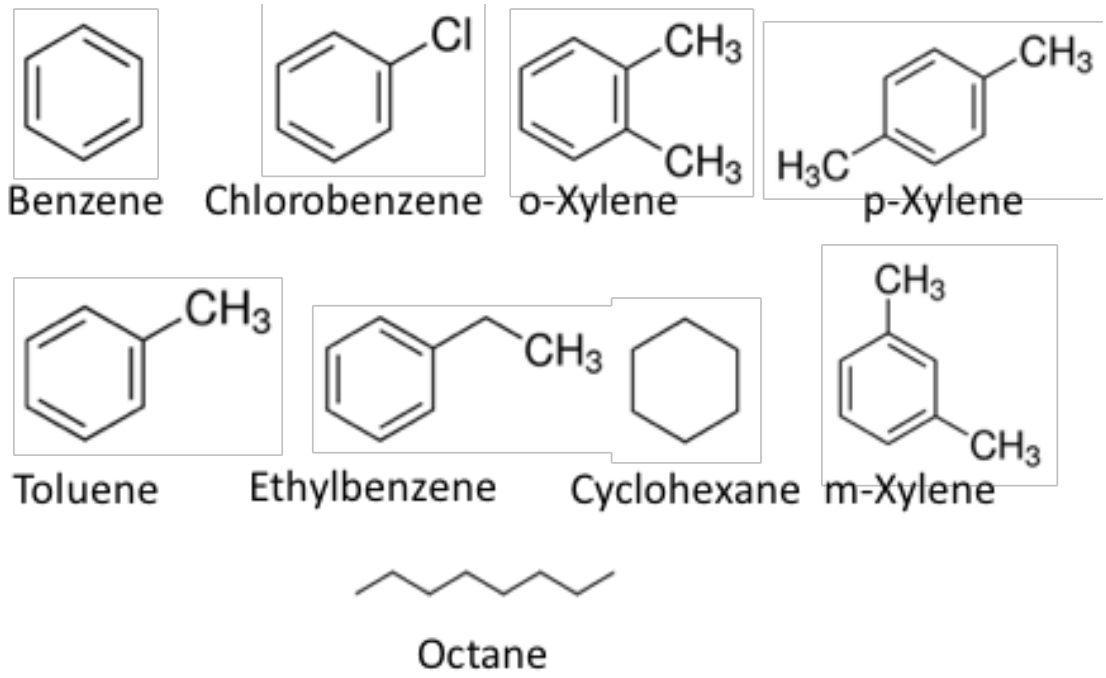

Figure 6.6. Chemical structure of the analytes being investigated.

6.3 Results and Discussion

6.3.1 RTILs Background Vapors

All 4 RTILs contained various background vapors before being cleaned, as seen in figure 6.3. All 3 of the hydrophilic RTILs ([EMIM] [ESO_4], [EMIM] [DEP], and [MTEOA] [$MeOSO_3$]) all contained a significant amount of water, with [MTEOA] [$MeOSO_3$] having the most. Water peaks are expected, as the vials are exposed to ambient conditions and these RTILs are hygroscopic. The hydrophobic RTIL ([EMIM] [NTF2]) also contained water but a much lower intensity was observed. [EMIM] [ESO_4] and [EMIM] [DEP], both contained ethyl ether, ethanol, acetone, and 1-methylimidazolium, all of which are commonly used in the synthesis and purification of the RTILs.[8-10] [EMIM] [DEP] contained the most background vapor to include the highest intensity peak of ethyl acetate. [EMIM] [NTF2] also contained ethyl acetate as well as being the only one in which acetonitrile was detected. [MTEOA] [$MeOSO_3$], was the only one that contained methanol and can be said to be the "cleanest" pre-cleaned RTIL. The cleaning of the RTILs by heating and purging vigorously with N_2 for approximately 24 hours appeared to be sufficient to rid the RTILs of virtually all contaminants.

6.3.2 Exploratory Experiments

The partition coefficient of volatile organic compounds (VOCs) over a wide range of solvents/ matrices and varying temperatures using either of the HS methods addressed above, are available in literature.[1-4, 11] 1 mL of water was used as the headspace solvent (β= 10.1) and Kp determinations for various VOCs were performed at 70 ℃ for an hour using the VPC method and compared to known available literature values. Results are

tabulated in table 6.3. Calibration and sample sets were prepared in triplicate. Linearity was observed throughout the 5-point calibration set and 5-point sample set with all analytes demonstrating an $r^2 \geq 0.995$. The average Kp value obtained by VPC (n=3 for all analytes) was found to have 12 – 30% difference from the available literature values for benzene, toluene, and o-xylene respectively. The same data set was then applied to pseudo-absolute quantitation (PAQ) (n=15 for all analytes).

The actual sample volume per analyte that reached the GC was determined using external calibration; the results are tabulated in table 6.4. It is not a surprise, that the actual sample volume calculated per analyte was approximately $\leq$ 20% of the 1 mL sample loop volume, which, can mainly be explained by the variation of pressure in the sample loop to that of the HS vial. The variation of volumes calculated between the analytes can be attributed to a multitude of things. Sample can be lost to vaporization during the sample preparation stage, as the VOCs are known to readily volatilize from solution. The gaseous sample can also experience wall adsorption effects within the HS vial.[3] Water, which originates from the humidity of the atmosphere and the natural humidity of samples, can be adsorbed by the inside of the glass vial due to hydrogen bonding to the surface silanol groups. This layer now acts as a partition system between the glass vial and the HS gas volume, which leads to a deviation in the actual volume calculated per analyte based on parameters of PAQ. The average volume calculated per analyte was used. This volume, was then used to determine the gas phase concentration of the analyte $[X]_G$ in the sample set. This allowed for Kp determination, based on equation 6.4. The results can be seen in table 6.3.

No significant differences in the precision of the two methods (VPC & PAQ) was observed. The percent relative standard deviation (RSD) observed with the VPC method were below 30% for all analytes except for octane, where we observed an RSD of 66%. A similar trend was observed with PAQ method where octane had high variability in the determination of Kp. This could be attributed to its relatively high $LogK_{OW}$ (octanol-water partition) value of approximately 5, meaning the partitioning into water is very low.[12]Thus, leading to below zero Kp values. Percent difference (% Dif.) between the average $Kp's$ obtained by VPC and PAQ are shown in table 6.3. Aside from octane, the % Dif. ranged from 6 – 26%, with p-xylene and m-xylene on the two extremes, respectively. Interesting to note that the extremes are for the co-eluting analytes m- and p- xylene. This may be due to the fact that concentrations of the coeluting analytes are nearing the saturation point of the detector, which could potentially lead to non-linearity of the individual contributions of the co-eluting analytes even though linearity was observed in the calibration and sample set curves, as mentioned above.[13]

Table 6.3. Average Kp determination of VOCs in water at 70 ℃ by the VPC and PAQ method along with percent relative standard deviation (RSD) and percent difference (% Dif.). VPC (n=3) PAQ (n=15)

Compound	Lit. Value	This Work (VPC)	RSD (%)	Difference (%) Lit.-VPC	This Work (PAQ)	RSD (%)	Difference (%) VPC-PAQ
Benzene	1.71*	1.52	17	12	1.64	23	8
Toluene	1.49**, 1.52*	1.16	26	25, 27	1.37	23	17
o-Xylene	1.01**	1.31	24	26	1.50	19	13
Ethylbenzene	-	1.03	23	-	1.22	26	17
m-Xylene	-	1.19	19	-	0.92	33	26
p-Xylene	-	1.26	21	-	1.19	25	6
Octane	-	0.31	66	-	0.47	48	41

(*) reference[1] (**) reference[2]

Table 6.4. Calculated actual volume of sample per analyte that reached the GC at 70 ℃.

Compound	Calc. Vol. (μL)
Benzene	172 ± 4
Toluene	175 ± 4
o-Xylene	150 ± 4
Ethylbenzene	171 ± 4
m-Xylene	172 ± 5
p-Xylene	134 ± 6
Octane	200 ± 5

6.3.3 Kp Determination of VOCs in RTILs at Varying Temperatures

VPC is the method of choice when it comes to Kp determinations of analytes in RTILs, as it has shown to be linear for Kp values be 1 -10^4 Kp.[2, 10, 14-15] Varona-Torres and colleagues investigated the use of 3 hydrophilic RTILs [EMIM] [ESO_4], [EMIM] [DEP], and [MTEOA] [$MeOSO_3$] and one hydrophobic [EMIM] [NTF2] for soil HS analysis. [16] The 3 hydrophilic RTILs were found to largely normalize the analyte response between the varying soil types. These findings require further knowledge of the relationship between the RTILs and the environmental contaminants. Unfortunately, to our knowledge, thermodynamic information of these environmental contaminants and the RTILs at the temperatures being investigated are not readily available. The widely accepted VPC method to determine Kp was performed with all 4 of the RTILs at temperatures from 70 to 110 ℃ , in 10-degree increments. The determination gas phase concentration was obtained by PAQ and applied for Kp determinations. The results were then compared to the values obtained by VPC. The RTILs were equilibrated for 30 min at the varying temperatures, as this was enough time for all components to reach equilibrium at the lowest temperature being investigated (70 ℃) as shown in figure 6.7. Cyclohexane was used as an internal standard in [EMIM] [ESO_4] and the normalized response was plotted against equilibration time, which ranged from 5 to 50 min.

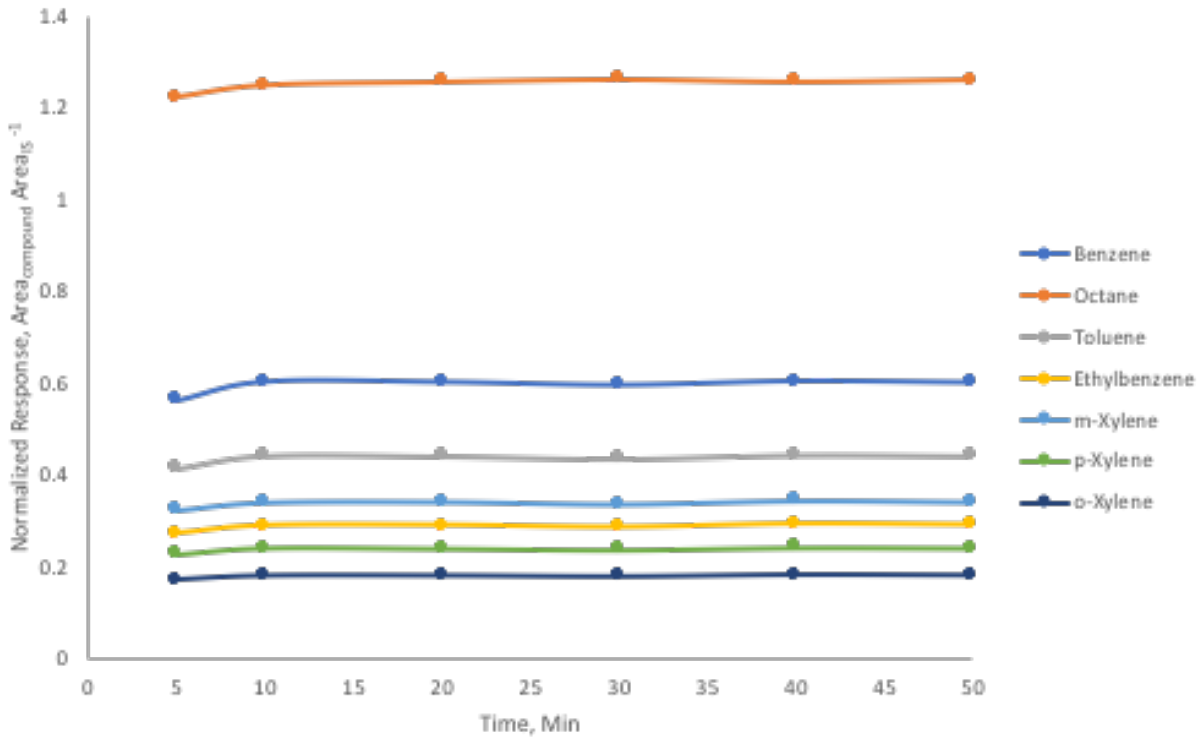

Figure 6.7. Optimization of heating equilibration times in [EMIM] [ESO_4] using cyclohexane as internal standard.

At 70 ℃, linearity was observed throughout the 5-point calibration set and 5-point sample set with all analytes demonstrating an $r^2 \geq 0.995$ for all analytes in all of the RTILS investigated in this work. The results of the experiments using [EMIM] [ESO_4] demonstrated percent RSD values of $<$ 10% for all analytes in both VPC and PAQ methods, as seen in table 6.5. In comparing the % Dif. of average Kp's, the largest difference was observed for m-xylene (20%) and octane at (14%). The use of [EMIM] [DEP] (21, 18%), [MTEOA] [$MeOSO_3$] (18, 24%) and [EMIM] [NTF2] (22, 18%) had significantly higher % Dif. for m- and p- xylene, respectively, as seen in table 6.6 – 6.8. Using [MTEOA] [$MeOSO_3$], octane had the most variability, thus the higher RSD value of

40%, a value similar to that attained using water, as seen when comparing tables 6.4 (water) and 6.7 ([MTEOA] [$MeOSO_3$]). At this temperature (70 ℃), [EMIM] [NTF2], the hydrophobic RTIL, returned the highest Kp values for all analytes except octane (Kp =17), in which [EMIM] [DEP] had the highest ($Kp = 24$) as seen in tables 6.8 and 6.6. At this temperature, with the exception of octane just mentioned, the RTILs can be arranged by overall analyte retention as: [EMIM] [NTF2] (highest Kp value) > [EMIM] [DEP] > [EMIM] [ESO_4] > [MTEOA] [$MeOSO_3$] (lowest Kp value). For our purpose we would want to see low Kp values. Relatively low % Dif. observed throughout the various RTILs at this temperature, it can be said PAQ is a suitable method for Kp determinations.

Table 6.5. Average Kp determination of VOCs in [EMIM] [ESO_4] at 70 ℃ by the VPC and PAQ method along with percent relative standard deviation (RSD) and percent difference (% Dif.). VPC (n=3) PAQ (n=15)

Compound	This Work (VPC)	RSD (%)	This Work (PAQ)	RSD (%)	Difference (%) VPC-PAQ
Benzene	81.7	2	85.1	3	4
Toluene	114	2	120	2	5
o-Xylene	238	2	250	3	5
Ethylbenzene	153	2	161	3	5
m-Xylene	129	3	157	3	20
p-Xylene	189	3	174	4	8
Octane	3.03	7	3.48	9	14

Table 6.6. Average Kp determination of VOCs in [EMIM] [DEP] at 70 ℃ by the VPC and PAQ method along with percent relative standard deviation (RSD) and percent difference (% Dif.). VPC (n=3) PAQ (n=15)

Compound	This Work (VPC)	RSD (%)	This Work (PAQ)	RSD (%)	Difference (%) VPC-PAQ
Benzene	121	2	121	1	<1
Toluene	193	4	197	2	2
o-Xylene	422	6	432	2	2
Ethylbenzene	312	5	317	2	2
m-Xylene	243	3	299	3	21
p-Xylene	379	3	316	4	18
Octane	24.2	1	24.3	2	<1

Table 6.7. Average Kp determination of VOCs in [MTEOA] [$MeOSO_3$] at 70 ℃ by the VPC and PAQ method along with percent relative standard deviation (RSD) and percent difference (% Dif.). VPC (n=3) PAQ (n=15)

Compound	This Work (VPC)	RSD (%)	This Work (PAQ)	RSD (%)	Difference (%) VPC-PAQ
Benzene	9.39	9	9.56	10	2
Toluene	12.1	11	12.1	10	<1
o-Xylene	24.6	9	23.3	9	5
Ethylbenzene	13.3	10	13.3	11	<1
m-Xylene	11.7	9	14.0	11	18
p-Xylene	18.2	9	14.3	13	24
Octane	0.35	8	0.49	40	33

Table 6.8. Average Kp determination of VOCs in [EMIM] [NTF2]] at 70 ℃ by the VPC and PAQ method along with percent relative standard deviation (RSD) and percent difference (% Dif.). VPC (n=3) PAQ (n=15)

Compound	This Work (VPC)	RSD (%)	This Work (PAQ)	RSD (%)	Difference (%) VPC-PAQ
Benzene	142	1	144	1	1
Toluene	250	1	260	1	4
o-Xylene	602	1	618	2	3
Ethylbenzene	386	2	393	2	2
m-Xylene	346	1	430	3	22
p-Xylene	524	3	441	4	17
Octane	17.4	2	17.0	2	2

For the remainder of the temperatures (80, 90, 100, 110 ℃), the chromatographic conditions where adjusted to include 2 more analytes (cyclohexane and chlorobenzene). Chlorobenzene was kept a constant concentration, thus only the PAQ could be applied. The GC temperature program was altered to hold at 35 ℃ for 2 min, increasing to 60 ℃ at a rate of 30 ℃ min^{-1}, then a slow temperature ramp of 4 ℃ min^{-1} to 100 ℃, where there is another increase at 30 ℃ min^{-1} to 200 ℃ and hold for 1 min. The total program time is 17.2 mins. Figure 6.8 shows the modified chromatograms with analytes of interest. Linearity was observed at all temperatures of all analytes in all RTILs with $r^2 \geq 0.995$. The Kp's for each individual analyte in each of the 4 RTILs at the varying temperature are shown in figures 6.9A – 6.9D. As can be expected, [EMIM] [NTF2] had the larger values of Kp for all analytes except both cyclohexane and octane in which, [EMIM] [DEP] demonstrated a slightly higher value for Kp. The general trend over the temperature range [EMIM] [NTF2] (highest Kp value) > [EMIM] [DEP] > [EMIM] [ESO_4] > [MTEOA] [$MeOSO_3$] (lowest Kp value) with the exception of the two unsaturated hydrocarbons mentioned above. No decreasing trend of Kp values were observed for octane or cyclohexane in [MTEOA] [$MeOSO_3$] the most hydrophilic RTIL being examined. Based on the data obtained, [EMIM] [NTF2] may not be the best HS co-solvent to improve sensitivity for the analytes investigated as higher Kp values indicate stronger analyte solvent interactions.

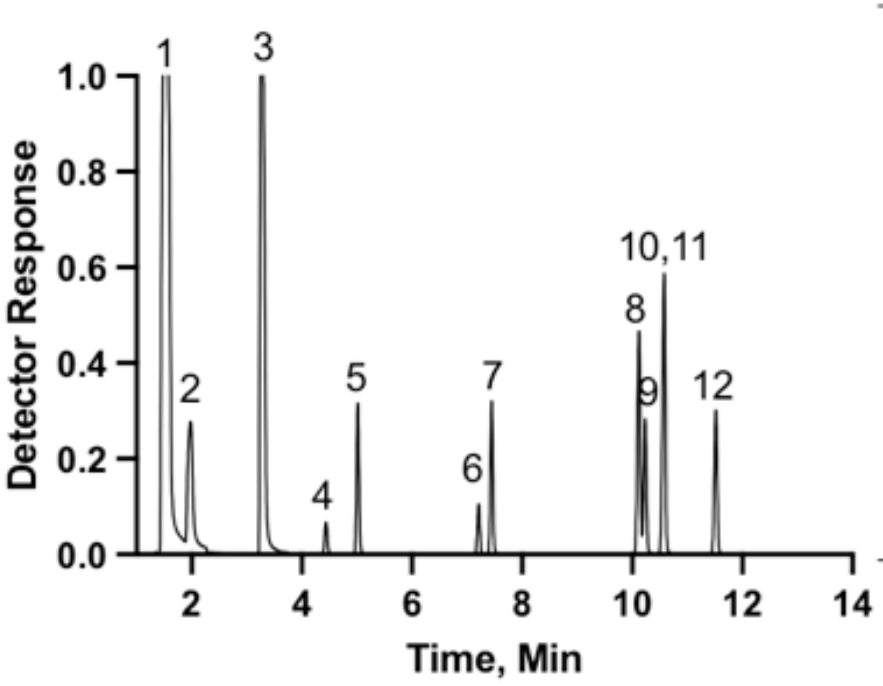

Peak #	Compound
1	Air
2	Water
3	DCM
4	Cyclohexane
5	Benzene
6	Octane
7	Toluene
8	Chlorobenzene
9	Ethylbenzene
10,11	m-/p-Xylene
12	o-Xylene

Figure 6.8. Chromatogram of analytes of interest in [MTEOA][$MeOSO_3$] at 110 ℃.

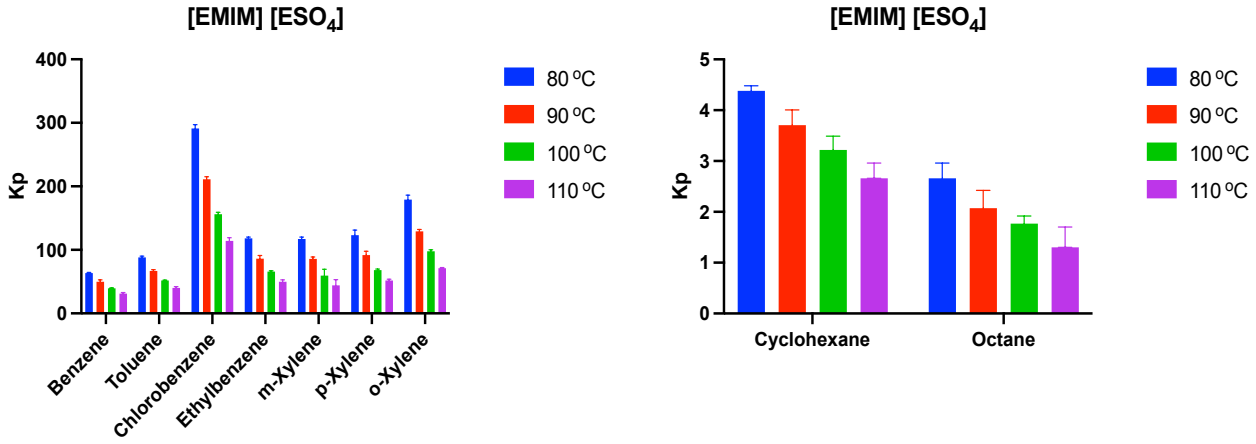

Figure 6.9A. Partition coefficients obtained at varying temperatures using PAQ for analytes investigated in [EMIM] [ESO_4].

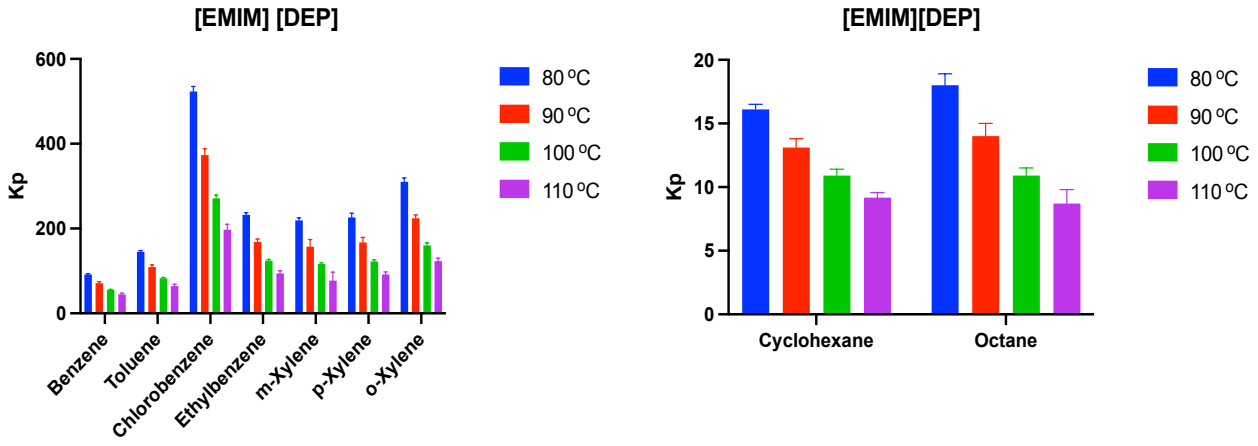

Figure 6.9B. Partition coefficients obtained at varying temperatures using PAQ for analytes investigated in [EMIM] [DEP].

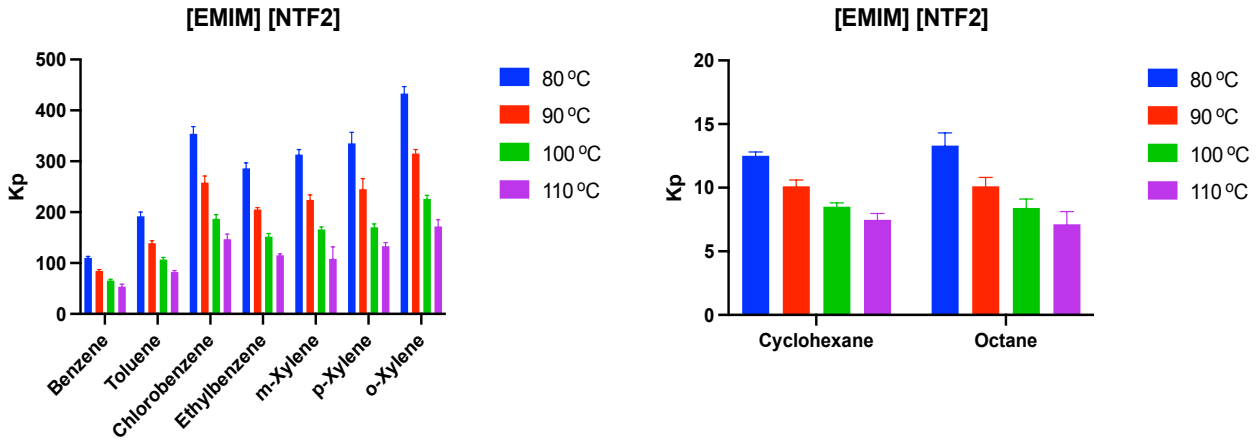

Figure 6.9C. Partition coefficients obtained at varying temperatures using PAQ for analytes investigated in [EMIM] [NTF2].

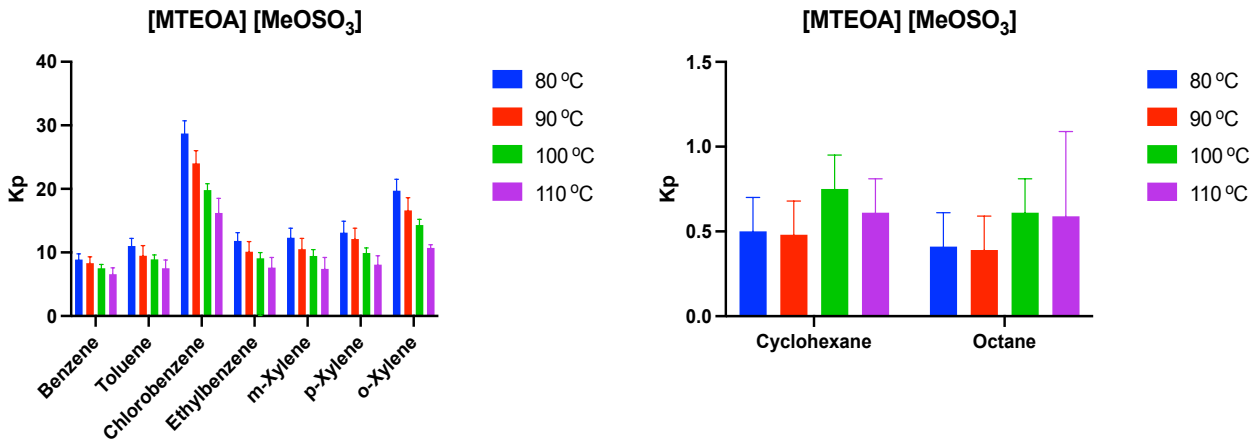

Figure 6.9D. Partition coefficients obtained at varying temperatures using PAQ for analytes investigated in [MTEOA] [$MeOSO_3$].

6.3.4 van't Hoff Plots for Determination of Enthalpy and Entropy

van't Hoff plots allow for the further understanding of the molecular-scale energetics (enthalpy (ΔH) and entropy (ΔS)) of the system. The van't Hoff plot relates the change in equilibrium constant (Kp) of a system to the change in temperature as seen in equation 6.5, where *R* is the gas constant and T is the temperature in Kelvin.

$$lnKp = -\frac{\Delta H}{RT} + \frac{\Delta S}{R} \text{ (Equation 6.5)}$$

The obtained Kp values by the PAQ approach were used for the determination of ΔH and ΔS of each analyte in each of the RTIL by creating van't Hoff plots and the results are shown in figure 6.10A-I. [MTEOA] [$MeOSO_3$] displayed deviation from linearity for all analytes but most noticeable with cyclohexane (fig.6.9A) and octane (fig.6.9C) with r^2 values of 0.427 and 0.329 respectively. This is a clear indication that ΔH and ΔS are not constant over this temperature range for these systems. Aside for the deviation just discussed, negative ΔH was observed for all compounds in all of the RTILs. As shown in

figures 6.9A-I, [EMIM] [ESO_4], [EMIM] [DEP] and [EMIM] [NTF2] show similar ΔH and ΔS values for all components. [MTEOA] [$MeOSO_3$] displayed the less exothermic system (less negative ΔH) for all of the compounds except, the two (cyclohexane and octane) mentioned above.

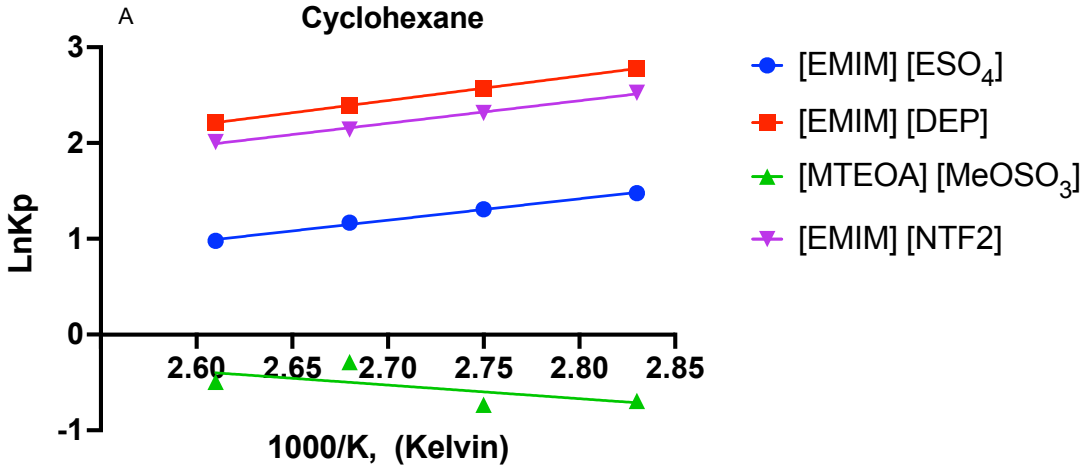

RTIL	ΔH $(kJ\ mol^{-1})$	ΔS $(J\ K^{-1})$	r^2
[EMIM] [ESO_4]	-18.6 ± 0.9	-40.3 ± 2.5	.995
[EMIM] [DEP]	-21.3 ± 0.2	-37.3 ± 0.5	.999
[MTEOA] [$MeOSO_3$]	11.8 ± 9.7	27.5 ± 26.3	.427
[EMIM] [NTF2]	-19.6 ± 1.1	-34.6 ± 3.0	.994

B

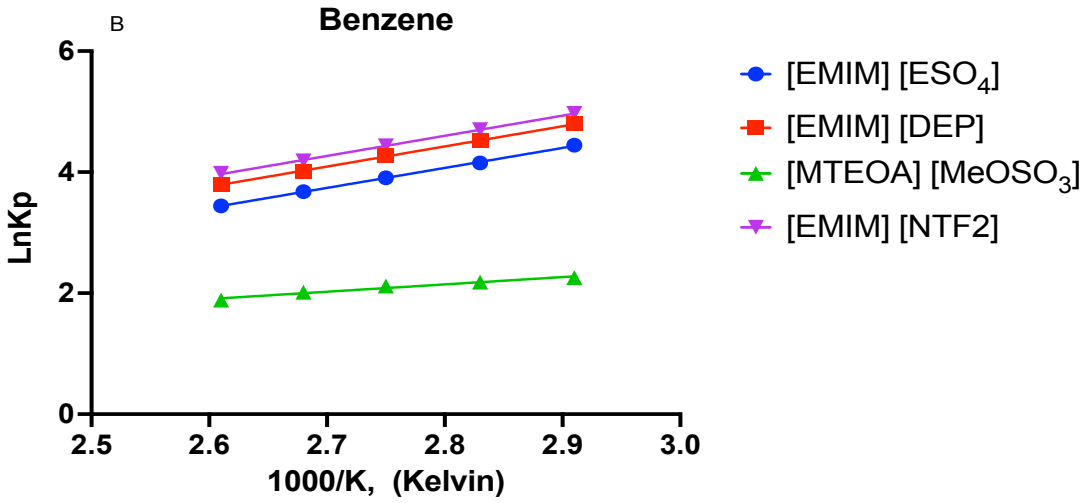

RTIL	ΔH $(kJ\ mol^{-1})$	ΔS $(J\ K^{-1})$	r^2
[EMIM] [ESO_4]	-27.4 ± 0.4	-43.0 ± 1.2	.999
[EMIM] [DEP]	-27.7 ± 0.4	-40.7 ± 1.0	.999
[MTEOA] [$MeOSO_3$]	-10.1 ± 1.0	-10.4 ± 2.9	.968
[EMIM] [NTF2]	-27.7 ± 0.4	-39.2 ± 1.1	.999

C

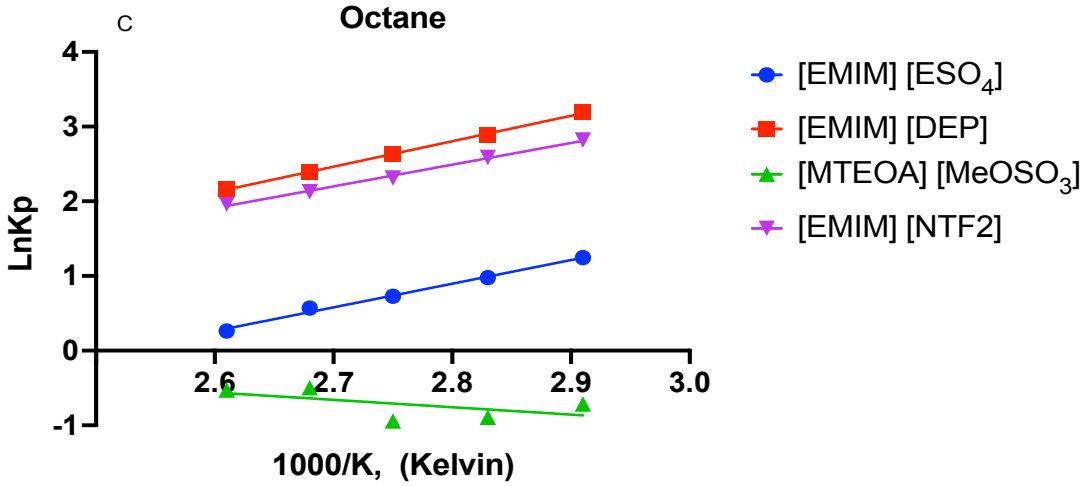

RTIL	ΔH $(kJ\ mol^{-1})$	ΔS $(J\ K^{-1})$	r^2
[EMIM] [ESO_4]	-26.3 ± 1.3	-66.3 ± 3.7	.993
[EMIM] [DEP]	-28.3 ± 0.5	-56.0 ± 1.2	.999
[MTEOA] [$MeOSO_3$]	8.2 ± 6.8	16.7 ± 18.6	.329
[EMIM] [NTF2]	-24.2 ± 0.9	-47.0 ± 2.5	.996

D

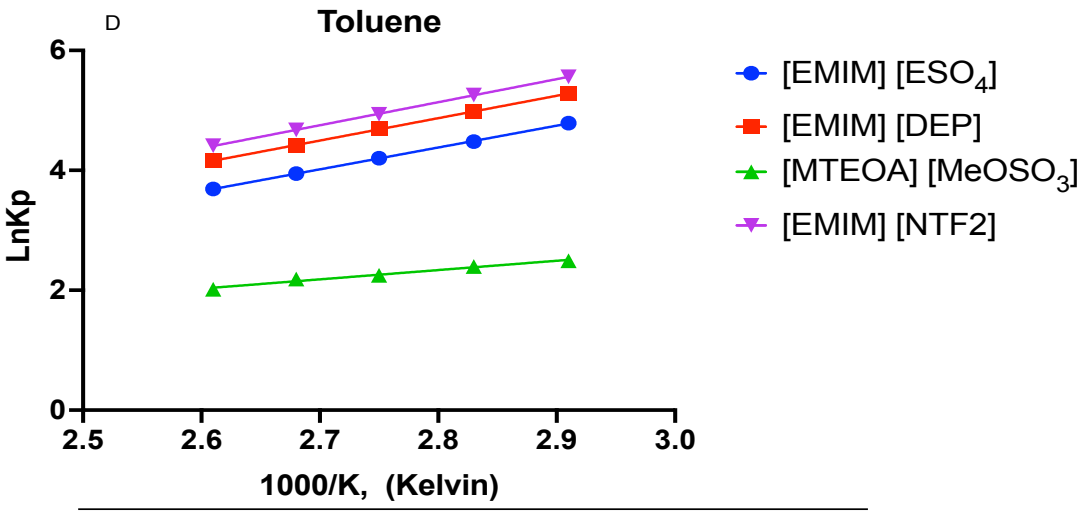

RTIL	ΔH $(kJ\ mol^{-1})$	ΔS $(J\ K^{-1})$	r^2
[EMIM] [ESO_4]	-30.3 ± 0.2	-48.4 ± 0.7	.999
[EMIM] [DEP]	-31.1 ± 0.2	-46.5 ± 0.6	.999
[MTEOA] [$MeOSO_3$]	-12.9 ± 1.0	-16.7 ± 2.8	.982
[EMIM] [NTF2]	-32.0 ± 0.3	-46.8 ± 0.7	.999

E

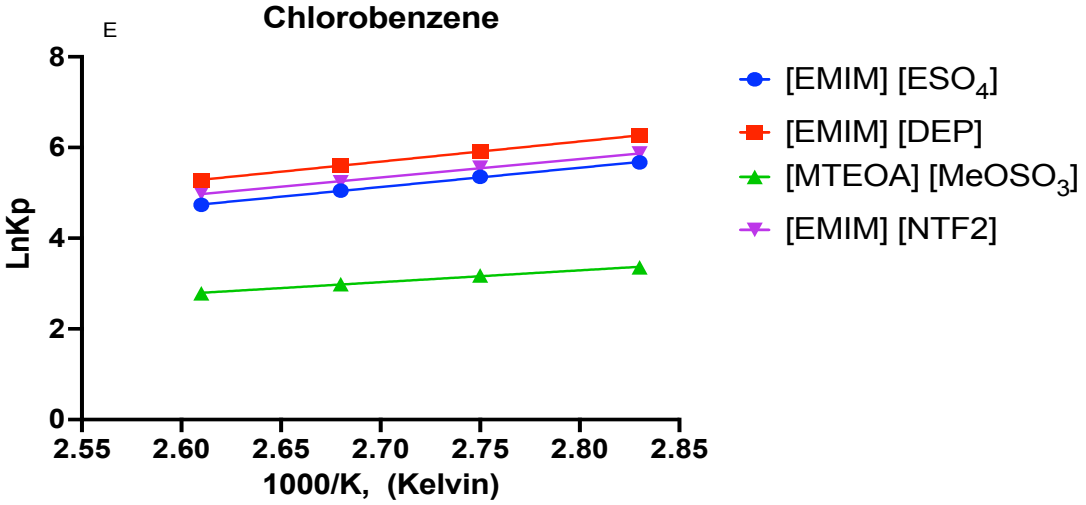

RTIL	ΔH $(kJ\ mol^{-1})$	ΔS $(J\ K^{-1})$	r^2
[EMIM] [ESO_4]	-35.4 ± 0.6	-53.0 ± 1.7	.999
[EMIM] [DEP]	-37.0 ± 0.5	-52.5 ± 1.4	.999
[MTEOA] [$MeOSO_3$]	-21.7 ± 0.9	-33.4 ± 2.4	.997
[EMIM] [NTF2]	-33.7 ± 1.2	-46.6 ± 3.3	.999

F

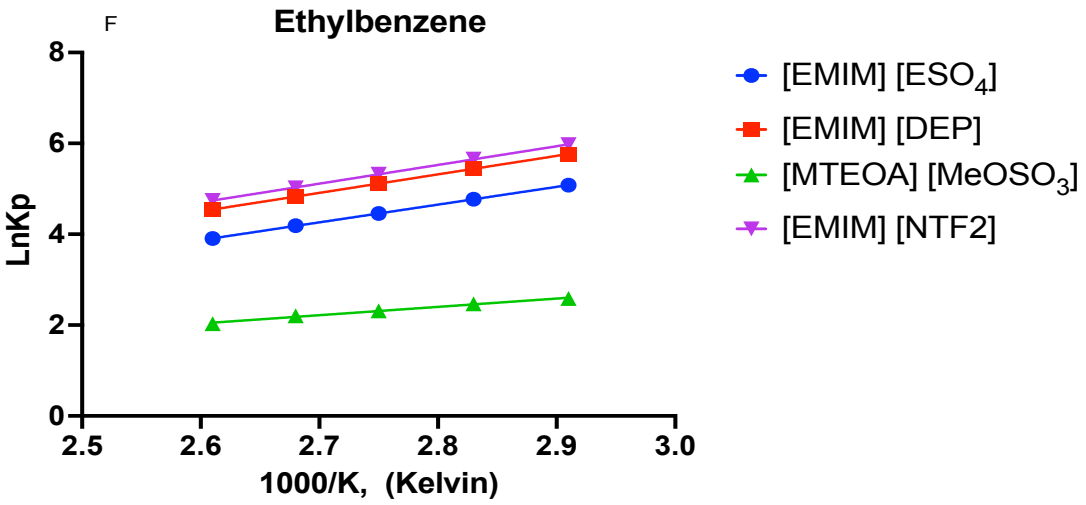

RTIL	ΔH $(kJ\ mol^{-1})$	ΔS $(J\ K^{-1})$	r^2
[EMIM] [ESO_4]	-32.5 ± 0.1	-52.3 ± 0.2	.999
[EMIM] [DEP]	-33.9 ± 0.3	-50.6 ± 0.9	.999
[MTEOA] [$MeOSO_3$]	-15.2 ± 0.8	-22.7 ± 2.1	.993
[EMIM] [NTF2]	-34.2 ± 0.2	-50.0 ± 0.7	.999

G

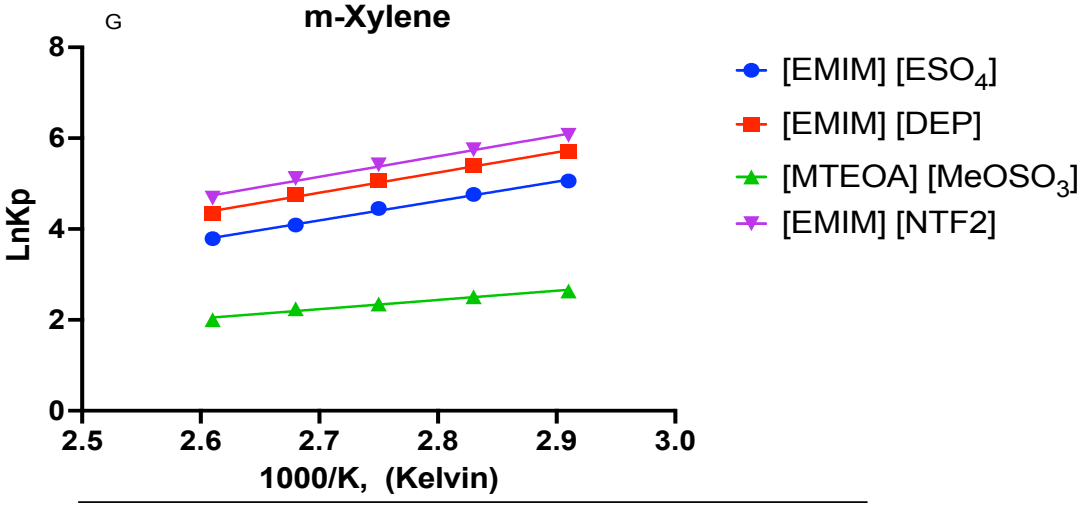

RTIL	ΔH $(kJ\ mol^{-1})$	ΔS $(J\ K^{-1})$	r^2
[EMIM] [ESO_4]	-35.5 ± 1.3	-61.0 ± 3.5	.996
[EMIM] [DEP]	-37.0 ± 1.7	-60.1 ± 4.8	.994
[MTEOA] [$MeOSO_3$]	-16.9 ± 1.5	-27.1 ± 4.2	.977
[EMIM] [NTF2]	-37.6 ± 1.9	-58.6 ± 5.3	.992

H

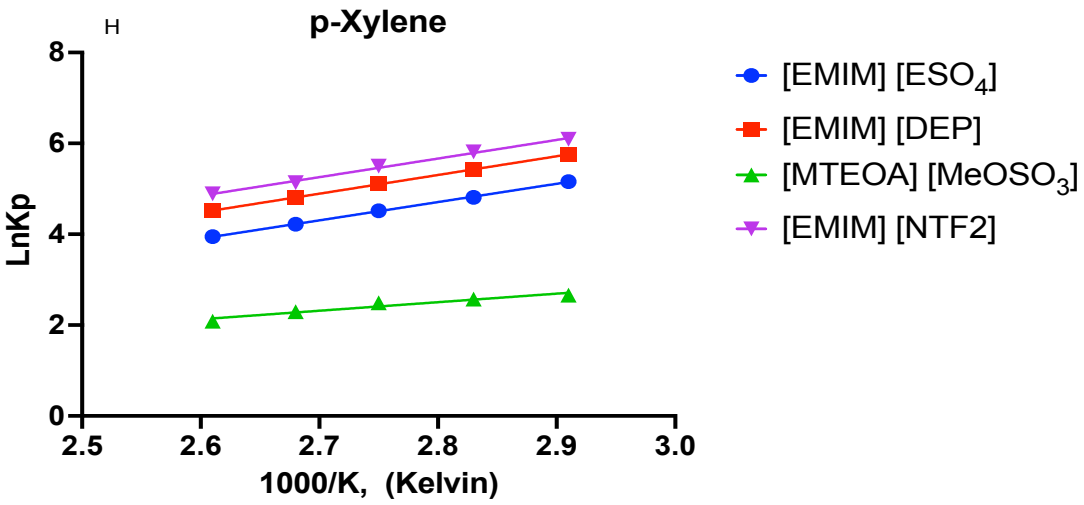

RTIL	ΔH $(kJ\ mol^{-1})$	ΔS $(J\ K^{-1})$	r^2
[EMIM] [ESO_4]	-33.5 ± 0.5	-54.5 ± 1.2	.999
[EMIM] [DEP]	-34.2 ± 0.4	-51.8 ± 1.2	.999
[MTEOA] [$MeOSO_3$]	-15.6 ± 2.3	-22.9 ± 6.4	.937
[EMIM] [NTF2]	-34.0 ± 1.4	-48.2 ± 3.7	.995

I

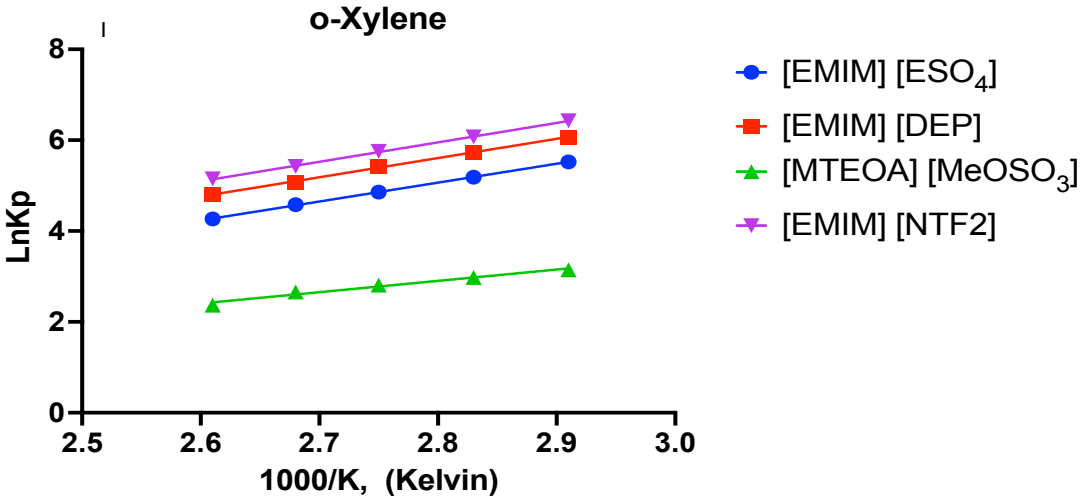

RTIL	ΔH $(kJ\ mol^{-1})$	ΔS $(J\ K^{-1})$	r^2
[EMIM] [ESO_4]	-34.6 ± 0.4	-54.7 ± 1.1	.999
[EMIM] [DEP]	-35.2 ± 0.6	-51.9 ± 1.7	.999
[MTEOA] [$MeOSO_3$]	-20.7 ± 1.9	-33.9 ± 5.1	.976
[EMIM] [NTF2]	-35.6 ± 0.5	-50.1 ± 1.5	.999

Figure 6.10. van't Hoff plots and calculated ΔH and ΔS values A) cyclohexane, B) benzene, C) octane, D) toluene, E) chlorobenzene, F) ethylbenzene, G) m-xylene, H) p-xylene and I) o-xylene in all 4 RTILs.

6.4 Conclusion

As discussed previously, RTILs are promising HS co-solvents that can be used to dissolve / homogenize various matrices. Understanding the interaction of analytes and the RTILs are of key interest when eliciting one for a task. Here we demonstrated a novel way to determine partition coefficients by pseudo-absolute quantitation (PAQ) using the HS-20 (pressure-loop) headspace system with gas chromatography vacuum ultraviolet detection (HS-GC-VUV). The determination of the headspace gas phase concentration, then leads to quick assessments of Kp values. Little to no difference observed between the mean values of $Kp's$ obtained by the vapor phase calibration (VPC) and PAQ. van't Hoff plots were used to determine change of enthalpy and entropy in the system. The negative enthalpy values obtained demonstrates strong solute-RTILs interaction which lead to a decrease of HS sensitivity (less analyte in the gas phase). The [EMIM] based RTILs showed to have the highest retention and behaving fairly similarly for aromatic compounds. Suggesting, such RTILs may not be suitable for increasing sensitivity of such components in HS analysis.

6. References

1. Ettre, L. S.; Welter, C.; Kolb, B., Determination of gas-liquid partition coefficients by automatic equilibrium headspace-gas chromatography utilizing the phase ratio variation method. *Chromatographia* **1993,** *35* (1), 73-84.
2. Kolb, B.; Welter, C.; Bichler, C., Determination of partition coefficients by automatic equilibrium headspace gas chromatography by vapor phase calibration. *Chromatographia* **1992,** *34* (5), 235-240.
3. Kolb, B., *Static Headspace-Gas Chromatography : Theory and Practice*. 2nd ed. ed.; John Wiley & Sons, Inc.: Hoboken, 2006.
4. Ettre, L. S.; Kolb, B., Headspace-gas chromatography: The influence of sample volume on analytical results. *Chromatographia* **1991,** *32* (1), 5-12.
5. ProEZGC Chromatorgram Modeler. https://www.restek.com/proezgc.
6. *GraphPad Prism* 2021.
7. Bai, L.; Smuts, J.; Walsh, P.; Qiu, C.; McNair, H. M.; Schug, K. A., Pseudo-absolute quantitative analysis using gas chromatography – Vacuum ultraviolet spectroscopy – A tutorial. *Analytica Chimica Acta* **2017,** *953*, 10-22.
8. Welton, T., Room-Temperature Ionic Liquids. Solvents for Synthesis and Catalysis. *Chemical Reviews* **1999,** *99* (8), 2071-2033.
9. Płotka-Wasylka, J.; de la Guardia, M.; Andruch, V.; Vilková, M., Deep eutectic solvents vs ionic liquids: Similarities and differences. *Microchemical Journal* **2020,** *159*, 105539.
10. Von Wald, G.; Albers, D.; Cortes, H.; McCabe, T., Background vapor from six ionic liquids and the partition coefficients and limits of detection for 10 different analytes in those ionic liquids measured using headspace gas chromatography. *Journal of Chromatography A* **2008,** *1201* (1), 15-20.
11. Voice, T. C.; Kolb, B., Static and dynamic headspace analysis of volatile organic compounds in soils. *Environmental Science & Technology* **1993,** *27* (4), 709-713.
12. Octane. National Library of Medicine: PubChem.
13. Schenk, J.; Mao, J. X.; Smuts, J.; Walsh, P.; Kroll, P.; Schug, K. A., Analysis and deconvolution of dimethylnaphthalene isomers using gas chromatography vacuum ultraviolet spectroscopy and theoretical computations. *Analytica Chimica Acta* **2016,** *945*, 1-8.
14. He, X.; Jiang, Y.; Lei, L.; Li, J.; Ni, M., Quantitative Prediction of Ionic Liquid-Gas Partition Coefficients for Residual Solvents by HS-GC. *Chromatographia* **2011,** *74* (1), 157.
15. Ni, M.; Sun, T.; Zhang, L.; Liu, Y.; Xu, M.; Jiang, Y., Relationship study of partition coefficients between ionic liquid and headspace for organic solvents by HS-GC. *Journal of chromatography. B, Analytical technologies in the biomedical and life sciences* **2014,** *945-946*, 60-7.
16. Varona-Torres, E.; Carlton, D. D.; Hildenbrand, Z. L.; Schug, K. A., Matrix-effect-free determination of BTEX in variable soil compositions using room temperature ionic liquid co-solvents in static headspace gas chromatography mass spectrometry. *Analytica Chimica Acta* **2018,** *1021*, 41-50.

Conclusion

In this body of work a brief history and the theoretical basis of gas chromatography and static headspace extraction were discussed in detail. The use of headspace gas chromatography mass spectrometry was used for the analysis of environmental contaminants in soil related to the oil and gas industry. It was found that soil texture was a contributing factor in total detection of the volatile contaminants rather than distance from identifiable emission sources.

Hydrophilic room temperature ionic liquids (RTILs) were investigated for their potential use as a headspace co-solvent in soil analysis. It was found that not only were they able to reduce thermostatting time, by operating at a higher temperature than common methods, but to also normalize between soil textures. This allows for less dependence on sample information, i.e. the determination of soil texture, moisture content, and pH, prior to analysis.

Understanding the thermodynamics associated with interactions between an analyte and a solvent can improve the selection of a solvent for a specific task. The interactions between RTILs and environmental contaminants were determined by headspace gas chromatography vacuum ultraviolet detection (HS-GC-VUV). The constant vial conditions provided by the HS-20 (pressure-loop headspace system) allowed for constant gas volume to reach the detector. Govern by the Beer-Lambert law the pseudo-absolute quantitation (PAQ) capabilities of the VUV, allowed for the calculation of molecules that read the detector and thus, allowed direct calculation of the gas phase concentration in the HS vial without the need of a calibration curve. This allowed for the determination of partition coefficient by rearranging the equilibrium static

headspace equation. The method was compared to widely accepted vapor phase calibration and was determined to be comparable. van't Hoff plots revealed that 1-ethyl-3-methylimidazolium cation [EMIM] based RTILs retain aromatics compounds similarly with negative values for enthalpy.

Further investigation is necessary to fully understand the "complete system" dynamic; that is, analyte/ co-solvent/ sample matrix. Continuing using the HS-20-GC-VUV and its PAQ capabilities we could rapidly determine thermodynamic data for various contaminants at various temperatures. The ability to investigate the analyte-solvent interaction, but as well as the analyte-matrix and define a 3-phase equilibrium model.